Analysis and generation of highly dynamic motions of anthropomorphic systems : application to parkour

Galo Maldonado

THÈSE

En vue de l'obtention du

DOCTORAT DE L'UNIVERSITÉ FÉDÉRALE TOULOUSE MIDI-PYRÉNÉES

Délivré par :
l'Université Toulouse 3 Paul Sabatier (UT3 Paul Sabatier)

Présentée et soutenue le *08/12/2017* **par :**

GALO XAVIER MALDONADO TORO

Analysis and Generation of Highly Dynamic Motions of Anthropomorphic Systems: Application to Parkour

---

JURY

AGNÈS ROBY-BRAMI	Directeur de Recherche	Rapporteur
FRANK MULTON	Professeur des Universités	Rapporteur
ETIENNE BURDET	Professeur des Universités	Examinateur
BRUNO WATIER	Maître de Conferences	Directeur de Thèse
PHILIPPE SOUÈRES	Directeur de Recherche	Directeur de Thèse

École doctorale et spécialité :
EDSYS : Robotique 4200046
Unité de Recherche :
Laboratoire d'analyse et d'architecture des systèmes
Directeur(s) de Thèse :
Bruno WATIER et *Philippe SOUÈRES*
Rapporteurs :
Agnès ROBY-BRAMI et *Frank MULTON*

Acknowledgments

First of all, I would like to thank my thesis supervisors Bruno WATIER and Philippe SOUÈRES for giving me the opportunity of conducting my research at LAAS-CNRS and for guiding me throughout the realization of this thesis. I would also like to thank my thesis jury for reviewing my work and for their pertinent comments and advices regarding my research. I gratefully acknowledge the Region Midi-Pyrénées for founding the Anthropomove project which made possible the realization of this thesis. I also thank the University of Toulouse III, EDSYS, LAAS-CNRS and the Gepetto team for their hospitality and the environment provided to do research.

Furthermore, I would like to thank the members of the Gepetto team who where involved in the achievement of this thesis. Particularly, I thank François BAILLY who was my principal collaborator in the mathematical development of the motor control study. I would also like to thank Justin CARPENTIER who contributed with the technical development of my work, especially in the use of the learning of the Pinocchio software and in the motion generation study. Thanks also to my colleagues who made this 3 years enjoyable inside and outside the laboratory. Thanks to François B., Florent F., Thomas F., Alexis M., Dinesh A., Justin C., Joseph M., Ganesh K. and the others.

I would also like to thank the people who were involved in the experimental sessions. Firstly, thanks to CREPS-Toulouse for the utilization of the motion capture room, to Hugo BITARD for lending us the parkour structure to perform the experiments and to Xavier DOLLAT who co-designed and build the adaptation elements for the parkour structure. Thanks to all the participants who volunteered to the exhausting experimental sessions of this thesis for their time and collaboration. Thanks also to Doc. Xavier DELANNOY and all the interns who helped me to set-up the recording sessions. Particularly, many thanks to Xavier DELANNOY for helping me with the palpation and localization of the participants surface muscles and for his contribution with the epidemiological study.

Finally, but not less important, thanks to all members of my family and to my friends outside the laboratory. Thanks to my wife Lizette for her love and support during this period, and during all the adventures since we arrived at France. Thanks to my parents for the education, motivation, advices, support and love not only during my thesis, but throughout my life.

Contents

List of Figures

List of Tables

Glossary

AMD Angular momentum derivative.

CNS Central nervous system.

CoM Center of mass.

CoP Center of pressure.

DPSI Dynamic postural stability index.

FAMD Frontal angular momentum derivative.

GRF Ground reaction force.

IC Initial contact with the ground.

ITC Index of task control.

LMD Linear momentum derivative.

MEE Mechanical energy expenditure.

RoM Range of motion.

SAMD Sagittal angular momentum derivative.

TAMD Transversal angular momentum derivative.

Traceurs Parkour practitioners.

TTS Time to stabilization.

UCM Uncontrolled Manifold.

Chapter 1

General Introduction

Contents

How does the central nervous system select and coordinate several degrees of freedom to execute a given movement? The difficulty of this question, formulated in the middle of the last century [Bernstein 1967], arises because each motion is the result of a motor control strategy from a redundant and large set of possible solutions. If some invariants of movement can be identified, it exists however an important variability that shows that motor control favors rather an envelope of possible movements than a single stereotypy. However, the central nervous system is able to find extremely fast solutions to the problem of muscular and kinematic redundancy by producing safe, optimal, robust, stable and/or precise movements.

This thesis provides an interdisciplinary approach for the treatment of whole-body human movement through the synergistic utilization of biomechanics, motor control and robotics. It's originality arises from the case study utilized throughout the manuscript which is the study of highly dynamic parkour movements. The complexity of the study result from its interdisciplinary nature and the complexity of the analyzed parkour motions.

This introductory chapter aims at providing a general overview of the thesis explaining the motivations behind this work, synthesizing the organization of the manuscript and summarizing the principal contributions.

1.1 Main Definitions and Historical Perspectives

The principal definitions and the historical perspective of the three main components of this thesis: biomechanics, motor control and robotics, are presented in this section.

1.1.1 Biomechanics of human movement

Biomechanics studies the structure and functioning of biological systems such as humans by means of mechanics.

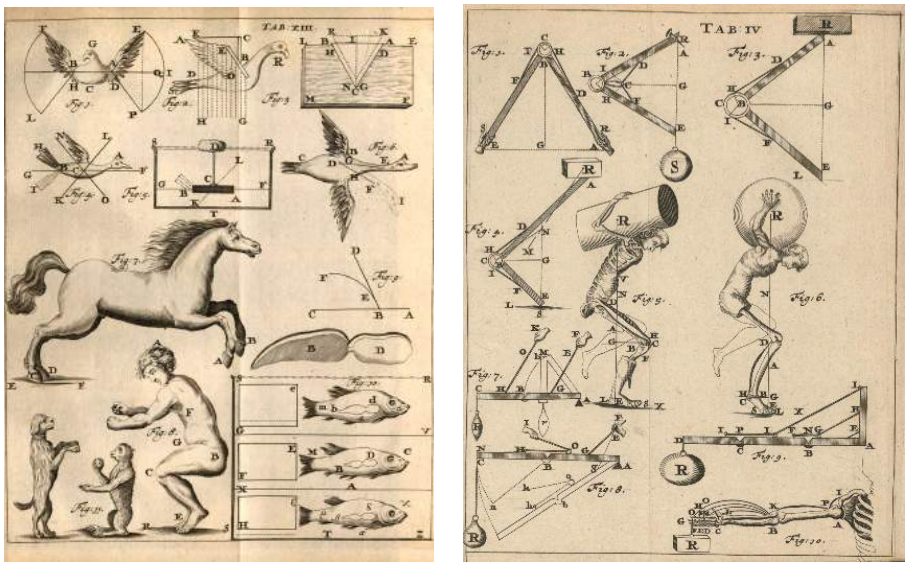

(a) **(b)**

Figure 1.1: Borellis' drawings from "De Motu Animalium I"(1680).

1.1.1.1 Elements of history

Biomechanics of human motion can be traced back to **Aristotle** (384-322 BC) who wrote the treatise *"About the movement of Animals"* (350 BC) and provided the first analysis of gait. Afterwards, **Archimedes** (287-212 BC) provided for the first time the notion of levers and statics which can be summarized in his famous phrase *"Give me a place to stand on, and I will move the Earth"*. Later, **Galen** (AD 129-201), considered as the first "sport physician" explained the difference between motor and sensory nerves, and agonist and antagonists muscles, while he was the team doctor of the Roman gladiators. From the Renaissance to beyond,

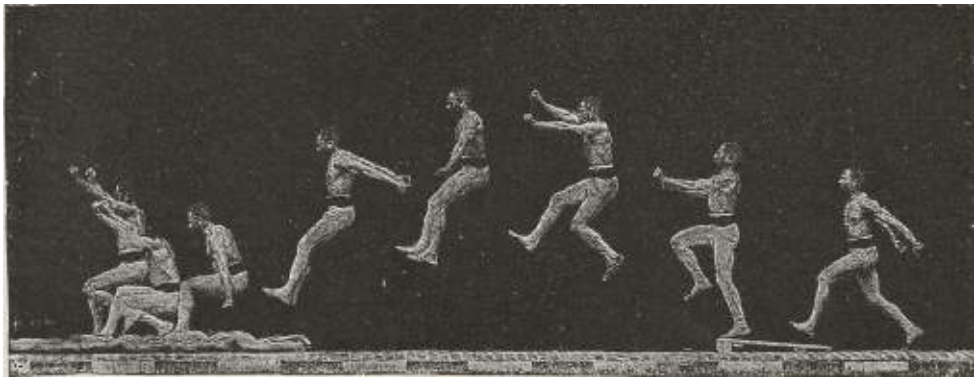

Figure 1.2: Successive phases of a jump motion for kinematics study. The image was taken at 5 [Hz] using chrono-photography on fix plate. The photo appears in the book "Le MOUVEMENT" by Étienne-Jules Marey, 1984.

we have to mention **Leonardo da Vinci** (1452-1519) who studied the anatomy and the mechanical functions of the skeletal system along with the forces that were applied to it. **Alfonso Borelli** (1608-1679) who published "*De Motu Animalium I*" and "*De Motu Animalium II*" in 1680 symbolizes the classic historical beginning of biomechanics. In fact Borelli is considered as the "father of biomechanics". Borelli brought out the general concepts of center of mass and center of pressure of a body in contact with the ground. Borelli calculated the forces required for equilibrium in various joints of the human body well before Newton published *"The Laws of Motion"*. Borelli was the first to understand that the levers of the musculoskeletal system magnify motion rather than force, so that muscles must produce much larger forces than those resisting the motion. (Fig. 1.1).

Modern biomechanics was marked by the research of **Étienne-Jules Marey** (1830-1904) pioneer of motion analysis technology (MoCap) who invented the chrono-photographic gun (1882). The chronophotographic gun was capable of recording up to 12 consecutive frames by second (Fig. 1.2). The work of Marey was inspired in great part by the work of the photographer **Muybridge** (1830-1904) who carried out photographic investigation. Marey was also the first to correlate ground reaction forces with movements.

Nevertheless, biomechanics as an established field can be considered young. The first specialized journal, the *Journal of Biomechanics* has been published since 1968, the first international research seminar took place in 1969 and the International Society of Biomechanics (ISB) was founded in 1973.

1.1.2 Motor control

Motor control can be defined as a field that studies how the central nervous system produces purposeful and coordinated movements considering the interaction within the human body and with the environment. Two aspects of motor control have been studied separately. The first one relates to the nature of physiological variables used

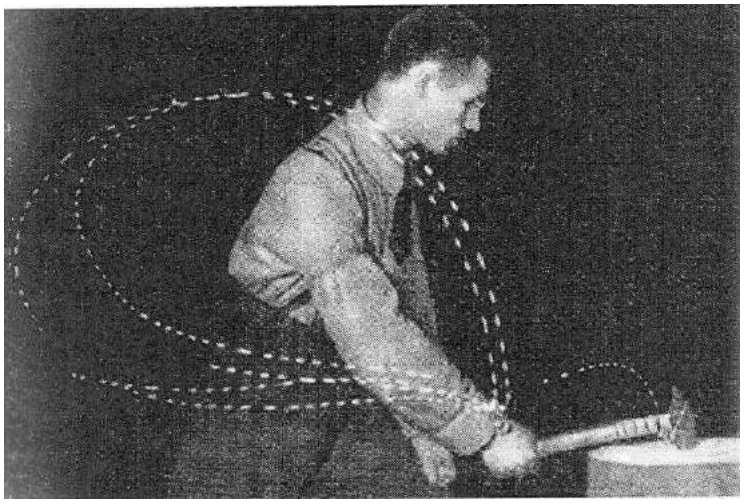

Figure 1.3: An example of variability in human movement or "repetition without repetition" [Bernstein 1967].

by the brain to control muscles. The second one relates to the "problem" of motor redundancy [Bernstein 1967]. In this thesis, we mainly focus on the second aspect.

1.1.2.1 Elements of history

Motor control can also be traced back to **Aristotle** (384-322 BC) who was the first paying attention to the concept of motion coordination by comparing coordination with harmony. He attributed both to design of creation. It was not until the famous experiments performed by **Nicolas Bernstein** (1896-1966) in the last century that motor control made a significant advance in the understanding of human motion. In one of these experiments, Nicolas Bernstein recorded blacksmiths (Fig. 1.3) who were instructed to cut metal with a chisel and a hammer. The participants were equipped with electrical bulbs placed on different body locations for recording the motion kinematics. One of the principal and most remarkable conclusion was that skilled blacksmiths performed the given task with variable joint trajectories across repetitions "repetition without repetition" while the end-effector (the hammer) was relatively invariant across repetitions. Repetition without repetition explains one of the most important characteristic observed in human motion: variability.

Motor control is also a young established field. While Nicolas Bernstein, considered as the pioneer of motor control, published his first work half a century ago, the journal of *Motor Control* exists only since 1997. The first conference "*Progress in Motor Control*" was held at about the same time and the International Society of Motor Control was established in 2001.

1.1.3 Humanoid robotics

A humanoid robot is a robot whose body shape and structure is built to resemble the human body.

1.1.3.1 Elements of history

WABOT-1 (1973) [Kato 1973], built by Waseda University in Japan, was the first humanoid robot in history. It was able to walk, recognize objects and Japanese language, to manipulate objects, and to synthesize voice. Its next version, **WABOT-2** (1980) [Sugano 1987] was capable of playing the piano and was also able of accompanying a person while listening to the person singing. Some other robots were built during the next years by Honda, but it was not until 2000 that a remarkable robot was introduced, it was named **ASIMO** [Hirose 2001]. ASIMO had an impressive design suitable for human interaction and had the ability to recognize objects, postures, gestures, its surrounding environment, sounds and faces. Japan was the pioneer in the development of humanoid robots. The Japanese National Institute of Advanced Industrial Science and Technology (AIST) together with Kawada Industries developed the *Humanoid Robotics Project*(HRP) launched in 1998 by the Ministry of Economy, Trade and Industry of Japan. This project led to the creation of different humanoid robots with outstanding capabilities such as **HRP-2** (2004) [Kaneko 2004].

The development of humanoid robots inspired the creation of the DARPA Robotics Challenge (DRC) which aimed to develop semi-autonomous ground robots that could do complex tasks in dangerous, degraded, human-engineered environments. The DRC led to the creation of new impressive robots such as **WALK-MAN** [Tsagarakis 2017] and **ATLAS** robots. So far, Atlas is considered as the world's most dynamic humanoid robot. In 2017, the Gepetto team at LAAS-CNRS in France also presented a powerful humanoid robot designed for industrial applications called **Pyrène** [Stasse 2017], the first of the TALOS series developed by PAL-Robotics company in Spain. There are many other robots which have been skipped from this short review which merits to be mentioned such as **TORO**, **REEM-C**, **COMAN**, **Shaft** and **Valkyrie** (Fig. 1.4).

1.2 Motivations

In this section, the motivations behind the realisation of this thesis are presented.

1.2.1 AnthropoMove project

This PhD thesis was possible thanks to the AnthropoMove project generated by the University of Toulouse III and the Region Midi-Pyrénées. The AnthropoMove project is an interdisciplinary project grounded on biomechanics and robotics for studying the organization of whole-body human movement, for modeling its variability, and for simulating it. The project was created after the emergence of the

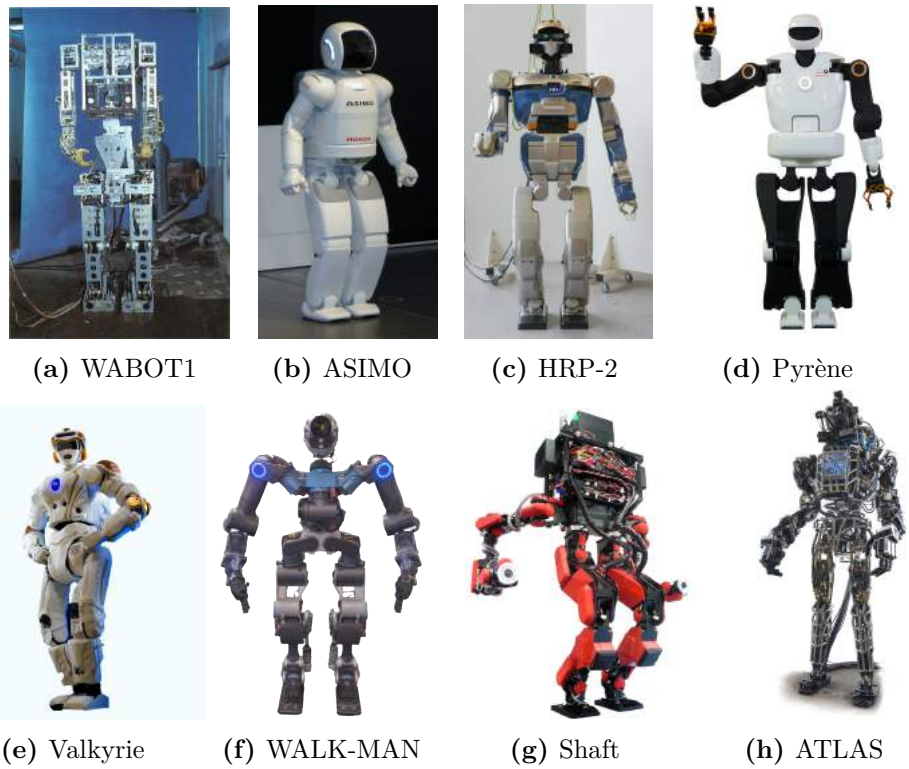

(a) WABOT1 **(b)** ASIMO **(c)** HRP-2 **(d)** Pyrène

(e) Valkyrie **(f)** WALK-MAN **(g)** Shaft **(h)** ATLAS

Figure 1.4: Examples of humanoid robots.

platform "Biomécanique et Analyse du mouvement" within the Toulouse campus. The aim of the AnthropoMove project is to better understand the criteria of motion synthesis in human movement generation and to take inspiration from human motion to improve the algorithms of motion generation in robotics. By better understanding some mechanisms of human motion generation, it could be possible to generate human-like motions with humanoid robots, virtual characters or robotic devices.

1.2.2 Why generating human-like motion?

During the 1990s, only 9% of the world's population was over the age of 60. Today, almost 15% is over 60 and this figure is predicted to increase to almost 20% by 2050 (Fig. 1.5). In Europe there are around 750 million people, from which around 100 million is elderly population and around 50 million people is estimated of having a disability. This demographic shift in world population will impose a large burden of care to treat the health risks associated with ageing. Assistive technology such as robotic solutions will help to tackle these issues and enable the elderly to regain their independence and maintain an enriching, fulfilling lifestyle [Dellon 2007].

According to the AFNOR NF EN ISO 9999 (2011), assistive robotics design are all products (including any device, equipment, instrument and software) used by or

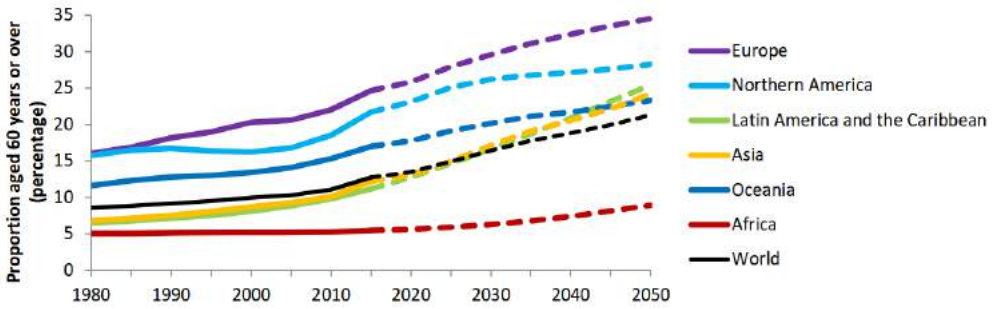

Figure 1.5: Percentage of the population aged 60 years or over, estimated for 1980-2017 and projected to 2050. Data source: *World Population Prospects: the 2017 Revision.*

for persons with disabilities. Assistive robotics are geared towards compensating for disabilities including grasping difficulties, mobility, performing domestic tasks, monitoring and comprehension. There are many types of rehabilitation robots including manipulators, orthosis, exoskeletons, prosthesis, wheel chairs, smart walker, nursing and cognitive robotics (Fig. 1.6).

(a) Re-Walk **(b)** Lokomat **(c)** Walking Assist

(d) ARMEO Spring **(e)** Nao **(f)** Robear

Figure 1.6: Examples of assistive robots.

Robots such as **Re-Walk**, **Lokomat** [Jezernik 2003] and **ARMEO Spring** are used to rehabilitate humans by teaching how to generate motions. Robots such as **Walking Assist** are used for augmenting force and facilitating human activities like carrying heavy loads. Social robots with human robot interaction capabilities such as **Nao** are being used to rehabilitate children with autism or to engage young

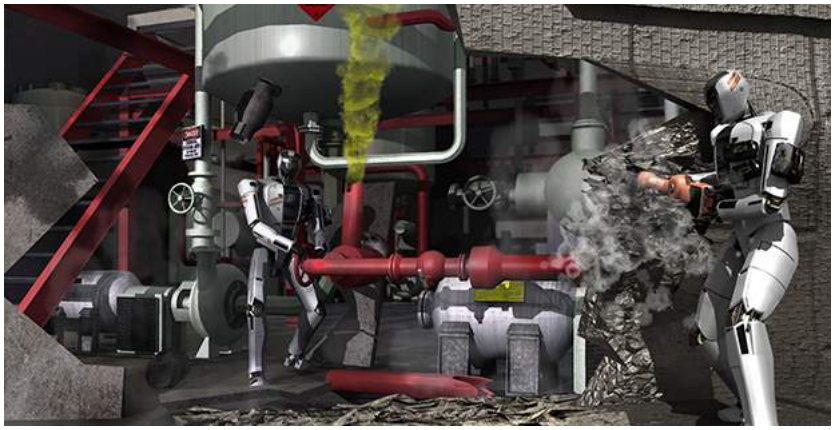

Figure 1.7: Robots for risking scenarios are developed within the DRC (DARPA Robotics Challenge).

patients for performing rehabilitation exercises. Robots such as **Robear** are being tested at home to help elderly population regain their independence. Rehabilitation robots are designed to provide force/torque ranges compatible with the human ones and to mimic as possible human kinematics. Moreover these robots aim to maximize interaction capacity and to exhibit transparency (the robot must be unnoticeable if the patient is capable of making the movement without assistance). Social robotics focus on developing robots able to collaborate with humans as their reliable partners [Breazeal 2003]. Moreover interacting with social robots has to consider body behaviours because these motions are instinctively used by humans to communicate [Asada 2009, Di Paolo 2012]. Assistive robots in human environments need to be adapted to move in places designed for human beings. Thus, it might be desirable to have robots with anthropomorphism and motion capabilities similar to humans.

Let us recall the principal motivation behind the DRC (DARPA Robotics Challenge): "*the primary goal of the DRC is to develop human-supervised ground robots capable of executing complex tasks in dangerous, degraded, human-engineered environments*"[1] (Fig. 1.7).

Sending robots to execute complex tasks in dangerous human environments might also require that robots could move in a human-like manner. Moreover, generating motions according to human motor control principles is a way to produce realistic anthropomorphic motions which are of interest in gaming and animation industries [Yamane 2003, Multon 1999, Hodgins 1998].

[1]Source: `https://www.darpa.mil/program/darpa-robotics-challenge`

1.2.3 Why is it so difficult to generate human-like motions with humanoid robots?

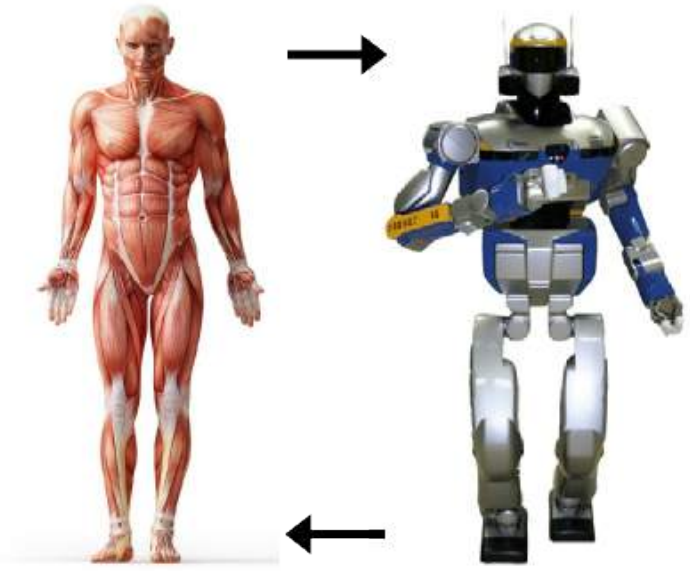

Figure 1.8: Human and HRP-2 humanoid robot. Understanding human motor control helps improving the algorithms of humanoid motion generation, while using the robotics formalism help modeling human motor control.

Since its beginnings, humanoid robotics has drawn inspiration from biomechanics. Despite the efforts made, humanoid motions are still far from human ones. One of the main reasons is without doubt, that humans and humanoid robots are very different systems whose complexity in their structure, actuation and sensing capabilities are far from being comparable.

Table 1.1: Comparative table of humans and HRP-2 humanoid robot characteristics.

	Human	**HRP-2**
Degrees of freedom	> 200	36
Muscles	> 600	–
Max torque $[N \cdot m]$	200	200
Max power $[W]$	1500	3000
Max angular velocity $[deg \cdot sec^{-1}]$	1500	300
Response time $[ms]$	100	150

Human and robot data are approximate.

As an example, let us compare the HRP-2 robot with a human (Table 1.1). There are five times more kinematic degrees of freedom in human motion as in HRP-2. This means that humans are largely more redundant systems than humanoid robots. In fact human motions are redundant not only at the joint level, but also at the level of muscles and neurons, which HRP-2 does not have. Moreover, human joints are complex and are driven by agonist and antagonist muscles while HRP-2

has simple joints that are driven by electrical motors. HRP-2 is composed of rigid bodies while humans include many soft bodies and their masses are distributed dissimilarly. Mechanical parameters such as the maximum angular velocity and power are also different (Table 1.1) which might prevent HRP-2 from executing highly dynamic motions. However, it is expected that technology advances in a near future will cope with the development of new materials and actuators for executing highly dynamic movements.

Despite their strong differences, humans and humanoid robots motion posses kinematic redundancy which refers to the ability to execute a motion in more than a unique way. How to choose one strategy among many possible ones?, the previous question is at the heart of this thesis. While in motor control we would try to answer why a participant of an experiment chooses a particular motor solution from many possible solutions, in robotics we might try to figure out which mathematical and computational approach is needed to generate a unique stable and optimal motion. Thus, this thesis presents an interdisciplinary approach for treating redundancy in humans and robots.

1.2.4 An interdisciplinary approach

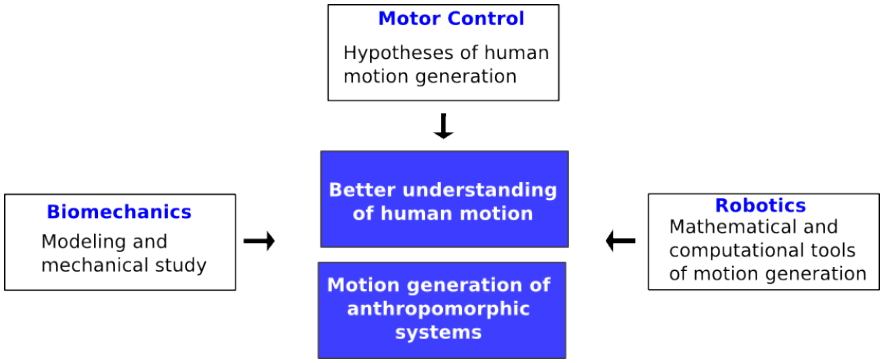

Figure 1.9: An interdisciplinary approach can provide a unified framework for better understanding human motion and for generating human-inspired motion with anthropomorphic systems such as humanoid robots, virtual characters or service robots

Biomechanics and motor control have created a powerful synergy to test hypotheses about the organization of human movement [Scholz 1999]. Biomechanics and robotics [Popović 2013] have also been used together to design human-like robots [Kim 2013] and to generate human-like motion [Khatib 2009]. Motor control and robotics [Burdet 2013] have lead to brain-inspired algorithms, computational models of biological neural networks and actual biological systems. In this manuscript we develop an interdisciplinary approach to treat redundancy in humans and humanoid robots. Our aim is to provide a unified framework for better understanding human motion, and for generating human-inspired motion. This synergy is represented in Fig. 1.9.

1.2.5 On highly dynamic motions

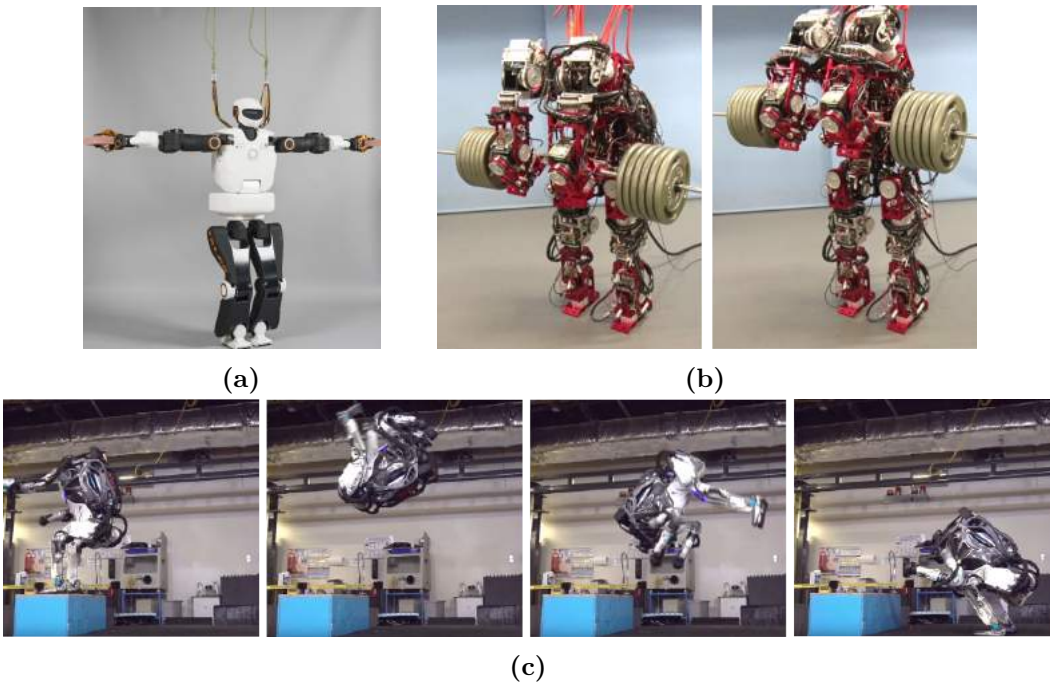

(a) (b)

(c)

Figure 1.10: In (**a**) Pyrène robot holding two bricks with the grippers. In (**b**) a humanoid robot presented by Waseda University and Mitsubushi Heavy Industries at IROS 2017 (2017 IEEE/RSJ International Conference on Intelligent Robots and Systems). In (**c**) snapshots of a recent video of Atlas robot performing a highly dynamic jump and landing.

Humanoid robotics is growing fast towards agile, robust, and powerful robots able to interact with their environment in which humans might be present [Stasse 2017]. To control these robots, motion generation algorithms are required to increase the robot stability, robustness, and efficiency. New generations of humanoid robots such as Pyrène or Atlas (Fig. 1.10) have powerful motor capabilities. Highly dynamic motor capabilities are necessary to perform reactive motions and maintain balance. In this thesis we propose to develop an interdisciplinary approach to investigate the question of highly dynamic motion generation. The case study of parkour motions was selected and used throughout the manuscript. Parkour movements are fascinating as they are highly dynamic and complex. Moreover, in the scientific literature there is a lack of understanding of these motions and several hypotheses could be formulated about their generation.

1.2.6 Parkour, the art of displacement

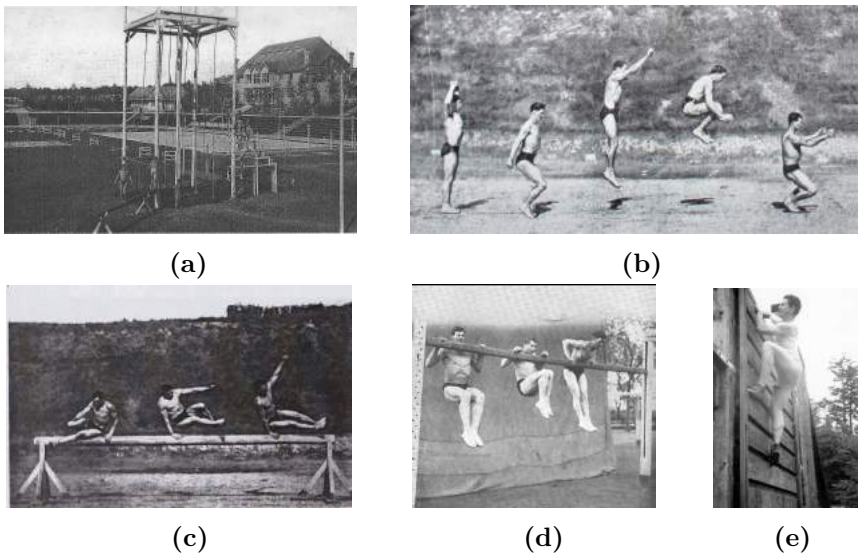

(a) (b) (c) (d) (e)

Figure 1.11: In (**a**), a training center in Reims, France, in 1913. The center was designated according to the principles of Georges Hébert. In (**b**)(**c**)(**d**)(**e**), examples of the natural method applied to jump and landing movements, to vaulting motions, to muscle-up technique and to climbing technique respectively.

Parkour is a lifestyle sport derived from the military method "methode naturelle" proposed by Georges Hébert before World War I. Georges Hébert was a French marine who taught physical education to marines (Fig. 1.11). The development of the method was inspired by Georges' observation of natural skilled movements performed by indigenous tribes in Africa. Later on, Raymond Belle, a French military utilized the method to improve his skills and introduced the term "le parcours" to describe his training. Training techniques included a combination of walking, running, jumping, landing, vaulting, balancing and quadrupedal techniques. His son, David Belle, developed further the methods and provided them its actual name of "parkour" in collaboration with Hubert Koundé.

The philosophy behind parkour is to create an harmony between mind and body, where practitioners can express themselves through the movement they perform "Overcoming and adapting to mental and emotional obstacles as well as physical barriers" [2]. In terms of sports, parkour can be considered as a lifestyle discipline in which practitioners – called "traceurs" – have to overcome obstacles in the environment in the most efficient manner and where movements look risky, highly dynamic and complex [Cazenave 2008, Gilchrist 2011, Kidder 2012]. Moreover, parkour motions are commonly performed in urban spaces on hard surfaces and from uncontrolled drop heights Fig. 1.12.

[2]Belle, Châu; Belle, Williams; Hnautra, Yann and Daniels, Mark (director). Generation Yamakasi (TV-Documentary in French). France: France 2.

Figure 1.12: Parkour motions performed in urban spaces. The photo corresponds to a parkour expert who was part of this study.

1.3 Thesis Organization

Following this introductory chapter, we introduce in **Chapter 2** the mathematical and computational background needed to study human movement in the context of biomechanics. Only notions which are linked to the development of the manuscript, are taken into account. Then, we present a epidemiology study of parkour practice in France. Afterwards, the biomechanics of key parkour techniques are presented. For this a whole-body musculoskeletal model is built and described. Performance variables that are representative of the studied parkour techniques are identified and a mechanical mean behavior of parkour practitioners executing each of the techniques is extracted. **Chapter 3** introduces the main concepts of motor control used in this thesis. Then, the mathematical framework of the uncontrolled manifold theory (UCM) in human motor control and the task function approach used in robotics are detailed. After, an extension of the UCM theory to the case of dynamic motions is presented. At the end of the chapter, this extension is applied to a case study of the parkour take-off and landing motions. **Chapter 4** recalls the motion generation tools of robotics based on the task-space formalism. Then, based on the performance variables identified in the biomechanics (Chapter 2) and motor control (Chapter 3) studies, and the presented whole-body model presented in Chapter 2, the robotics framework of motion generation is used to generate whole-body parkour motions. At the end, we discuss how our interdisciplinary approach based on biomechanics, motor control and robotics can be utilized to generate and also to understand human movement.

1.4 Contributions

1.4.1 Journal articles

- G. Maldonado, P. Souères and B. Watier (2017). Strategies of parkour practitioners for executing soft precision landings. Under review at Journal of Sports Sciences.
- G. Maldonado, P. Souères and B. Watier (2017). From Biomechanics to Robotics. In Press, *Springer Tracts in Advanced Robotics (STAR), "Biomechanics of Anthropomorphic Systems"*.
- G. Maldonado, F. Bailly, B. Watier and P. Souères (2017). Extending the Uncontrolled Manifold theory to dynamic movements: application to take-off and landing motions in parkour. Submitted to PLOS Computational Biology.

1.4.2 Conference articles

- G. Maldonado, H. Bitard, B. Watier and P. Souères (2015). Evidence of dynamic postural control performance in parkour landing (2015). *Computer Methods in Biomechanics and Biomedical Engineering, 18*(1), 1994–1995.
- G. Maldonado, P. Souères and B. Watier (2016). Optimal criteria of parkour landings. European Society of Biomechanics (ESB - Lyon).
- G. Maldonado, P. Souères and B. Watier (2017). A First Step in Identifying Motor Tasks in Highly Dynamic Motions. European Society of Biomechanics (ESB - Seville).
- G. Maldonado, F. Bailly, B. Watier and P Souères (2017). Souères. Angular momentum regulation strategies for highly dynamic landing in Parkour. In Press, *Computer Methods in Biomechanics and Biomedical Engineering.*

Chapter 2

Biomechanics of Parkour

"The art of displacement"

Contents

The main goals of this chapter are to present the biomechanics of key parkour techniques, to build a skeletal model for analyzing and generating parkour motion, to identify performance variables that are representative of the studied parkour techniques and to obtain a mechanical mean behavior of parkour practitioners executing each of the techniques. The identified performance variables and the quantified mean behavior are not presented in the chapter but will be used in Chapter 3 for generating human inspired motion.

This chapter is organized in the following manner:

- First, we introduce the notions and the mathematical background needed to study human movements in the context of biomechanics. The presented biomechancis methods are used for recording, processing and analyzing human motion.
- Secondly, an epidemiology study of parkour in France is presented. The epidemiological study allows for identifying a set of parkour motions that are interesting from a biomechanics and injury prevention perspective. It also contributes to understanding parkour practice in France.
- Afterwards, a whole-body musculoskeletal model appropriate for studying parkour motion is created based on existing models in the literature. The created model allows for analyzing (this chapter and Chapter 3) and generating (Chapter 4) parkour motions.
- Then, the biomechanics of key parkour techniques identified in the epidemiological analysis is presented in two studies.
- At the end of this chapter, we make a general conclusion of the presented research and the ongoing work.

2.1 Biomechanics of Human Motion

Biomechanics aims at applying the physical laws of mechanics to study human motion in order to provide a better understanding of the mechanical strategy used by the central nervous system (CNS) to coordinate the motion [Winter 2009, Zatsiorsky 2002]. In fact, biomechanics provides the basis for testing hypothesis about how the brain coordinates a given movement and most

of motor control theories of human motion are based on biomechanical studies (e.g. [Feldman 1995, Scholz 1999, Todorov 2002]). Biomechanic information can also be used to generate human-inspired motions with humanoid robots [Duffy 2003, Dasgupta 1999] or anthropomorphic systems such as animation avatars [Sok 2007, Yamane 2010]. In this section we make a summary of the mathematical and computational background needed to study the biomechanics of human motion.

2.1.1 Motion capture

Motion capture "MoCap" is a technology that allows to record motion online. In biomechanics, it is used to record the movements of humans and animals for quantitative analyses. The motion is tracked using cameras that record the 2D positions of markers placed on the body. When more than one camera is available, the 3D marker coordinates can be computed by the MoCap system. Two types of markers can be used depending on the motion capture system: active and passive markers. Active systems use infra-red light-emitting diodes placed on markers that are activated in a predefined sequence by a control unit to correctly identify markers. Passive systems use markers covered by a reflective tape which are lighted by infrared cameras to reconstruct the markers position. Coordinate data are calculated by the system with respect to a laboratory fixed reference frame. Data are then processed to obtain kinematic variables describing segment or joint movements.

A motion capture system might also synchronize analog data such as reaction forces, or muscular activity. External forces are those caused by the human interacting with the environment. Common sensors are force platforms which measure net ground reaction forces (GRFs) under the feet. Recording external forces allow to perform kinetics analysis of human motion and to compute other variables such as internal joint torques and forces, joint power or joint mechanical energy [Winter 2009]. The forces produced by the muscles and transmitted through tendons, ligaments, and bones can be measured directly with indwelling force sensors, or estimated by modeling the musculoskeletal system [Delp 2007]. Moreover, the activation patterns of the muscles can be measured through electromyography (EMG) sensors. Typically, these sensors are placed over the skin of the human body using surface EMGs [Hermens 2000].

2.1.1.1 Data collection and reporting

In order to communicate motion data, an experimental protocol must be carefully designed and followed. The recording protocol should take into account recommendations for reporting biomechanic data based on international standards. For example, kinematic data are collected and reported based on recommendations from the International Society of Biomechanics (ISB) [Wu 2002, Wu 2005], and surface muscular activity is recorded and communicated based on the recommendations from the European project of Surface ElectroMyoGraphy for the Non-Invasive Assessment of Muscles (SENIAM).

2.1.2 Motion reconstruction

Recorded motion data has to be reconstructed and processed. Data reconstruction consists in labelling marker trajectories recorded by the MoCap system, interpolating trajectory gaps, and removing noise from the signals.

2.1.2.1 Labelling and interpolating

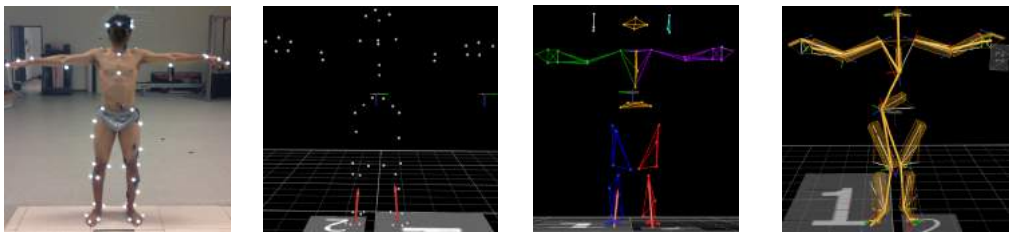

(a) **(b)** **(c)** **(d)**

Figure 2.1: In (**a**), a human with passive markers on his body during a static trial recording. In (**b**), Vicon Nexus reconstruction of the static trial. In (**c**) the labelling of markers for each body segment. In (**d**), the linkage of the kinematic chain for reconstructing motion trials using this model.

2.1.2.2 Filtering

Filtering consists in removing the noise from the recorded signals. The noise normally appears in higher frequencies than the signals and might arise from different sources as: soft-tissue artifacts (STA), sensors, or white noise. STA is referred to the movement of the markers placed on the skin with respect to the underlying bones due to skin deformations. These deformations depend on the body characteristics, on the location of the markers on the body and the nature of the motion. Particularly, STA affects the estimation of joint kinematics [Dumas 2014, Bonci 2014, Camomilla 2015].

For filtering raw data coming from cameras (marker positions) and force platforms (GRFs), a 4th order low-pass Butterworth digital filter applied in a zero-phase can be implemented at the same cut-off frequency to avoid inconsistencies with inverse dynamics computations [Kristianslund 2012, Mccaw 2013]. To select the optimal cut-off frequency f_c at which a signal is filtered, two types of analyses are commonly performed: power spectral analysis and/or residual analysis [Winter 2009].

Power spectral analysis Power spectral analysis is a technique in which the power of the recorded signals can be studied in the frequency domain. Frequency analysis is done based on a spectral density plot which displays the power of each frequency component against frequency. Power spectral density can be estimated using the Fast Fourier Transform (FFT). Based on this evaluation, a decision can be

made to determine how much to accept or reject from the raw signals. Commonly, f_c is chosen as the frequency that contains more than 95% of the signal power.

Residual analysis The residual analysis [Winter 2009] allows to evaluate noise by comparing the difference between the unfiltered signals and signals filtered at different cut-off frequencies. Let N_f be the number of i sampled frames in a signal, the residual ε at a given cut-off frequency f_c is calculated as follows:

$$\varepsilon(f_c) = \frac{1}{N_f} \sum_{i=1}^{N_f} \left(s_i - \hat{s_i}(f_c)\right)^2, \tag{2.1}$$

where s_i is the raw signal, $\hat{s_i}$ is the filtered signal with cut-off frequency f_c. Eq. (2.1) is calculated recursively for a set of given cut-off frequencies that is arbitrary but should be chosen so that the frequencies of the signal can be represented. Residuals are later displayed as function of these cut-off frequencies to evaluate the noise and to select the cut-off frequency. Criteria to chose the cut-off frequency based on residual analysis can be found in [Winter 2009].

2.1.2.3 Center of rotation and axes of rotation

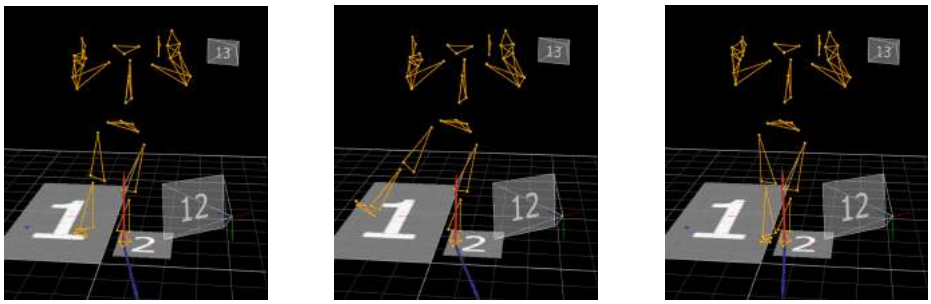

Figure 2.2: Vicon Nexus reconstruction of a trial that allows the computation of the hip center of rotation.

After data have been filtered, joint center of rotations can be estimated from markers. Three methods can be used to this end: virtual models (e.g. in OpenSim software [Delp 2007]), regression tables (e.g [Dumas 2007b]) and/or functional methods (e.g. [Ehrig 2005]). In general, the center of rotation of ball-modeled joints such as the shoulder and hip are computed using functional methods (2.2). The SCoRe method provides a good estimation [Ehrig 2005] and can be computed as:

$$\min_{\boldsymbol{c1},\ \boldsymbol{c2}} \quad \sum_{i=1}^{N_f} \left\| R_{1_i}\boldsymbol{c}_1 + \boldsymbol{t}_{1_i} - (R_{2_i}\boldsymbol{c}_2 + \boldsymbol{t}_{2_i}) \right\|^2, \tag{2.2}$$

where $\boldsymbol{c_1} \in \mathbb{R}^3$ and $\boldsymbol{c_2} \in \mathbb{R}^3$ are the centers of rotation in the body segment coordinate system, $(R_{1_i}, \boldsymbol{t}_{1_i})$ and $(R_{2_i}, \boldsymbol{t}_{2_i})$ are the transformation matrices of body 1

and body 2 respectively from segment (local) to world (global) coordinates. The solution to this minimization problem provides two trajectories c_1 and c_2 for the same joint and thus the mean value of both can be used as an estimate. Functional methods can also be used to determine the optimal axes of joints rotations (e.g. for calculating the knee axes [Ehrig 2007]). Other joint centres can be computed based on regression tables.

2.1.3 Scaling of human anthropometry

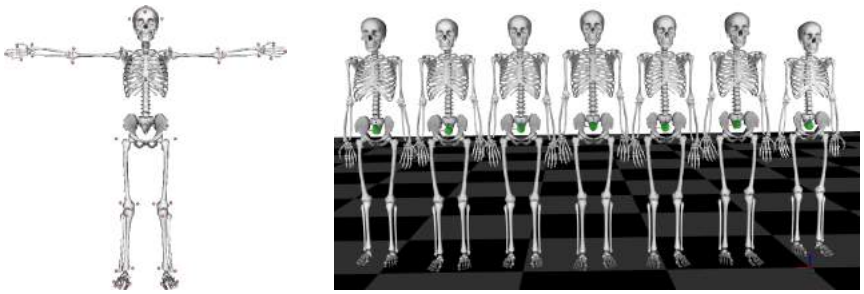

(a) **(b)**

Figure 2.3: In (**a**), a virtual skeleton model created based on OpenSim models which can be used for scaling human anthropometry. In (**b**), 7 participants which were scaled with the virtual skeletal model.

The human body is composed of hundreds of muscles and bones. In order to calculate the kinematics and the dynamics, a physical model representing the skeletal or musculosketal system is needed. The model is simplified by the assumption that the human body can be described by a collection of rigid bodies (segments) representing bones or a combination of them (for example when modeling the torso or the foot segments). In spite of this simplification, this model is usually called skeletal model and we will use the same convention in this manuscript. In the case of muscle studies, a more complex model of the system is needed: a musculoskeletal model.

The scaling of anthropometry allows for the estimation of segment properties of the human body (modeled as rigid segments) such as segment lengths, inertia matrices, and center of mass positions. To estimate human anthropometry, cadaver studies [Dumas 2007b], mathematical modeling [Havana 1964], scanning and imaging techniques [Zatsiorsky 1983, Durkin 2002], kinematic measurements [Hatze 1975], or motion capture and kinetic measurements [Venture 2008], can be used. Commonly, experimental marker data from a static trial is used to scale the anthropometry of the recorded participant using the regression equations provided by cadaver studies or by fitting these data to a virtual skeletal model (Fig. 2.3). Further details about the virtual musculoskeletal model are given in Section 2.1.3.1 whereas the data fitting technique is presented later in Subsection 2.1.4.

2.1.3.1 Human musculoskeletal models

A skeletal model is an effective tool for visualizing and analyzing human motion. When building a virtual 3D-model, the following information has to be considered:

- **The model** contains the description of the kinematic chain including joint types and joint ranges of motion.
- **The segment data** gives the specification of the physical characteristics of the body segments such as the masses, the inertia matrices, and the position of the centers of mass of each segment.
- **The virtual markers** contain the positions of the markers placed on the model according to the experimental protocol. Markers are normally placed in accordance with the International Society of Biomechanics (ISB) standards with a minimum of 3 virtual markers per segment for a 3D analysis [Wu 2002, Wu 2005].
- **The visual** elements are the 3D meshes that will be displayed, which can be created using 3D software. This data is useful for visualization purposes but cannot replace biomechanics computations.
- **The muscle set:** contains the information of the muscles used in the model such as the lever arm, the maximum isometric force that the fibers can generate, the optimal length of the muscle fibers, the resting length of the tendon, the angle between tendon and fibers at optimal fiber length, the time constant for ramping up and down muscle activation, the tendon strain at maximum isometric force, the passive muscle strain at maximum isometric force and the maximum normalized lengthening force.

2.1.4 Inverse kinematics of human motion

The inverse kinematics of the human motion consists in converting experimental marker positions into joint angles by minimizing errors of the reconstructed motion and soft tissue artifact "STA". STA corresponds to the relative motion of soft tissues with regard to the underlying bone. Two classes of methods are commonly used in the literature to calculate 3D angles: segment optimization methods [Chèze 1995] and global optimization methods [Lu 1999]. In segment optimization methods, a frame is attached to each segment according to the ISB recommendations. The axes of the reference frames are also created based on the ISB which allows the communication of kinematic data. Angles are then calculated from Euler angle sequences by computing the optimal bone pose from a marker cluster. Global optimization methods, usually referred to as "Inverse Kinematics", can also be used to calculate joint angles and constitute a promising methodology [Duprey 2010]. Using global optimization it is possible to add physically realistic joint constraints while taking into account the whole kinematic chain structure and joint ranges of motion. Let n be the total number of DoF of the skeletal system and m the number

of recorded markers. The inverse kinematics problem can be addressed through the following optimisation:

$$\begin{aligned} \min_{\boldsymbol{q}} \quad & \sum_{i=1}^{N_m} w_i \left\| \boldsymbol{x}_i^{exp} - \boldsymbol{x}_i(\boldsymbol{q}) \right\|^2 \\ \text{s.t.} \quad & \underline{\boldsymbol{q}} \leq \boldsymbol{q} \leq \overline{\boldsymbol{q}}, \end{aligned} \tag{2.3}$$

where N_m is the total number of markers, $\boldsymbol{q}$ are the generalized coordinates, $\underline{\boldsymbol{q}}$ and $\overline{\boldsymbol{q}}$ are minimum and maximum ranges of motion of the joint coordinates $\boldsymbol{q}$, $\boldsymbol{x}_i^{exp}$ is the experimental marker position of the i^{th} marker, $\boldsymbol{x}(\boldsymbol{q})$ is the corresponding virtual model marker position, and w_i is the marker weight, which specifies how strongly the marker error should be minimized.

2.1.4.1 Center of mass

By knowing the anthropometry and the configuration of the body, its center of mass position (CoM) can be computed. Denoting by n_s the number of segments of the system, m_{s_i} the mass of the i^{th} segment and $\boldsymbol{c}_i \in \mathbb{R}^3$ its CoM position, the whole-body CoM position $\boldsymbol{c} \in \mathbb{R}^3$ can be computed as follows:

$$\boldsymbol{c} = \frac{\sum_{i=1}^{n_s} m_{s_i} \boldsymbol{c}_i}{\sum_{i=1}^{n_s} m_{s_i}}. \tag{2.4}$$

2.1.5 Kinetics of human motion

The kinetic study of the human motion consists in determining the external forces acting on the body and internal forces "or stress" whiting the body that might be the consequence of external forces application. External forces include gravity force and any reaction force produced through contact with the environment. Internal forces are produced by ligaments, muscles and joint articular surfaces.

2.1.5.1 Center of pressure

By knowing the reaction forces, the center of pressure (CoP) can be calculated. Center of pressure analysis is used to study mechanical stability in human motion. The CoP can be interpreted as the neuromuscular response to the imbalances of the body's CoM. The CoP is also used to compute inverse dynamics. Typically GRFs measurements obtained through force platforms are used. GRFs measurements provide the net force vector $\boldsymbol{f}_{grf} = [f_x \;\; f_y \;\; f_z]^T$ and the net moment vector containing the components about the principal axes of the force platform $\boldsymbol{\eta}_{grf} = [n_x \;\; n_y \;\; n_z]^T$. The components of the CoP position $\boldsymbol{cp} \in \mathbb{R}^2$ can be computed as follows:

$$cp_x = \frac{f_x d_z - n_y}{f_z}, \quad cp_y = \frac{f_y d_z + n_x}{f_z}, \tag{2.5}$$

where d_z is the distance from the platform origin to the top surface. These equations apply to force platforms instrumented with one central pillar that supports an upper flat plate such as Amti force plates (AMTI, Watertown, MA, USA).

2.1.6 Inverse dynamics of human motion

Inverse dynamics consists in calculating internal forces and torques at the joints that generate a given motion. To this end, the body model described before (skeletal model), the movement kinematics and the measured external forces produced in case of contact with the environment are used. Three formalisms are available to compute inverse dynamics: Hamiltonian, Euler-Lagrange and Newton-Euler. In particular, the Newton-Euler formulation expresses dynamic equations for each link and performs calculations recursively by propagating reaction forces and applying Newton third law of motion (principle of action and reaction). Euler's first and second equations of motion form the so called Newton-Euler equations. The first equation states that the sum of external forces equals the variation of the linear momentum:

$$\sum \boldsymbol{f}_{ext} = \frac{d}{dt}(m\boldsymbol{v}_c) = m\boldsymbol{a}_c, \tag{2.6}$$

The second equation states that the sum of external torques equals the variation of the angular momentum at the center of mass:

$$\sum \boldsymbol{\eta}_{c,ext} = \frac{d}{dt}(I\boldsymbol{\omega}) = I\dot{\boldsymbol{\omega}} + \boldsymbol{\omega} \times I\boldsymbol{\omega}, \tag{2.7}$$

Eq. (2.6) and Eq. (2.7) are commonly propagated at each joint using a bottom-up approach. This method can be computed numerically though the application of the recursive formulation of the Newton-Euler equations [Kuo 1998]. Four inverse dynamics methods have been proposed in the literature based on vectors and Euler angles, wrenches and quaternions, homogeneous matrices, or generalized coordinates and forces [Dumas 2007a].

2.1.7 Energetics of human motion

Energetics in human motion can be analyzed by means of mechanical power and work. By making the assumption that the human body can be modeled as a poly-articulated system composed of rigid body segments, and by assuming that joints are frictionless, net internal forces and torques at the joints computed though inverse dynamics can be used to compute joint power and joint mechanical work [Zatsiorsky 2002].

The mechanical power $\boldsymbol{P}_{mec}$ (joint mechanical power and work will be expressed in upper-case for avoiding confusion with the notations of linear momentum and angular velocity respectively) of the i^{th} joint is calculated as follows:

$$\boldsymbol{P}_{mec,i} = \boldsymbol{\eta}_i \times \boldsymbol{\omega}_i = \boldsymbol{\eta}_i \times (\boldsymbol{\omega}_d - \boldsymbol{\omega}_p), \tag{2.8}$$

where η_i is the net joint torque of the i^{th} joint, $\boldsymbol{\omega}_p$ is the angular velocity of the proximal segment and $\boldsymbol{\omega}_d$ is the angular velocity of the distal segment. Thus, $\boldsymbol{\omega}_i$ represents the relative angular velocity of the i^{th} joint. Joint mechanical work $W_{mec,i}$ can be then calculated as the time integral of the joint power:

$$W_{mec,i} = \int_{t1}^{t2} \boldsymbol{P}_{mec,i}\ dt. \tag{2.9}$$

Note that joint work is positive when joint torque and joint angular velocity are in the same direction, otherwise it is negative.

2.1.7.1 Mechanical energy expenditure

Because work is computed by means of positive and negative joint power, its summation in a poly-articulated system might be close to zero if muscles produced work and dissipated energy. A more practical measure of the mechanical energy expenditure (*MEE*) was proposed in [Aleshinsky 1986b, Aleshinsky 1986a]. The *MEE* is calculated as the time integral of the sum of individual absolute joint powers:

$$MEE = \int_{t1}^{t2} \sum_i |\boldsymbol{P}_{mec,i,+}|\ dt + \int_{t1}^{t2} \sum_i |\boldsymbol{P}_{mec,i,-}|\ dt. \tag{2.10}$$

The first part of the equation represents the work for accelerating the body segment while the second part of the equation represents the work that decelerates the body segment [Zatsiorsky 2002]. *MEE* is a "worklike" measure used to determine the amount of energy expended for motion.

2.1.8 Linear and angular momenta of human motion

The linear momentum of a poly-articulated system, such as the human body, is obtained as follows:

$$\boldsymbol{p} = m_b \boldsymbol{v_c}, \tag{2.11}$$

where m_b is the total mass of the poly-articulated system and $\dot{\mathbf{c}}$ is the center of mass velocity. Let S be the number of body segments, the whole-body angular momentum expressed at its center of mass position $\mathbf{c}$ is calculated as follows:

$$\boldsymbol{\mathcal{L}}_c = \sum_{s=1}^{S} \left[(\boldsymbol{c}_s - \boldsymbol{c}) \times m_s \boldsymbol{v}_s + I_s \boldsymbol{\omega}_s \right], \tag{2.12}$$

where $\boldsymbol{c_s}$ is the center of mass position of the s^{th} segment, m_s is the mass of the s^{th} segment, $\boldsymbol{v_s}$ is the segment linear velocity, I_s is the inertia around the segment center of mass and $\boldsymbol{\omega_s}$ is the segment angular velocity around the segment center of mass. Similarly the linear and angular (expressed at the center of mass position) momenta derivative can be calculated as the time derivative of Eq. (2.11) and Eq. (2.12) respectively.

2.2 Epidemiology of Parkour in France

This section presents a descriptive epidemiological study of parkour practice in France. This study was done in collaboration with the French parkour association LFREP (Laboratoire Français de Recherches et d'Etudes sur le Parkour). It identifies potential risk factors associated to parkour practice in the context of injury prevention. Moreover, the study will contribute to determine a set of key parkour techniques for further biomechanical analysis in the next sections.

2.2.1 Introduction

Before starting the epidemiology study, let us briefly introduce the main parkour techniques. Parkour movements contain a base of techniques that are combined together for adapting to a particular situation or environment. Parkour techniques include principally jump/landing, climbing, swinging, vaulting, running and quadrupedal movement techniques. In this subsection, jump/landing, vaulting, arm jump and climbing techniques are presented. Based on this introduction, we will present the epidemiological study in the next subsections.

2.2.1.1 Parkour jumping and landing techniques

Parkour jump and landing techniques are the foundation of most of the Pakour movements. They aim at providing practitioners with the necessary strategies to execute precise and safe motions. The principal techniques are presented below:

Precision technique The precision jump/landing technique is used for relative small drops. It requires practitioners to jump and land with precision on the forefoot without heel contact with the ground, to bend their lower limbs without any varus-valgus motion of the knees and to use their arms to counterbalance the movement and stabilize themselves (Fig. 2.4).

(a) **(b)**

Figure 2.4: Parkour precision jump (**a**) and landing (**b**) techniques performed in a urban space. The photos were taken at Toulouse (France) with a parkour expert who was part of the current study.

Roll technique The roll landing technique is used when landing from greater heights. It consists in landing over the forefoot without heel contact with the ground and putting both feet almost parallel, then pushing-off from the ground and rolling in the direction of the movement placing both hands on the ground and rotating the body from one shoulder to the opposite hip across the back along a diagonal (Fig. 2.5). It might be compared to the judo fall technique of forward roll (known as Zenpo Kaiten). However, it differs from it in the feet and hands placement.

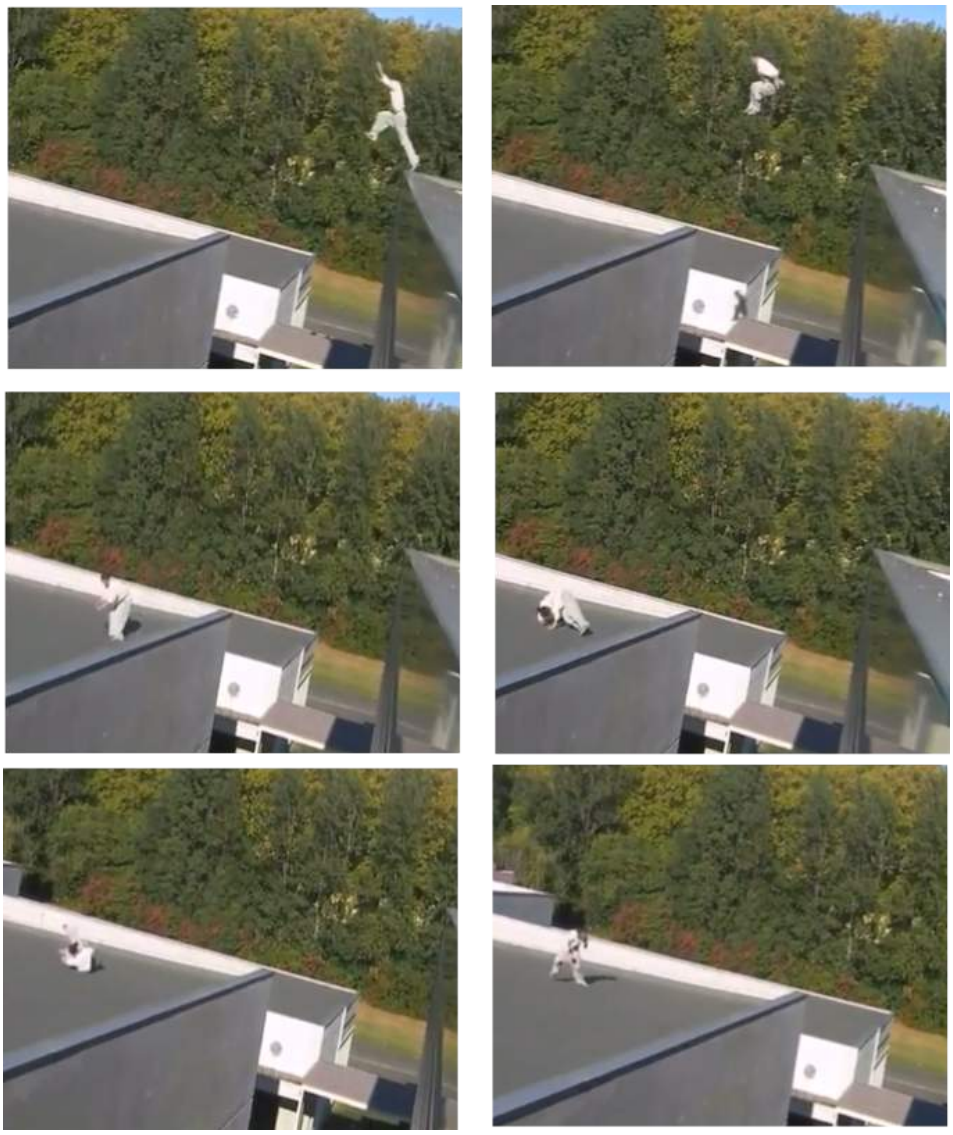

Figure 2.5: Parkour roll landing technique performed in a urban space. The photos were taken at Toulouse (France) with a parkour expert who was part of the current study.

2.2.1.2 Parkour vaulting techniques

Parkour vaulting techniques are used to overcome obstacles of the environment quickly and efficiently.

(a) **(b)**

Figure 2.6: Safety vault (**a**) and Kong vault (**b**) techniques performed in urban spaces. The safety vault technique is one of the simplest and often the first technique to be learned in parkour vaultings. The kong vault is a more complex technique which goal is to gain power and distance.

2.2.1.3 Parkour arm jump technique

The arm jump is a technique that is used when the distance/height between the take-off location and the intended destination is too far to simply jump onto with the feet. The technique can be performed from a running or standing configuration. The principal goal is to land safely on walls. The technique is normally followed by parkour landing or climbing techniques.

Figure 2.7: Parkour arm jump technique performed in a urban space.

2.2.1.4 Parkour climbing techniques

Climbing techniques in parkour are used by traceurs to move vertically (both up and down). For example to muscle-up on the top of a wall. These techniques require high conditioning of the upper body and whole-body coordination. The conditioning for executing parkour climbings is to perform closed-chain bodyweight techniques. The most used ones are pull-up and muscle-up.

Figure 2.8: Parkour climbing technique performed in a urban space. The photos were taken at Toulouse (France) and corresponds to a parkour expert who was part of the current study.

2.2.2 Sate of the art

Parkour might be considered a risky discipline because of the nature of the movements which are highly dynamic and complex, and the changing environment which includes irregular and hard surfaces. [Cazenave 2008] suggested that traceurs adopt a risk-taking bahavior that contributes to a positive regulation of their self-esteem. An injury rate of 61.5%, considering the % of traceurs that suffered a musculoskeletal injury while practicing parkour in the last six months, has been reported in the literature [Da Rocha 2014]. In the same study, 41% of these injuries prevented traceurs from training for more than four weeks. Moreover, it was reported that lower-limbs accounted for more than half of the injuries due to parkour practice

(57.1%). The authors also suggested that age and practice time might be linked to injury, that adults might have greater caution in conducting this type of activity and that training should not be longer than three hours.

In this study, we propose to extend this epidemiological study and to contribute to the understanding of parkour practice in France. This study will also serve for identifying key parkour techniques which might be of interest from biomechanical and injury prevention perspectives. Our contribution in this work was to translate, process and analyze a database containing information related to parkour practice in France. This is explained in the sequel.

2.2.3 Methods

Data from a survey of 85 parkour male practitioners that was collected and processed in France. The questionnaire was designed by the members of the French parkour association LFREP. The type of questions and how the data was processed is explained in the following items:

- The expertise in parkour. In our study, parkour experts were considered to be practitioners with more than 5 years of parkour practice.
- The type of injury suffered from parkour practice. The injury type was later classified into 4 categories by a rehabilitation doctor as follows: ligament, musculotendinous disorder, fracture and wounds.
- The injury severity level. In this study, injury severity was graded from 1 (low severity) to 3 (high severity) depending of traceurs feeling of severity.
- Whether traceurs belonged or not to a parkour association. One of the main goals of parkour associations is to train traceurs. So this information might be linked to performance and injury prevention.
- The technique used when getting injured. The technique was later classified into 5 categories: landing, vaulting, climbing, arm jump and others. Others includes mostly free-running techniques, tictac parkour technique and injuries suffered during conditioning.

2.2.4 Results

Ligament was the most suffered injury accounting for the 53% of cases (Fig. 2.9a). Across techniques, landing (41%) was the most prone to induce injuries (Fig. 2.9b). Ligament was the most frequent injury independently of expertise or technique (Fig. 2.10a and Fig. 2.10b). Musculotendinous disorder was the second most suffered injury in climbing (33%)(Fig. 2.10b). In landing and vaulting techniques, musculotendinous disorder, fracture and wound were similarly suffered (Fig. 2.10b). In arm jump, there was an important prevalence of ligament injuries (76%) (Fig. 2.10b). The injury with highest severity score was fracture (60% of the total injuries

(a) **(b)**

Figure 2.9: The most frequent injuries **(a)**, and the most used techniques when getting injured **(b)**. Most of the traceurs suffered from a ligament injury and most of the injuries where suffered when performing parkour landing techniques.

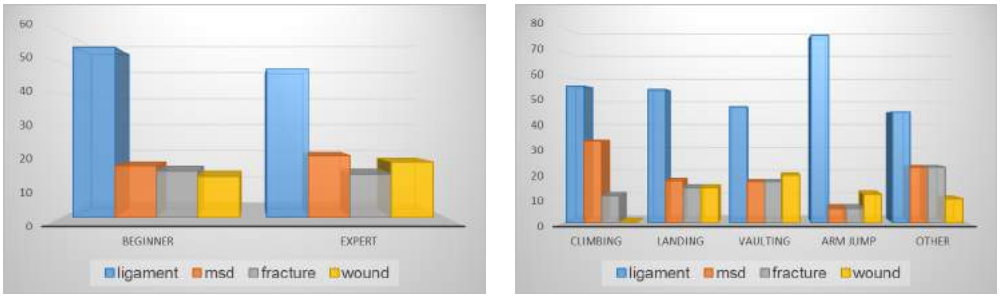

(a) **(b)**

Figure 2.10: Percentage of injury type according to parkour expertise **(a)** and technique **(b)**. Ligament was the most suffered injury independently of the expertise or technique used.

with score equal to 3) while the other injury types reported a low severity score (Fig. 2.11a). Severity score was low in all techniques (Fig. 2.11b) and increased with expertise (In Fig. 2.11c low severity decreased while high severity increased). Finally, the data also shown that 75 % of traceurs belonged to a parkour association and only 25% of traceurs had more than 5 years of parkour practice.

2.2.5 Discussion

Ligament injury is the most common

Although the severity level of ligament injuries was low, the frequency of ligament injuries appear to be high across parkour techniques. Particularly, it seems that ligament injuries are very frequent in the arm jump technique (76%). This result is not surprising if we consider that in sports like gymnastics, were athletes perform highly dynamic motions such as in parkour, the ankle and wrist are commonly prone to ligament injuries [Caine 2005].

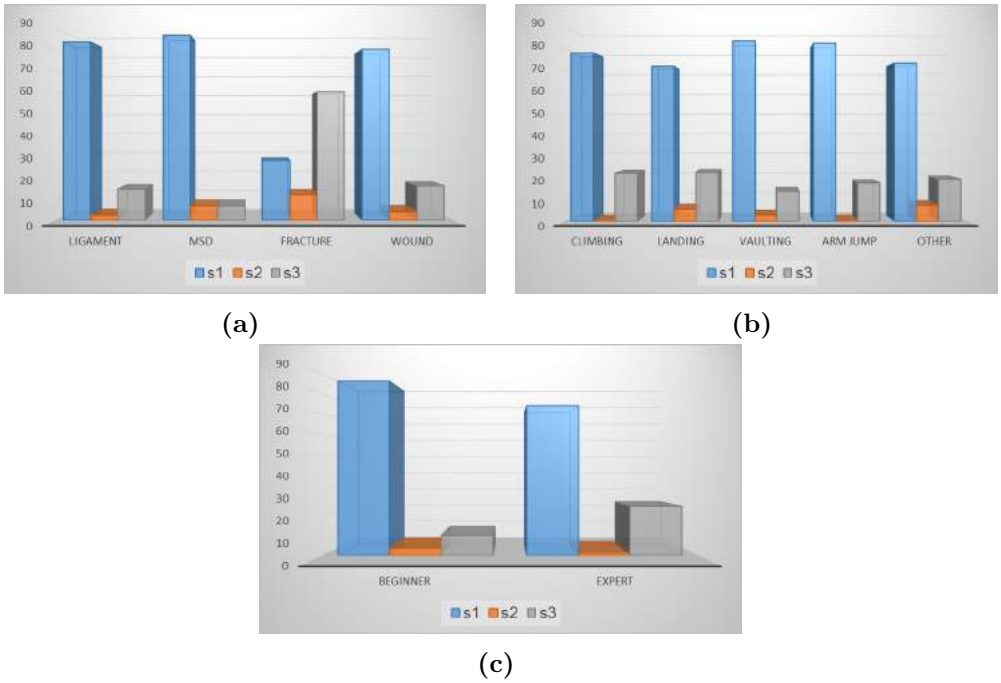

(a) **(b)**

(c)

Figure 2.11: Severity level as percentage according to injury type **(a)**, technique **(b)** and expertise **(c)**. In the legends of the figure, low severity is labeled "s1", medium severity is labeled "s2" and high severity is labeled "s3".

Landing techniques are the most prone to injury

Parkour landings are the techniques in which injuries happen most frequently (41% of total injuries). This makes sense because landing techniques are highly utilized during parkour practice as they are part of most of the parkour motions. This result is also in accordance with the literature of related sports like gymnastics. A descriptive epidemiology of collegiate women's gymnastics injuries has shown that the majority of competition injuries (approximately 70%) resulted from either landings in floor exercises or dismounts [Marshall 2007]. This result is also in accordance with a recent study of parkour injuries in United States where most of the injuries were reportedly caused by landings [Rossheim 2017].

Severity of the injuries

In all techniques, the reported score of injury severity showed to be low. This result contradicts the results of [Da Rocha 2014] where 41% of the injuries were relatively severe. In our study, only fracture reported a high score of severity which is not surprising due to the nature of the injury type. The score of severity increased with practice. Experts (practitioners with more than 5 years expertise in this study) appear to suffer from more dangerous injuries. This result is in accordance with the literature of similar sports, where it has been demonstrated that expertise increases the injury risk [Zetaruk 2005]. Moreover, it is reasonable to think that traceurs'

risk-taking behavior might increase with expertise.

The previous paragraph should be only used as guide. In fact, results of severity in this study are very subjective. A better way to analyze severity of injury is to use standardized methods such as the Injury Severity Score (ISS) [Baker 1974]. Such an analysis was not possible in this study because the questionnaire did not include information about the exact location of the injury.

2.2.6 Conclusion

The most critical parkour techniques for the purpose of injury prevention appear to be landing, vaulting, arm jump and climbing, as injuries are more frequent when using these techniques. Despite the risking nature of parkour practice, most of the reported injuries are of relative low severity. Although parkour is a young discipline, which is not yet considered as an official sport, most of the traceurs are trained with a parkour association in France. When training and practicing parkour, special effort should be put to avoid injuries during landing phases. For example, to improve landing performance with a trainer and to use recommended equipment for parkour practice.

In the context of our research, we have identified the parkour precision landing technique as the most critical for injury prevention. Moreover, jumps and landing techniques are of interest for generating highly dynamic motions as future new generation of robots will allow to cope with the dynamics of these motions (see for example the snapshots of the Atlas robot while jumping and landing in Chapter 1). These results encourage us to quantify the performance of parkour landings and to generate these movements. In the next sections we will present biomechanics studies of this technique. Before that, let us start by introducing a whole-body musculoskeletal model that was built for performing these studies.

2.3 Selection of a Whole-body Musculoskeletal Model

In order to analyze and generate parkour motions, a musculoskeletal model (Fig. 2.12) was created. To build the model, the following criteria were considered:

- The model should express the main elementary motions of the studied parkour techniques. This implies that the model might be more complicated than a humanoid robot model, but not as a complex as a physiological human model
- The model should be whole-body and three dimensional as parkour practice requires whole-body coordination (e.g. for accomplishing complex motions).
- The model should include surface joint stabilizer muscles that favor the study of muscular activity in highly dynamic motion. For example the agonist-antagonist muscles that perform abduction-adduction, flexion-extension or plantar flexion-dorsiflexion.

In the rest of the section we describe the main components of the model.

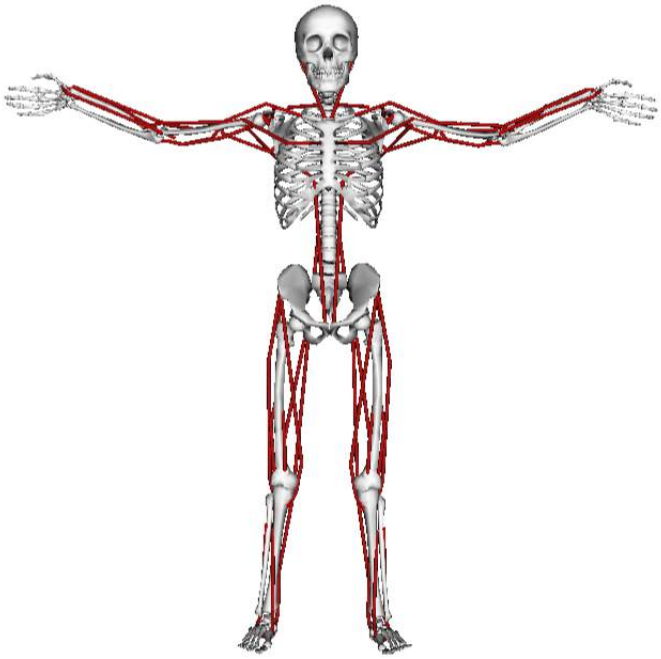

Figure 2.12: Musculoskeletal model. The visual elements are based on the running model of Hammer [Hamner 2010].

2.3.1 Joints modeling

A whole-body 3D model including 42 degrees of freedom (Table 2.1) was used to reconstruct the main elementary movements of the parkour athlete. The characteristics of the model are listed below:

- The lower limb, pelvis and upper limb anthropometry are based on the running model of Hammer et al. [Hamner 2010]. Mass properties of the torso and head segments (including the neck) are estimated from the regression equations of [Dumas 2007b, Dumas 2007c]. Hands anthropomorphic data are based on regression equations [Leva 1996].

- Each lower extremity has 7 DoF. The hip is modeled as a ball-and-socket joint, the knee is modeled as a hinge joint, the ankle is modeled as 2D hinge joints (flexion-extension and inversion-eversion), and the toes are modeled with one hinge joint at the metatarsals.

- The pelvis joint is modeled as a free-flyer joint to permit the model to translate and rotate in the 3D space. This 6D joint is attached to the free-floating base (root frame) of the under-actuated systems. The lumbar motion is modeled as a ball-and-socket joint [Anderson 1999] and the neck joint is also modeled as a ball-and-socket joint.

- Each arm is modeled with 8 DoF. The shoulder is modeled as a ball-and-socket joint, the elbow and forearm rotations are modeled with hinge joints to represent flexion-extension and pronation-supination [Holzbaur 2005], the wrist flexion-extension and radial-ulnar deviations are modeled with hinge joints, and the hand fingers are modeled with one hinge joint for all fingers.

Lower limb joints

	Hip	Knee	Ankle	Toes
Type	ball and socket	hinge	hinge (×2)	hinge

Upper limb joints

	Shoulder	Elbow	Wrist	Fingers
Type	ball and socket	hinge (×2)	hinge (×2)	hinge

Trunk and head joints

	Pelvis	Lumbar	Neck
Type	free flyer	ball and socket	ball and socket

Table 2.1: Synovial joints and free flyer joint of the whole body model.

2.3.2 Muscles modeling

The model contains 48 superficial muscles (Fig. 2.12) that represent the more relevant joint stabilizer muscles to study parkour movements. Muscles are modeled using hill-type models based on the works described in [Thelen 2003, Schutte 1993]

which are used in OpenSim [Delp 2007]. The muscles and their principal mechanical actions in the execution of parkour movements, are presented in Table 2.2 for the lower limb muscles, in Table 2.3 for the upper limb muscles and in Table 2.4 for the trunk and head muscles.

2.3.2.1 Lower limbs muscles

Twenty three superficial muscles that stabilize the hip, knee and ankle joints were selected based on a functional analysis of the muscles mechanical action in the execution of parkour jumps and landing techniques (Table 2.2).

Lower limb muscles

Muscle	Main Functions
Gluteus medius	Abduct an rotate medially the thigh at the hip.
Sartorius	Flex, abduct, and rotate laterally the thigh at the hip. Flex the leg at the knee.
Tensor fasciae latae	Extend the thigh at the hip.
Biceps femoris	Flex and rotate the leg laterally at the knee. Extend the thigh at the hip.
Semitendinoseus	Flex and rotate the leg medially at the knee. Extend the thigh at the hip.
Vastus lateralis	Extend the leg at the knee.
Vastus medialis	Extend the leg at the knee.
Lateralis gastrocnemius	Plantar flex the foot at the ankle.
Medialis gastrocnemius	Plantar flex the foot at the ankle and flex the leg at the knee.
Soleus	Plantar flex the foot at the ankle.
Tibialis posterior	Plantar flex the foot at the ankle. Slight inversion of the foot at the ankle.
Tibialis anterior	Dorsiflex the foot at the ankle. Slight inversion of the foot at the ankle.

Table 2.2: Lower body muscles of the whole body model and their mechanical action

2.3.2.2 Upper limbs muscles

Twenty one superficial muscles that stabilize the shoulder, elbow and wrist joints were selected based on a functional analysis of the muscles mechanical action in the execution of climbing techniques (Table 2.3).

Upper Limbs	
Muscle	**Main Functions**
Anterior deltoideus	Abduction, flexion and medial rotation of the forearm at the shoulder joint
Posterior deltoideus	Abduction, extension and lateral rotation of the upper arm at the shoulder joint
Medial deltoideus	Abduction of the upper arm at the shoulder joint
Pectoralis major	Flexion, adduction and medial rotation of the upper arm at the shoulder joint
Latisimus dorsi	Extension, adduction, horizontal abduction, flexion from an extended position, and medial rotation of the upper arm at the shoulder joint
Triceps brachii longus	Extension of the forearm at the elbow joint. Also adducts and may assist in extension of the shoulder joint.
Triceps brachii lateralis	Extension of the forearm at the elbow joint.
Biceps brachii longus	Supination and flexion of the forearm at the elbow joint.
Brachioradialis	Flexion of the forearm at the elbow joint
Carpi radialis flexor	Flexion and radial abduction of the hand at the wrist joint
Carpialis extensor	Extension and radial abduction of the hand at the wrist joint.

Table 2.3: Upper body muscles of the whole body model and their mechanical action

2.3.2.3 Trunk and head muscles

Trunk	
Muscle	**Main Functions**
Erector spinae longissimus	Extension of the lumbar spine at the lumbar joint
Rectus abdominis	Flexion of the lumbar spine at the lumbar joint
Sternocledomastoid	Oblique rotation and flexion of the head at the neck joint
Trapecius ascendus	Scapulae motion and extension of the head at the neck joint

Table 2.4: Trunk muscles of the whole body model and their mechanical action

Four superficial muscles that stabilize the lumbar and neck joints were selected based on a functional analysis of the muscles mechanical action in the execution of the parkour techniques 2.4. The sternocledomastoid and the trapecius ascendus muscles were used for studying the motion of the head. Nevertheless, the trapecius ascendus muscle is also important for the scapulae movement in the execution of climbing techniques.

2.3.3 Marker set

The model includes a whole-body marker set with 48 markers placed on anatomical bony landmarks (2.13) selected based on the recommendations of the International Society of Biomechanics (ISB) [Wu 2002, Wu 2005].

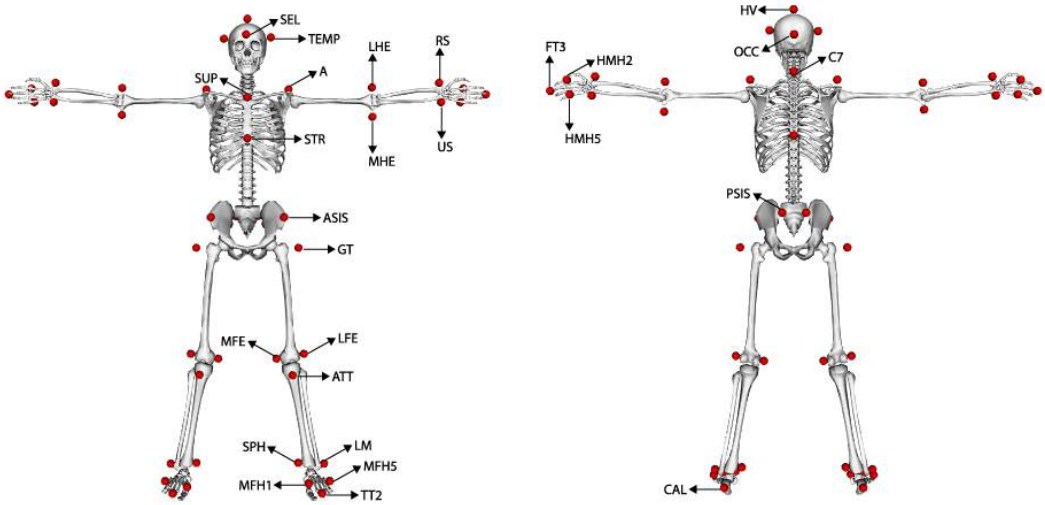

Figure 2.13: Marker set depicted on the whole body skeletal model

2.4 Strategies of Parkour Practitioners for Executing Soft Precision Landings

In this section we present a biomechanical study of the parkour precision and roll landing techniques. To this end, biomechanical methods introduced at the beginning of this in chapter are applied (Section 2.1), and the lower limb part of the skeletal model presented in the previous section is utilized (Section 2.3). In this part of the research, we made a lower-limb biomechanical study of parkour precision landing technique, parkour roll landing technique and landings performed in a natural style by untrained participants (recreational athletes). We compare the landing techniques at two different drop heights. This study allows to quantify some performance factors of traceurs executing these movements and to identify the mechanisms for pain avoidance and injury prevention in parkour landings. The results also draw attention to the possibility of using parkour landing strategies in other sports such as gymnastics.

2.4.1 Introduction

Various types of analyses are proposed in this study including injury prevention, energetic performance, postural control and motion smoothness. In what follows we present the state of the art of these topics in the context of our research.

2.4.1.1 Injury prevention in parkour landings

Parkour movements look risky, highly dynamic and complex [Kidder 2012, Gilchrist 2011, Cazenave 2008]. One of the most repeated and risky motion is landing (see the epidemiological study in Sec. 2.2), which is commonly performed in urban spaces with hard surfaces and uncontrolled drop heights. Biomechanical studies assessing kinetics of parkour landings have shown that traceurs can decrease peak vertical ground reaction forces (GRFs) which, according to specialists of injury prevention, may be dangerous for the human body when they are high [Puddle 2013, Standing 2015]. In these studies, only vertical forces were reported despite the fact that antero-posterior forces may be high when landing and the stopping abruptly. This movement could induce injuries like ACL ruptures [Steele 1990]. Moreover, if GRF peaks are lowered and the motion is smooth, then joint torques, joint angular velocities and joint power peaks might also be lowered, which is fundamental for injury prevention in landing [Devita 1992, Bisseling 2007, Bisseling 2008, Rosen 2015]. Thus, a stable, less demanding in terms of joint power and torque peaks, and a safer technique for landing from higher drops, may also be of interest in other highly dynamic and complex sports such as gymnastics.

The first part of this comparative study is based on the previous analysis of injury prevention and mechanical performance. This drove us to formulate a list of hypotheses that will be enumerated and preceded by "**H**" so that we can refer to

them in the results and discussion sections.

- **H1** We hypothesized that antero-posterior GRF will be reduced in parkour landings as traceurs seem to lower vertical GRF [Standing 2015].
- **H2** We hypothesized that the parkour techniques would induce a reduction of angular velocity, torque and power, because of the soft landing that traceurs seem to perform and their ability to lower the vertical GRF.
- **H3** We expect that increasing the landing height will induce an increment of the assessed GRFs, peak angular velocity, joint torques and power.

2.4.1.2 Energetic performance of parkour landings

Such a dynamic and complex discipline as parkour requires rigorous training [Grosprêtre 2016]. In fact, it has been shown that parkour training induces high development of muscular capacity [Marchetti 2012]. Therefore performing an energetic study to quantify the contribution of joints in energy dissipation may provide clues about how lower-limbs should be conditioned for landing. Furthermore, learning how multi-joint control changes with increased landing height may be of interest to practitioners who may so learn how energy is being dissipated by their lower-limbs [Yeow 2009].

Following this reasoning, we formulate the following hypotheses:

- **H4** We hypothesized that traceurs will extended landing phase duration for shock absorption and that this would lead to more mechanical energy dissipation.
- **H5** We expected that traceurs executing the precision technique would use especially knee extensors to absorb the energy as it has been demonstrated by related studies of soft landings [Devita 1992]

2.4.1.3 Postural control in parkour landings

Postural control consists in maintaining, achieving or restoring a state of balance. In the literature, it has been associated to injury prevention. For example, it has been reported that postural control is significantly related to ankle and knee injuries [Hrysomallis 2007]. Postural control has also been associated to athletic performance. For example, it has been shown that the more proficient athletes display a best postural control and that, among athletes, gymnasts tend to have the best balance ability [Hrysomallis 2011].

Gymnasts and traceurs share some similarities. In fact, both athletes are commonly exposed to land from important heights. Thus, it seems consistent to think that as in gymnastics, a key performance factor in parkour precision landings is postural control. If postural control in traceurs is not significantly better than postural control in recreational athletes, then parkour training must be modified to

improve stability and prevent injuries. In fact, impacts in parkour are more considerable than in gymnastics, because parkour is performed onto hard surfaces while gymnastics is performed onto soft surfaces.

In order to study postural control during the parkour precision landing technique (the roll technique was excluded from this analysis as there is a continuation of the motion without stabilization) the following parameters were considered: Time to stabilization (TTS) [Colby 1999], dynamical postural stability index (DPSI) [Wikstrom 2005], and confidence ellipsoid area of the center of pressure (CoP) displacement [Takagi 1985]. TTS is a dynamic test of postural control that quantifies the time it takes for an individual to return to a baseline or stable state following a jump or drop landing. A longer TTS indicates more difficulty in controlling posture at landing (it might also indicate impaired neuromuscular control [Brown 2004]). DPSI provides an index of stabilization for antero-posterior (A-P), medial-lateral (M-L) and vertical (V) anatomical axes. A large DPSI value indicates that the athlete performed more effort to control the stability in a given direction. A confidence ellipsoid of the center of pressure contains information about the center of pressure excursion for postural control. A large value of the confidence ellipsoid area is related to difficulties in controlling posture after landing.

Based on the previous analysis and the clinical tests of postural control presented, we formulate the following hypotheses:

- **H6** We hypothesize that parkour practitioners will have a better dynamical postural control performance in terms of a lower DPSI value and a lower area of the center of pressure confidence ellipsoid than untrained participants.
- **H7** We further hypothesize that TTS will be less in traceurs than in recreational athletes because practitioners appear to land in a pose where the center of mass (CoM) is closer to the center of the support polygon.
- **H8** Finally, we hypothesize that the landing height effect on stability is not statistically significant for both populations.

2.4.1.4 Motion smoothness of parkour landings: fluidity and aesthetics

Freerunning is a derivation of parkour which objective is to express fluidity and aesthetics of the motion. While fluidity and aesthetics are not as important as efficiency and pain/injury prevention in parkour, they constitute an interesting component of the parkour movements. For example, a parkour landing where peak GRFs are lowered and the time duration of the motion is extended might look smoother than a landing performed by untrained jumpers where peak GRFs are high and the time duration of the motion is short.

According to the biomechanical literature, a final knee flexion of more than 90 degrees from full extension corresponds to a soft landing, otherwise it is classified as a stiff landing [Devita 1992]. Moreover, it has been proposed that in order to quantify the smoothness of a movement, jerk [Hogan 1984, Flash 1985] is a good parameter. For example, it has been shown that the application of the *minimum-jerk*

criterion induced smooth end-effector (e.g. the hand) trajectories whose profiles are bell shaped and seem more natural (human-like). When computing the *minimum-jerk*, only the kinematics of the end-effector is considered. In order to generate smooth trajectories considering the dynamics and the joint space (body joints), the *minimum-torque-change* criteria [Uno 1989] can be used. Finally, note that, although these criteria could be used to formulate hypotheses about how the CNS solves redundancy from a motor control perspective, our interest in this study is to compare mechanical cost functions related to smoothness in the landings executed by traceurs and untrained participants. The results from this analysis are intended to enrich the understanding of the strategies used by traceurs when performing parkour landings.

Based on the previous reasoning and the presented criteria, we formulated our scientific hypotheses as follows:

- **H9** We hypothesized that traceurs will perform soft landings and that joint range of motion (RoM) will increase with drop height.
- **H10** We hypothesized that the jerk of the CoM trajectory "J_{jerk}" will be minimized in parkour landings.
- **H11** We hypothesized that parkour landings will induce a lower cost value of the *minimum-torque-change* "J_{tc}" than in landings performed by untrained participants.

2.4.2 Methodology

2.4.2.1 Participants

Twelve healthy untrained male participants (age: 22.3 ± 3.3 y, height: 1.79 ± 0.08 m, mass: 71.2 ± 5.6 kg) and twelve healthy trained male traceurs (age: 22.2 ± 4.8 y, height: 1.73 ± 0.04 m, mass: 66.6 ± 5.1 kg) volunteered for this study. The traceurs' experience in parkour practice was 5.4 ± 2.1 y. The subject exclusion criterion was based on history of lower extremity injuries or diseases that might affect landing biomechanics. The experiments were conducted in accordance with the standards of the Declaration of Helsinki (rev. 2013) and approved by a local ethics committee.

2.4.2.2 Data acquisition

Kinematic data were collected using 11 infrared cameras sampling at 200 Hz (Vicon, Oxford Metrics, Oxford, UK) and recording reflective markers placed on the participants (Fig.2.14 and Fig.2.15). As previously remarked, only lower-limbs motions were considered for this study. Markers were set based on Wu recommendations [Wu 2002] as follows: the first and fifth metatarsal, calcaneus, lateral and internal malleolus, anterior tibial tuberosity, lateral and medial epicondyles of knee, greater trochanter, posterior superior iliac spine and anterior superior iliac spine

(see marker set for the lower limbs in Fig. 2.13 in Subsection 2.3.3). Two force plates (AMTI, Watertown, MA, USA) embedded into the floor were used to record GRF and moments at 2000 Hz for each limb.

2.4.2.3 Experimental protocol

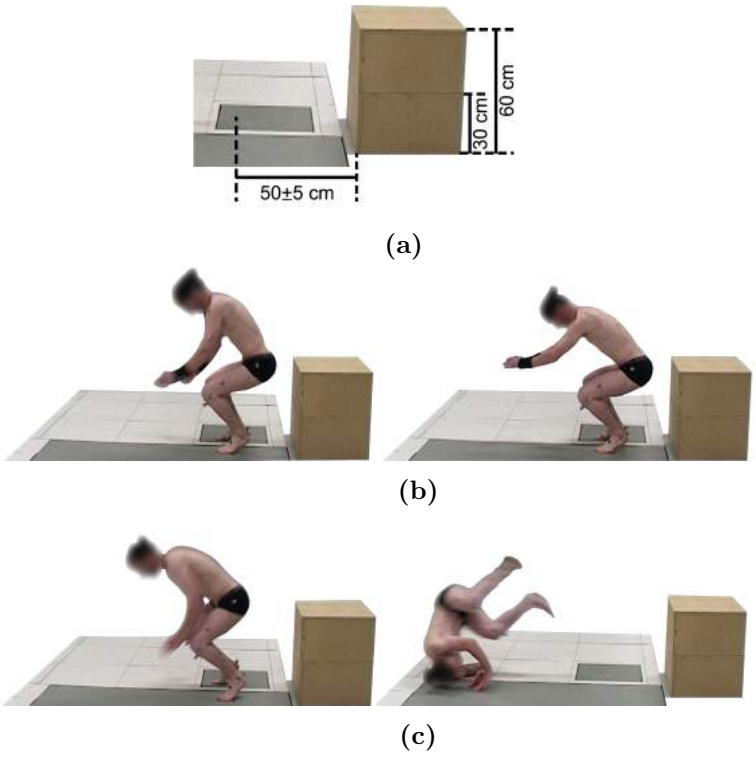

Figure 2.14: Parkour landing techniques studied when landing from 60 cm height. In **(a)** the two boxes used for the protocol and the way the distance to the target (50 ± 5 cm) was calculated. In **(b)**, the landing phase of parkour precision technique. On the right in **(c)**, the landing phase of parkour roll landing technique. On the left in **(c)**, the roll strategy that follows the landing phase.

All participants started with 5 min of warming up that was followed by 5 min of self-stretching. Two boxes of 30 cm height were used to create two landing heights: 30 cm and 60 cm (Fig. 2.14a). For each height, 2 blocks of 3 successful trials without randomization were executed as follows: one block of familiarization, followed by a second one of recording including 30 seconds of rest in between. Untrained participants' trials were labeled as untrained trials while parkour trials were divided into precision and roll trials. All participants were instructed to land barefoot in a specified target and to avoid jumping up to do not exceed the initial height. No instruction was provided regarding the use of arms. The target was set with marker landmarks placed on the landing surface to limit the minimal and maximal horizontal landing distance at 50 ± 5 cm (Fig. 2.14a). In the untrained

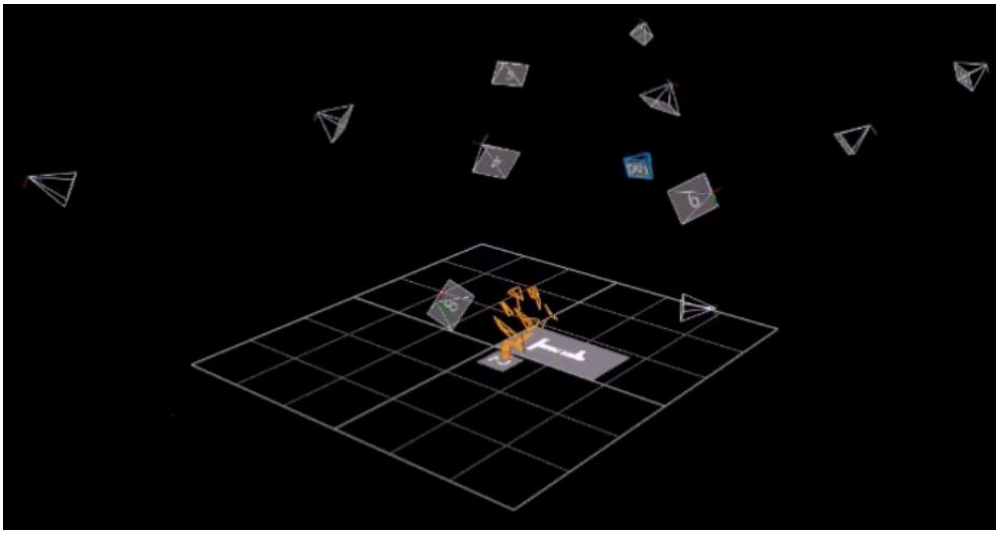

Figure 2.15: Reconstruction of a landing motion using Vicon Nexus software. In the image, 11 optoelectronic cameras used for recording the 3D marker trajectories on the participants' body, 1 digital video camera utilized for verifying the recordings, and two force platforms used for recording the ground reaction forces can be observed.

trials, participants were asked to land as they preferred and stabilize themselves on the force platform. In the precision and the roll trials, traceurs were instructed to land using the parkour precision and roll technique (Fig. 2.14b and Fig. 2.14c respectively).

2.4.2.4 Data analysis

Definition of the landing phase For untrained and precision trials, the landing phase was defined as the time duration between the initial contact with the ground "IC" — defined as the time instant when the vertical GRF was more than 50 N [Puddle 2013] — and the maximum knee flexion (100%) [Mccaw 2013] (Fig. 2.16a and Fig. 2.16b). In the roll trials, the landing phase was defined from IC until the time instant before the roll (100%) that was prior to the antero-posterior displacement of the hip at the beginning of the roll (Fig.2.16c). Note that Fig. 2.14c does not represent the landing phase duration of the roll landing, as rolling on the shoulder strategy is not part of the provided definition. In fact the roll analysis was outside the scope of this study.

Kinematics, dynamics and energetics Data were reconstructed using the Nexus software (Fig. 2.15) from the Vicon motion capture system (Vicon, Oxford Metrics, Oxford, UK). Reconstructed data were processed using a custom-made Matlab program. Kinematics and GRFs were filtered at the same cutoff frequency [Kristianslund 2012, Mccaw 2013] with a low-pass Butterworth digital filter of 4th

order applied in a zero-phase. A cut-off frequency of 30 Hz was used after a residual analysis [Winter 2009]. The geometric model was scaled with OpenSim [Delp 2007] and the scaling parameters were modified according to anthropomorphic tables [Dumas 2007b]. Inverse kinematics and inverse dynamics were performed using OpenSim [Delp 2007]. Results were exported to Matlab in order to compute joint power and mechanical work, evaluate the data and perform the statistical analysis. Only hip, knee and ankle joints were considered. The assessed variables were: GRF peaks, time to maximum peak norm of GRF, loading rate of force, hip, joint angular configuration at IC, RoM, peak angular velocity, duration of the landing phase, joint torques, joint power and mechanical work (including total eccentric work, and positive and negative joint contribution for energy generation and dissipation (Eq (2.10)). Joint power was computed as the product of the joint torque and the joint angular velocity, and joint mechanical work was calculated by integrating the joint power along the time of the landing phase. Total eccentric mechanical work was calculated as the sum of the absolute value of the eccentric mechanical work generated by the hip, knee and ankle joints [Zatsiorsky 2002]. The work contribution for energy dissipation was calculated by normalizing each joint eccentric work by the total eccentric work (100 %). All these calculations are explained at the beginning of this chapter in Section 2.1. The cost value of the *minimum-jerk* criterion applied to the CoM trajectory was calculated as follows:

$$J_{jerk} = \frac{1}{T} \int_{IC}^{T} \dot{\mathbf{a}}_c{}^2 \, dt, \tag{2.13}$$

where T is the time duration of the landing phase, and $\dot{\mathbf{a}}_\mathbf{c}$ is the derivative of the CoM acceleration. The cost function value of the *minimum-torque-change* criterion applied to the lower-limb joints was calculated as follows:

$$J_{tc} = \frac{1}{T} \int_{IC}^{T} (\dot{\boldsymbol{\eta}}_{hip}^2 + \dot{\boldsymbol{\eta}}_{knee}^2 + \dot{\boldsymbol{\eta}}_{ankle}^2) \, dt, \tag{2.14}$$

where $\boldsymbol{\eta}$ is the joint torque.

Normalization and data reporting Forces, joint torques, joint power and mechanical work were normalized by the subject's body mass. Results were reported only for the landing phase and for the dominant leg as it has been reported to provide better conclusions for injury prevention [Niu 2011]. Leg dominance was defined as the most used leg for stabilization by comparing the mean GRF of each force platform during the landing phase [Niu 2011].

Clinical tests for assessing postural control during landing The time to stabilization TTS of the A-P component of the GRFs was calculated using sequential estimation and the "overall series mean $\pm$ 0.25 SD" [Colby 1999] threshold. Details of the calculation are provided by Algorithm 1 in which Nf is the number of frames.

where Nf is the number of recorded frames, grf denotes the ground reaction

Algorithm 1 Calculate the time to stabilization (TTS)

$\bar{y} \leftarrow mean(grf_{AP})$
$lowB \leftarrow \bar{y} - 0.25 \times std(grf_{AP})$
$uppB \leftarrow \bar{y} + 0.25 \times std(grf_{AP})$
for $n = 1$ **to** N_f **do**
  $\hat{y} \leftarrow \frac{\sum_{i=1}^{N_f} grf_{AP,i}}{n}$
  if $lowB \leq \hat{y} \leq uppB$ **then**
    $TTS \leftarrow time[n]$
  end if
end for

force of the antero-posterior (sub-index AP), medial-lateral (sub-index ML) and vertical (sub-index V) axes components. The DPSI (dynamic postural control index) [Wikstrom 2005] values were calculated as follows:

$$DPSI_{M-L} = \frac{\sqrt[2]{\sum_{i=1}^{N_f} \left(0 - grf_{ML,i}\right)^2}}{N_f}, \tag{2.15a}$$

$$DPSI_{A-P} = \frac{\sqrt[2]{\sum_{i=1}^{N_f} \left(0 - grf_{AP,i}\right)^2}}{N_f}, \tag{2.15b}$$

$$DPSI_{V} = \frac{\sqrt[2]{\sum_{i=1}^{N_f} \left(BW - grf_{V,i}\right)^2}}{N_f}, \tag{2.15c}$$

where BW is the body weight. Details of the confidence ellipsoid area of the center of pressure displacement calculation can be obtained in [Schubert 2014].

2.4.2.5 Statistical analysis

The average of three trials in each recording block was calculated for each participant. A threshold level of significance was set ($p \leq .05$) and then the Bonferroni correction was applied. Statistical tests for the height and technique factor were performed. Three correlated paired t-tests ($p/3$) were computed to assess the effect of dropping from the 30 and 60 cm heights on the assessed variables (untrained 30 cm vs untrained 60 cm, precision 30 cm vs precision 60 cm, roll 30 cm vs roll 60 cm). Similarly four independent t-tests ($p/4$) were computed to compare the assessed variables of untrained trials with each of the parkour trials at the same height (untrained 30 cm vs precision 30 cm, untrained 30 cm vs roll 30 cm, untrained 60 cm vs precision 60 cm, untrained 60 cm vs roll 60 cm). Then, two independent paired t-tests ($p/2$) were executed to compare roll with precision trials at the same height (precision 30 cm vs roll 30 cm, precision 60 cm vs roll 60 cm).

2.4.3 Results

2.4.3.1 Ground reaction forces

Technique factor All GRF components were lesser in parkour landings (**H1**) than in untrained landing. Time to maximum peak GRF was higher in the parkour precision-landing technique and the loading rate was lesser in both parkour techniques. Although not statistically different, at 30 cm height, peak GRF in precision technique were lesser than in roll technique ($p > .1$), but at 60 cm height, peak GRF in roll technique were lesser than in precision technique ($p < .05$) (Table 2.5).

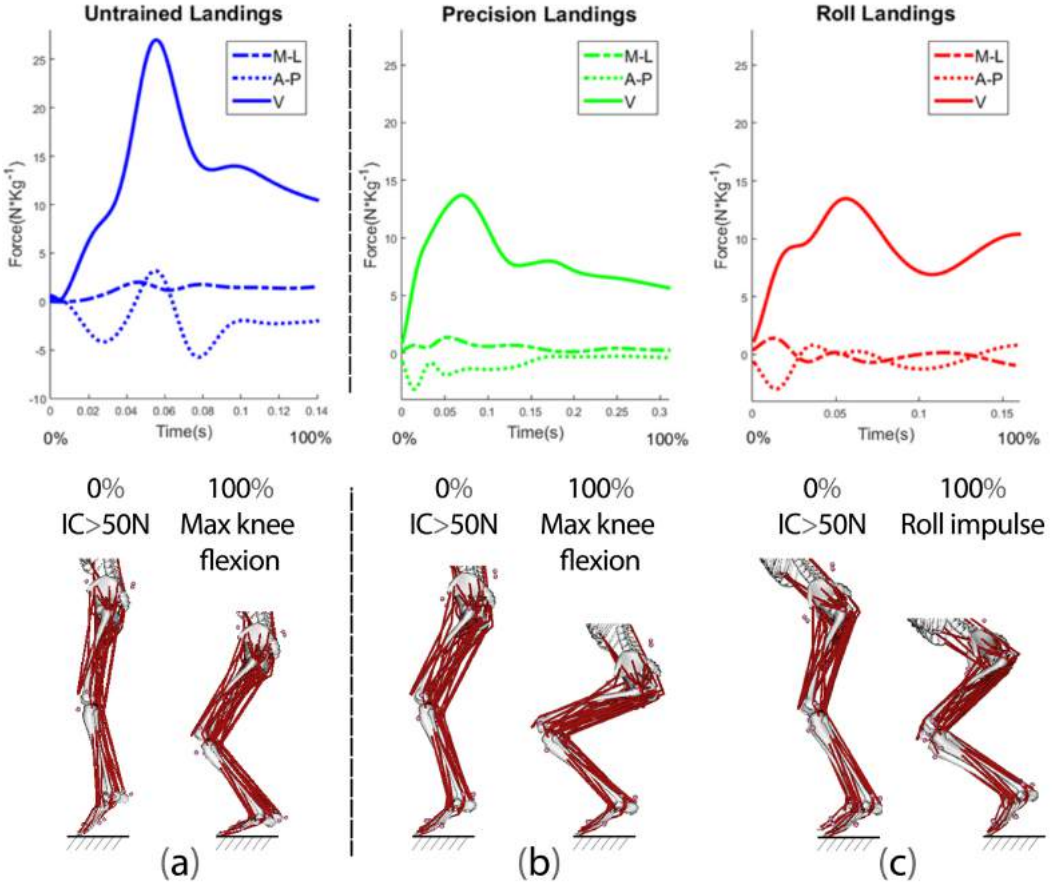

Figure 2.16: Landing phase definition for untrained, precision and roll trials. The schema corresponds to a landing of 60 cm height of an untrained participant executing a untrained trial (**a**), and to a traceur executing the precision (**b**) and the roll technique (**c**) respectively. IC denotes the initial contact with the ground. These images were obtained using the OpenSim software. Although muscles are displayed in the model of the figure, they were not used in this study. On the top of the images, a representative profile of the normalized GRFs during the landing phase for each of the landing techniques are displayed. Positive values represent vertical, anterior and medial GRFs induced on the force platform (of the dominant limb) by participants during the landing phase.

Height factor All GRFs and loading rate increased with landing height (**H3**) in all landing conditions (Table 2.5) while the time to maximum peak GRF decreased with landing height.

Table 2.5: Mean (*SD*) of force parameters assessed of the dominant leg. The p-values were corrected with Bonferroni method for the number of hypothesis.

	Untrained		**Precision**		**Roll**	
	30 cm	60 cm	30 cm	60 cm	30 cm	60 cm
Peak force $[N \cdot Kg^{-1}]$						
M-L	1.73(.7)†	2.15(1)‡	.97(.4)	1.28(.5)	1.51(.7)	1.53(.7)
A-P	3.22(1)†	4.38(1.4)†‡	2.07(.5)∗∘	2.7(.5)	2.91(.6)	3.08(.5)
V	17.79(4.3)†‡	22.23(4.7)†‡	10.28(1.8)∗	13.35(1.6)	11.78(1.7)	11.79(1.7)
N	19.58(4.5)†‡	23.98(5.3)†‡	10.79(1.81)∗	13.97(2.1)	12(1.7)	12.05(1.7)
Time to maximum peak force $[ms]$						
	68.9(20)	60.49(12)	106.06(53)	72.93(11)	65.46(46)	62.93(30)
Loading rate $[N \cdot Kg^{-1} \cdot s^{-1}]$						
	333(160)†	431(162)†	128(50)∗∘	198(48)	281(188)	264(186)

Note: **M-L**, medial-lateral force, **A-P**, antero-posterior force, **V** vertical force , **N** norm of force vector.
∗ landing from 30 cm significantly different to landing from 60 cm for the same trial ($p \leq .017$).
† untrained trial significantly different to precision trial for the same height ($p \leq .0125$).
‡ untrained trial significantly different to roll trial for the same height ($p \leq .0125$).
∘ precision trial significantly different to roll trial for same height ($p \leq .025$).

2.4.3.2 Time and kinematics

Technique factor The landing phase duration was significantly longer in precision techniques (54.5 % more than untrained landings and 57.7 % more than roll landings) (**H4**). Joints were more flexed at IC in parkour landings, especially at the hip joint ($p < .001$ in precision landings and $p < .0001$ in roll landings at 60 cm). Peak angular velocities of joints were lesser in parkour (**H2**), especially in the ankle joint ($p < .01$ in precision landings and $p < .001$ in roll landings).

Height factor The landing phase duration was similar between 30 cm and 60 cm heights for all landings. In the roll technique at 60 cm, traceurs landed with the hip and knee slightly more extended than when landing from 30 cm height, while in the precision technique joint angles were less modified at IC (**H9**). Results show that the hip was only 2.1 degrees more flexed, the knee was 1.6 degrees more flexed and the ankle was 3.1 degrees more flexed. Peak angular velocities of joints increased with height (**H3**). The peak angular velocity of the knee did not increase significantly with height in all techniques (see Fig. 2.16 and Table 2.6).

Table 2.6: Mean (*SD*) of kinematic parameters assessed of the dominant leg. The p-values were corrected with the Bonferroni method for the number of hypothesis.

	Untrained		**Precision**		**Roll**	
	30 cm	60 cm	30 cm	60 cm	30 cm	60 cm
Landing phase duration [*s*]						
Time	.15(.03)†	.14(.04)†	.33(.08)∘	.33(.09)∘	.14(.05)	.16(.06)
Joint angle at initial contact with the ground [*deg*]						
H-F	2.9(9.2)†‡	2.2(11.4)†‡	25.6(8.2)	23.5(9.4)	37.6(17.6)	29.5(9.5)
K-F	17.8(3.3)∗ † ‡	22.4(3.6)†‡	32.1(5.2)	33.7(5.6)	42.2(11.6)	36.6(7.1)
A-PL	19.1(10.7)	21.8(10.2)	21.7(10.8)	24.8(9.1)	9.9(12.9)	17.5(11.3)
Joint range of motion during the landing phase [*deg*]						
H-F	25.2(9.4)∗†	42.5(18.9)	48.1(8.6)∗	59.0(8.2)∘	38.7(13.3)	45.4(10.7)
K-F	47.0(5.8)∗ † ‡	61.3(9.4))†	84.1(16.4)∗	95.6(13.5)∘	67.0(18.4)	77.2(16.6)
A-PL	43.1(3.8)∗	50.1(5.0)	48.9(8.9)∗	54.4(9.0)	36.7(13.2)	44.8(12.7)
S	64.8	83.7	116.2	129.3	109.2	113.8
Peak joint angular velocity (deg/s)						
H-F	531(210)∗	782(291)†‡	380(66)∗	484(68)	462(122)	469(70)
K-F	669(116)‡	768(162)‡	658(93)∘	777(68)∘	693(93)	788(100)
A-PL	1174(163)∗ † ‡	1514(221)‡	927(205)∗	1234(226)	813(209)∗	1101(237)

Note: **H-F**, hip flexion; **K-F**, knee flexion; **A-PL** ankle plantarflexor; **S** knee flexion from anatomical pose.
∗ landing from 30 cm significantly different to landing from 60 cm for the same trial ($p \leq .017$).
† untrained trial significantly different to precision trial for the same height ($p \leq .0125$).
‡ untrained trial significantly different to roll trial for the same height ($p \leq .0125$).
∘ precision trial significantly different to roll trial for same height ($p \leq .025$).

2.4.3.3 Dynamics

Technique factor Peak joint torques and power were also lesser in parkour landings (**H2**). The knee extensor torque was significantly higher in untrained technique than in precision technique from both heights ($p < .01$ at 30 cm and at 60 cm), and it was significantly higher than the roll technique at 60 cm ($p < .01$). The ankle plantar-flexor peak power was significantly lower in the roll technique ($p < .00001$ when comparing with untrained landings and $p < .01$ with precision landings at 60 cm) (Fig. 2.17 and Table 2.7).

Height factor Peak joint torques and power increased with height of landing (**H3**). More eccentric mechanical work was generated during parkour landings by the lower-limbs when the height was increased ($p < .01$ in precision landings).

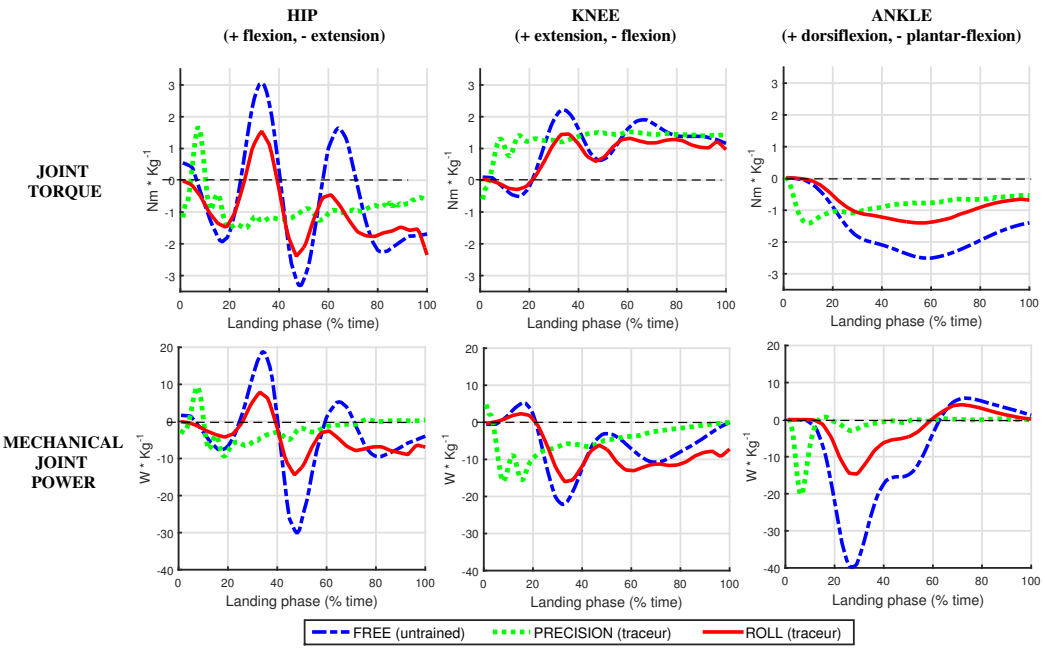

Figure 2.17: Representative untrained, precision and roll landing profiles of the dominant leg joint torques and joint mechanical power. The profiles correspond to the mean value of the landing trials performed from a 60 cm drop height by an untrained participant and by a traceur for the precision and the roll landings. The rows represent the assessed values and the columns the joints. Positive values represent flexion for the hip, extension for the knee and dorsiflexion for the ankle while negative values represent extension for the hip, flexion for the knee and plantar-flexion for the ankle.

Table 2.7: Mean (*SD*) of dynamic parameters assessed of the dominant leg. The p-values were corrected with the Bonferroni method for the number of hypothesis.

	Untrained		**Precision**		**Roll**	
	30 cm	60 cm	30 cm	60 cm	30 cm	60 cm
Peak joint torque $(N \cdot m \cdot Kg^{-1})$						
H-F	1.73(0.4)‡	2.24(0.8)	1.33(0.7)	1.60(0.6)	1.14(0.5)	2.05(1.4)
H-E	2.18(0.4)†‡	2.45(0.7)	1.61(0.5)	1.82(0.4)	1.58(0.5)	1.88(0.9)
K-E	1.84(0.3)∗†	2.41(0.5)†‡	1.50(0.2)∗	1.90(0.3)	1.43(0.4)∗	1.80(0.3)
A-PL	1.61(0.3)∗‡	1.98(0.3)‡	1.31(0.2)∗	1.67(0.3)	1.21(0.2)	1.31(0.5)
Peak joint power $(W \cdot Kg^{-1})$						
H-F	10.2(5.3)∗	21.3(10.4)†	5.9(3.4)	8.5(4.1)	6.0(3.3)∗	11.8(8.3)
H-E	12.4(5.0)	16.7(10.2)	8.3(3.3)∗	12.4(4.5)	9.3(5.1)	13.1(6.4)
K-E	15.4(5.9)∗	27.4(11.6)	11.8(3.2)∗	19.5(4.0)	12.3(3.7)∗	18.5(4.1)
A-PL	24.6(6.0)∗ † ‡	36.8(7.2)†‡	12.9(5.6)	23.4(7.0)∘	8.4(3.4)∗	13.3(6.2)

Note: **H-F**, hip flexor; **H-E**, hip extensor; **K-E**, knee extensor; **A-PL** ankle plantarflexor.
∗ 30 cm significantly different to 60 cm ($p \leq 0.025$).
† untrained significantly different to precision ($p \leq .0125$).
‡ untrained significantly different to roll ($p \leq 0.0125$).
∘ precision trial significantly different to roll trial ($p \leq .025$).

2.4.3.4 Energetics

Technique factor The ankle and knee only worked in eccentric mode while the hip worked in concentric and in eccentric mode. Hip concentric work was significantly higher in untrained landing than in precision technique ($p < .005$). More eccentric mechanical work was generated during parkour landings by the lower-limbs especially in the precision technique. The knee was always the most important contributor (around twice the contribution of the hip or the ankle) (**H5**) while the hip and ankle shared similarly the rest of the total energy dissipated by the lower-limbs (Table 2.8 and Fig. 2.18).

Height factor Mechanical work contribution per joint of parkour techniques did not change significantly with height. From 30 cm, untrained participants dissipated energy principally through their ankle plantar-flexors (47 % of the total eccentric mechanical work) while from 60 cm they dissipated energy principally through the knee extensors (48 % of the total eccentric mechanical work). Similarly in untrained landings, the work contribution of the ankle was significantly less at 60 cm than at 30 cm of landing (Table 2.8 and Fig. 2.18).

Table 2.8: Means (*SD*) of energetic parameters assessed of the dominant leg. The p-values were corrected with Bonferroni method for the number of hypothesis.

	Untrained		**Precision**		**Roll**	
	30 cm	60 cm	30 cm	60 cm	30 cm	60 cm
Mechanical work ($J \cdot Kg^{-1}$)						
H-C	0.16(0.1)†	0.27(0.2)†	0.07(0.1)	0.10(0.1)	0.11(0.1)	0.27(0.3)
H-E	0.23(0.1)†	0.32(0.3)†	0.53(0.2)∗	0.83(0.3)∘	0.42(0.3)	0.44(0.2)
K-E	0.72(0.2)∗†	1.12(0.4)†	1.26(0.5)∗	1.99(0.7)	0.88(0.4)	1.39(0.8)
A-E	0.85(0.2)†‡	0.88(0.3)	0.61(0.1)∗∘	0.96(0.3)∘	0.39(0.2)	0.56(0.3)
T-E	1.79(04)	2.32(0.8)†	2.41(0.7)	3.79(1.1)∘	1.69(0.7)∗	2.41(0.9)
Work contribution to energy dissipation per joint (%)						
H	12.17(4.9)†	13.10(8.6)	22.93(7.4)	22.44(7.6)	24.22(12.7)	23.14(17.4)
K	40.41(9.3)	48.05(11.6)	51.23(9.0)	52.45(7.2)	50.90(10.9)	53.95(15.2)
A	47.42(9.1)∗ † ‡	38.85(7.4)†‡	25.84(4.9)	25.11(4.2)	24.88(8.2)	22.91(12.2)

Note: **H-C**, hip concentric; **H-E**, hip eccentric; **K-E**, knee eccentric; **A-E** ankle eccentric; **T-E**, total eccentric; **H** hip; **K** kneel; **A**, ankle.
∗ 30 cm significantly different to 60 cm ($p \leq 0.025$).
† untrained significantly different to precision ($p \leq 0.0125$).
‡ untrained significantly different to roll ($p \leq 0.0125$).
∘ precision trial significantly different to roll trial ($p \leq 0.025$).

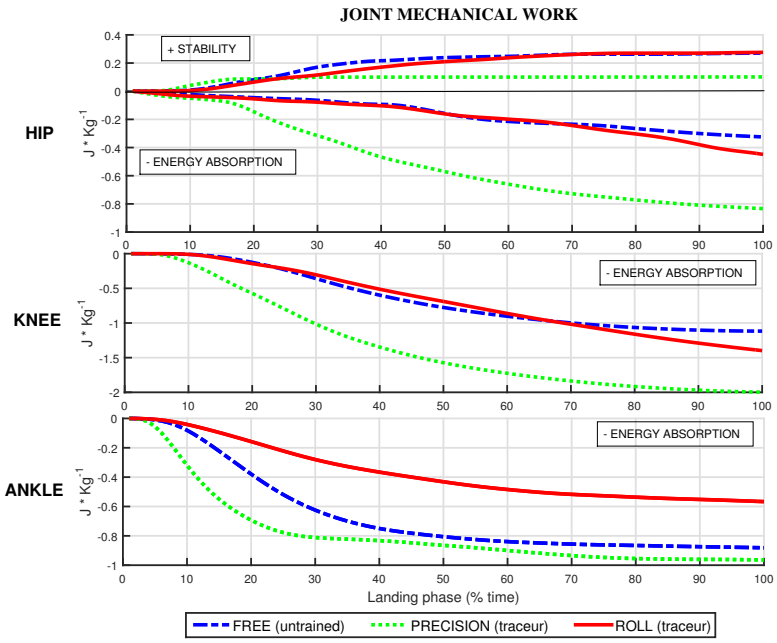

Figure 2.18: Representative untrained, precision and roll landing mechanical work profiles of the dominant leg. The profiles correspond to the mean value of the landing trials performed from a 60 cm height drop by an untrained participant and by a traceur for the precision and the roll landings. The rows represent different joints. Negative mechanical work represent the work performed for energy absorption through eccentric muscles of lower limbs, while positive mechanical work of the hip accounts for the stabilization of the upper trunk through the concentric muscles of the hip. Because positive and negative mechanical work cancel each other at the beginning of the landing phase, the hip mechanical work is illustrated using the absolute value of positive and negative joint power (See Eq. (2.10)).

2.4.3.5 Postural control

Table 2.9: Assessment parameters Postural control of parkour precision landing technique and untrained trials. DPSI and confidence ellipse area are normalized with the values of untrained population.

	Untrained		**Precision**	
	30 cm	60 cm	30 cm	60 cm
A-P Time to stabilization $[s]$	.42	.45	.45	.41
M-L dynamic postural stability index	1	1	.90	.81
A-P dynamic postural stability index	1	1	.54	.59
V dynamic postural stability index	1	1	.94	.93
Confidence ellipsoid area	1	1	.06	.05

Note: **M-L**, Medial-Lateral; **A-P**, Antero-Posterior; **V**, Vertical

Technique factor Confidence ellipsoid areas were significantly lower in parkour precision landing ($p < .0001$) (**H6**). In medial lateral (M–L) axis, there is no

significant difference of the CoP displacement, while in the A–P axis, the CoP of parkour practitioners is less displaced (Fig.2.19). Trial population did not affect the TTS (**H7**). A–P DPSI changes depending on the population (Table 2.9).

Height factor Trial height did not affect significantly the CoP area, the TTS and the DPSI value (**H8**).

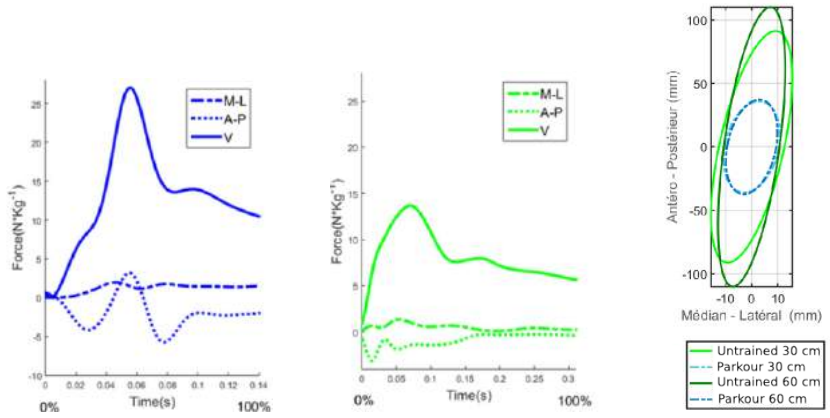

(a) (b) (c)

Figure 2.19: In **(a)** representative profiles of the GRFs of an untrained landing from 60 cm. In **(b)** representative profiles of the GRFs of a parkour precision landing from 60 cm. In **(c)** the CoP confidence ellipsoids of the untrained and precision landings at both heights: 30 cm and 60 cm.

2.4.3.6 Smoothness

Technique factor Parkour traceurs landed using a soft technique(**H9**). The knee joint was flexed to 116 degrees (30 cm) and to 129 degrees (60 cm) in the precision technique, and to 109 degrees and to 114 degrees respectively in the roll technique. Untrained participants landed stiffly with 65 degrees and 84 degrees of knee flexion respectively (Table 2.6). The jerk of the CoM trajectory and the cost value of the *minimum-torque-change* criterion were significantly different with the population factor. These criteria were minimized in parkour landings (**H10** and **H11**) (Table 2.10).

Height factor In spite that knee flexion increased with height in all trials (**H9**), untrained participants performed a stiff landing technique (84 degrees) at 60 cm. The jerk of the CoM trajectory was not significantly different with the height factor in untrained and roll landing trials. The cost value of the *minimum-torque-change* criterion was significantly different with the height factor in all trial types.

Table 2.10: Smoothness expressed in terms of maximum knee flexion and studied optimization criteria normalized with the cost values of the untrained population.

	Untrained		**Precision**		**Roll**	
	30 cm	60 cm	30 cm	60 cm	30 cm	60 cm
K-F'$[deg]$	64.8	83.7	116.2	129.3	109.2	113.8
$\mathbf{J_{jerk}}$	1†‡	1†‡	.35∗	.44	.36	.37
$\mathbf{J_{tc}}$	1† ‡ ∗	1†‡	0.22∗	0.22	0.56∗	0.56

Note. **K-F'**, knee flexion from anatomical pose;
$\mathbf{J_{jerk}}$ *minimum-jerk*; $\mathbf{J_{tc}}$, *minimum-torque-change*.
∗ 30 cm significantly different to 60 cm ($p \leq 0.025$).
† untrained significantly different to precision ($p \leq 0.0125$).
‡ untrained significantly different to roll ($p \leq 0.0125$).

2.4.4 Discussion

When landing and stabilizing, as in the precision technique, flexing more the lower extremity joints and extending the landing phase duration seems to help traceurs land smoothly, stably and to reduce the peaks of all GRF, the joint angular velocities, the joint torques and the joint power. The increase of the landing phase duration and a considerable flexion of the lower-limbs may allow traceurs to distribute torques along the landing phase in order to reduce the associated peak demands and damp the impact force. Also, it induces more mechanical energy generation for energy dissipation. When rolling after landing, traceurs preserve the softness of the technique but without extending the landing phase duration. Rather, they change the lower extremity joint configuration at IC and control the hip flexion later, to continue dissipating the energy of the impact with the roll that follows the landing.

2.4.4.1 Kinematics in parkour landings

At IC, traceurs landed with the hip and knee more flexed than untrained participants who landed straighter (**H9**). It has been reported [Cortes 2007] that when untrained participants land on their forefoot only (the heel does not touch the ground as in precision technique), they show significantly lower knee and hip flexion compared with landings that include heel contact. Moreover, in the same study, it was suggested that the forefoot technique requires the participants to have a straighter position at initial ground contact to stabilize themselves. However for traceurs executing precision landing, stability was significantly higher compared to untrained participants (see later Subsection 2.4.4.6 for the discussion about postural control) suggesting that a straight pose does not necessarily mean better stability. We suggest that in the case of precision landing, the body configuration at IC allowed traceurs to land with their center of mass closer to the center of the base of support. Moreover, landing on their forefoot and with the body more flexed, allowed traceurs to progressively flex their lower-joints in order to damp the impact and control their balance using eccentric loading. In the case of roll landing, traceurs landed also more flexed at IC but with the body tilted forward, to damp

the impact and to facilitate the impulse with the knee extensors afterwards. In the roll technique, we also observed that at 60 cm traceurs landed with the hip and knee slightly more extended than when landing from 30 cm height, while in the precision technique, the joint angles seemed to be less modified. This suggests that the precision technique remains more constant at IC when the height is changed, while the roll technique seems to be adjusted with the height by controlling the knee and hip extension to simplify the roll that follows the landing.

When increasing the height from 30 cm to 60 cm, precision and untrained techniques induced significantly more range of motion (RoM) of the hip, knee and ankle joints. The reason may be due to the initial landing velocity which is higher at 60 cm, which may have induced more flexion of the joints after contacting the ground. For untrained landing at 60 cm, ranges of motion and initial joint angles reported in the literature [Decker 2003] are similar to the results presented here. Moreover, only the hip and ankle angular velocities increased significantly with height in the untrained and precision landings, probably because the knee had more time to reduce the initial velocity to zero due to its higher RoM. Moreover, more mechanical work of the knee extensor muscles may allow to reduce the joint peak velocity. This was not the case for the roll technique (especially for the hip joint), because this technique does not require stabilization after landing, but rather rolling. Thus the hip angular velocity was not required to be zero at the end of the landing phase.

2.4.4.2 Kinetics in parkour landings

Peak GRF of untrained and parkour landings were similar to those reported in the literature [Puddle 2013, Standing 2015, Devita 1992, McNitt-Gray 1993], confirming that parkour landings reduce the impact GRF and the loading rate (**H1**). Moreover, we showed that parkour techniques allow for decreasing antero-posterior and medial-lateral forces (**H1**) which could help to avoid injuries like ACL ruptures [Steele 1990]. This may also help traceurs to land softly (**H8**) and control their balance without significantly deviating their center of mass (**H6**, **H8**). For the roll technique, it is suggested that traceurs do not dissipate all the energy in the landing phase, but also during the roll that follows the landing. This continuation of the motion into rolling could explain why roll landing requested significantly lower peak joint torques at the ankles plantar-flexors than untrained landing. Moreover, not contacting the heel with the ground in parkour landings increases the lever arm between GRF and ankle joint center but does not imply higher torques than those generated at the ankle joint by untrained participants to counteract the induced rotational motion around the ankle. However, if the height increases significantly and traceurs cannot continue rotating their lower extremity joints, higher torques might be necessary to counteract the motion.

2.4.4.3 Dynamics in parkour landings

Considering inverse dynamics in the untrained landings, our results are consistent with those in the literature [Devita 1992, Mccaw 2013, McNitt-Gray 1993]. The

reason why knee and ankle plantar-flexors torques increased significantly from 30 cm to 60 cm landings (**H3**), may be that both joints require more extension torques than the hip for damping the landing, while the hip flexion and extension torques are more involved in the stabilization of the upper trunk. It has also been suggested [Devita 1992] that the hip eccentric mode is used to absorb the impact whereas the hip concentric mode to keep the upper body aligned over the legs. In the present study, upper trunk stability was achieved by both eccentric and concentric modes because flexors and extensors were used to maintain balance (landing from a horizontal distance of 50 cm). This phenomenon was principally observed in untrained landings. In the precision technique, the concentric mode was significantly less used than in untrained landings, presumably because the landing was more stable due to a better postural control (See discussion in Subsection 2.4.4.6 about postural control and refer to **H6**).

It has been shown that traceurs can develop high eccentric joint torques in the knees when performing long jumps compared to other power athletes [Grosprêtre 2016]. In the present study, knee extensor torque was significantly higher in the untrained technique than in the precision technique when landing (**H2**). One reason might be that extending the landing phase duration allows traceurs to redistribute torques along the time and thus decrease the peak joint torques and peak joint power demands (**H2**, **H4**). Moreover, traceurs are able to reduce the GRF peak more significantly than untrained participants (**H1**) which influence the joint torque calculation.

2.4.4.4 Mechanical power in parkour landings

The ankle plantar-flexor peak power was significantly higher in untrained landing (**H2**) probably because of the heel contact with the ground. Because of this, the impact force may have induced higher peak angular velocity of the ankle (note that the GRF were higher during untrained landings (**H1**). Moreover plantar-flexor power in precision technique was significantly higher than in roll technique when the height increased to 60 cm (**H3**). This may imply that for greater heights and when it is feasible to roll, traceurs should avoid landing with the precision technique and use instead a different strategy such as the roll technique. Using the roll technique might prevent traceurs to experience an imbalance of the impact load with the ability of the musculoskeletal system to respond to the stress induced by this loading. Furthermore, it has been shown [Grosprêtre 2016] that eccentric torque capability was greater in traceurs than in power athletes and gymnasts. In the present study we observed that regardless of this capability, parkour techniques induced lesser peak torques and power at the joints (**H2**) than untrained landing.

2.4.4.5 Energetic performance in parkour landings

Mechanical work increased with height (**H4**), as reported in literature, essentially because of the increase in potential energy to be dissipated [Yeow 2009]. Total

eccentric work was significantly higher in precision technique than in roll and untrained landings (**H4**), because the landing phase duration is extended and the joint RoM increases with precision landing. Thus, precision technique induces more active energy dissipation with less efficiency in terms of energy transformation, and requires more conditioning of extensor muscles. We showed that in untrained technique, ankle plantar-flexors and knee extensors were the main mechanisms of energy dissipation through negative mechanical work, which is similar to previous results reported in the literature for stiff landing [Devita 1992, Zhang 2000]. Particularly, untrained participants performed more mechanical work with the ankle than traceurs from 30 cm, probably because they paid more attention to the stability and used their ankles to stabilize themselves. Also, untrained participants performed more eccentric work with the knee when landing from 60 cm. This observed change in strategy may be explained by the fact that when height increases, untrained participants use more their knee extensor muscles to dissipate energy. It is also interesting to see the way traceurs shared the mechanical work across lower-limbs, which was similar for the precision and the roll technique. In this allocation, the knee accounted for half of the mechanical work needed for energy dissipation (**H5**) while the hip and ankle uniformly shared the rest of the energy dissipated with the lower-limbs. This highlights the importance of the knee joint for energy dissipation, and an interesting compromise for sharing the loads with the hip and ankle joints in parkour landings.

2.4.4.6 Postural control in parkour precision landing

Parkour practitioners showed a significantly better dynamic postural control performance than untrained people when executing precision landings (**H6**), specially in the A-P direction (Fig. 2.19c). From the representative force profiles in Fig. 2.19a and b, it can be observed that there is more regulation of the force in the A-P axis during untrained trials. In fact, the area of the confidence ellipsoid of the CoP was significantly higher in untrained landings (Table 2.9). This result is also reflected in the A-P DPSI (which depends on the A-P force) that is significantly different in the A-P direction. In terms of TTS, there were not significant differences (**H7**). On the one hand, untrained participants landed stiff to get stable faster inducing as a consequence a short landing phase duration (see also the representative force profile in Fig. 2.19a). On the other hand, traceurs landed in a pose where the CoM is closer to the center of the support polygon (see Fig. 2.14) which improves stability (in spite of the induced longer duration of the landing phase in precision landings). Note that muscle pre-activation strategy, which is modulated with practice, affects the landing performance [Yeadon 2010].

2.4.4.7 Motion smoothness in parkour landings

Traceurs landed using a soft landing in precision and roll landing techniques (**H9**. This might allow traceurs to reduce the impact forces at landing (**H1**) [Devita 1992],

a highly important parameter in injury prevention. Moreover, executing a soft landing allow traceurs to perform aesthetic landings, for example, by minimizing torque change in the joints (**H11**). The smoothness of parkour motion is also reflected by the jerk trajectory of the CoM (**H10**) which is related to the global body motion and the interaction with external forces (Newton's laws of motion). These results show that augmenting knee flexion allows traceurs to decrease the impact forces and provide a good performance indicator of aesthetic motions (such as those performed in freerunning).

2.4.4.8 On parkour training and injury prevention

It has been reported that stiffer landing [Devita 1992] could manifest to patellar tendinopathy as peak joint velocities and torques increase [Bisseling 2008]. Therefore, parkour coaches should closely monitor the landing strategy and the joint load frequency to reduce the patellar tendon loading and the risk of injury. Hip flexion at IC and not contact of the heel with the ground seem to help traceurs execute soft landings [Devita 1992] by increasing the lower-joints flexion. However, high impact pressure concentrated in metatarsal bones and high vertical reaction forces may cause metatarsal fractures [Kavanaugh 1978]. Therefore, traceurs are encouraged to avoid using the precision technique when the height is important. Moreover, when the landing height is increased, ankle taping could be helpful to enhance peak plantar-flexion strength [Hopper 2014]. In the parkour community, an unwritten rule imposing a maximum knee flexion of 90 degrees in landings is commonly used. In this study, traceurs exceeded 90 degrees with both techniques and this strategy was beneficial compared to landings performed with less than 90 degrees because it helped to smooth the landing impact lowering the GRF. For an optimal performance (considering the eccentric force-velocity relationship of the muscles) during landing, extensor muscles should be properly warmed up and intense fatigue should be prevented. This may help to enhance and maintain the capacity of developing the required eccentric torques [De Ruiter 2001]. Extensor muscles should be well conditioned for executing parkour landings, taking into account that in both techniques, the knee accounted for half of the energy absorbed by the lower-limbs.

2.4.5 Conclusion

Parkour techniques appear to be optimal to reduce impact forces, peak joint torques, peak angular velocities and peak power in the lower joints, and to improve postural control and motion aesthetics because of the soft landing that traceurs perform. Recommendations about how to avoid injuries and how to condition the lower limbs were provided, which are of special interest in parkour landings that turns out to be the most risking parkour technique (see Section 2.2). Moreover, this study can be used to improve parkour training and performance. It can also be of interest for

other sports where landing dynamics is high such as gymnastics.

In this study, GRFs, kinematics, dynamics, energetics, postural control and motion smoothness of parkour landings were presented for the first time. For a better understanding of the rolling technique, landings with higher horizontal speeds and an analysis of the roll phase are needed. A limitation of this research is that traceurs were recorded inside a laboratory and at limited heights (because of untrained participants), which differs from natural parkour practice. Moreover, this study did not consider upper-limbs which might also be of interest when studying parkour motions. The next study will consider full body motion and higher heights.

2.5 Regulation of Angular Momentum in Parkour Precision Landing Technique

So far, our parkour motion analysis has been limited to the biomechanics of lower-limbs and the study has only considered landings from low heights. In this last section, we consider the whole-body model introduced in Section 2.3 and analyze higher jumps from higher heights. From the previous study, several mechanical variables were computed and presented. However, key performance variables that could account for whole-body dynamics and that might be useful for generating parkour landing motions have not been yet clearly identified. The objective of this study was to analyze whole-body motion. In particular, we studied angular momentum regulation in parkour precision landing.

2.5.1 Introduction

Angular momentum was shown to be regulated during daily life activities such as walking [Herr 2008] or during more complex motions (also observed in parkour and freerunning) like somersaults and twists [Frohlich 1979]. In [Herr 2008] it was suggested that during gait, segment-to-segment angular momentum cancellations regulate the total angular momentum expressed at the CoM position and that active generation of angular momentum is a key strategy for bipedal manoeuvrability and stability. According to Euler's second law of motion, the derivative of the angular momentum (AMD) expressed at the CoM position is equal to the sum of the external net torques applied to the body. This sum can be regulated by humans when contacting the ground at landing to maintain equilibrium and avoid tipping motions [Sardain 2004]. In relatively recent studies, information from angular momentum observed in human movements has been transferred to anthropomorphic avatars [Hofmann 2009] and to bipedal robots [Yun 2011, Goswami 2004] control.

Motivated by these studies, we proposed to conduct a whole-body biomechanical study by analyzing the AMD expressed at the CoM in parkour precision landings performed by experts. We hypothesized that traceurs regulate the AMD among the three principal axis of rotation to achieve such a dynamic motion as precision landing. To extend our analysis, we also studied postural control strategies by looking into segmental contributions to the total AMD expressed at the CoM position.

2.5.2 Methodology

2.5.2.1 Experimental protocol

Five healthy trained male traceurs (age: 22.2 $\pm$ 4.8 y, height: 1.73 $\pm$ 0.04 m, mass: 66.6 $\pm$ 5.1 kg) volunteered for the study. The traceurs' experience in parkour practice was 5.4 $\pm$ 2.1 years. The subject exclusion criterion was based on history of lower extremity injuries or diseases that might affect jump and landing biomechanics. The experiments were conducted in accordance with the standards of the Declaration of Helsinki (rev. 2013) and approved by a local ethics committee.

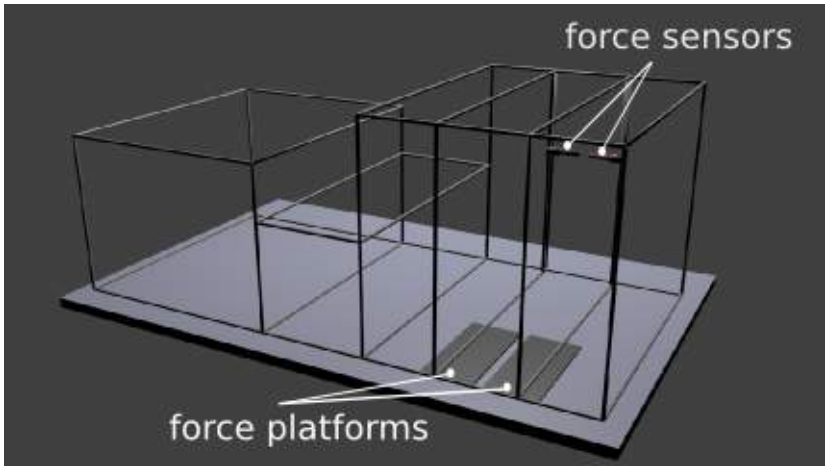

Figure 2.20: 3D modeling of the adapted tubular structure utilized for accomplishing the experimental protocol.

(a) **(b)**

Figure 2.21: Parkour precision jump (**a**) and landing (**b**) techniques performed inside a motion capture laboratory.

Participants performed a warming up session followed by a familiarization period during which the protocol instructions were provided to them, and during which they familiarized with the lab environment. The landing protocol was designed to include a jump height of 75 % of the height of the participant and a landmark placed at a distance equals to the square of the jump height. For setting-up the protocol, a tubular structure used for parkour training was modified and assembled according to the design shown in Fig. 2.20. During the recording protocol, participants were asked to land on the target specified by a landmark on each force plate using the parkour precision technique as shown in Fig. 2.21.

2.5.2.2 Data acquisition

A total of 8 successful repetitions per participant was recorded. 3D whole-body kinematic data were collected using 14 infra-red cameras sampling at 400 Hz (Vicon,

Oxford Metrics, Oxford, UK) and recording 48 reflective markers placed on the participant's body. Note that in comparison with the previous study, in this research we used two more cameras (14 instead of 12), full body motion (considering upper limbs, trunk and neck), and we use the double of the sample frequency because the recorded motion was more dynamic (in the previous study we sampled at 200 Hz). Markers were located on the participants' body based on Wu and Dumas recommendations [Dumas 2007b, Dumas 2007c, Wu 2002, Wu 2005] as follows: the first, and fifth metatarsal, second toe tip, calcaneus, lateral and internal malleolus, anterior tibial tuberosity, lateral and medial epicondyles of knee, greater trochanter, posterior superior iliac spine and anterior superior iliac spine, procesuss xiphoideus, incisura jugularis, seventh cervicale, tenth thoracic vertebra, acromioclaviculare, medial and lateral epicondyle, ulnar and radial styloid, second and fifth metacarpal heads, second fingertip, sellion, occiput, right and left temporal (See Fig. 2.13 for more details). Two force plates (AMTI, Watertown, MA, USA) embedded into the floor in order to record landing GRFs and two rigid handle bar sensors (SENSIX, Poitiers,Vienne, France) with a diameter of 63 mm placed on a parkour tubular structure to record take-off GRFs, were used sampling at 2000 Hz (see Fig. 2.20). Force data were used to define the onsets used to divide the parkour motion into phases.

2.5.2.3 Data analysis

Kinematics and kinetics were processed with the same cut-off frequency [Kristianslund 2012] using a low-pass Butterworth digital filter of 4th order applied in a zero-phase. A cut-off frequency of 35 Hz was used after a residual analysis [Winter 2009]. The score method was used to better estimate the center of hip and shoulder joints [Ehrig 2005]. Inverse kinematics was solved by minimizing the squared distance between recorded and virtual markers (global optimization method [Lu 1999]) using OpenSim software with the model introduced in Section 2.3. All momenta computations were performed using a custom made program with a whole-body model and a physics engine [Carpentier 2015]. The landing phase was defined in the same way as in Subsection 2.4.2.4. *AMD* expressed at the CoM was computed based on the equations provided in Section 2.1.8. The three components of the *AMD* vector were labelled as "FAMD", "SAMD" and "TAMD". *AMD* was normalized by the height and the body weight of each participant.

2.5.3 Results

Regulation to zero of the 3 components of the *AMD* was observed (Fig. 2.23). A recurrent segment cancellation strategy is revealed (Fig. 2.22). It appears that at the beginning of the landing phase, pelvis, torso and head are not used for stabilization while upper and lower limbs work together to regulate the *AMD* of angular momentum. Small adjustments of total *AMD* at the CoM were observed in the end of the motion by upper limbs at the frontal and transversal planes.

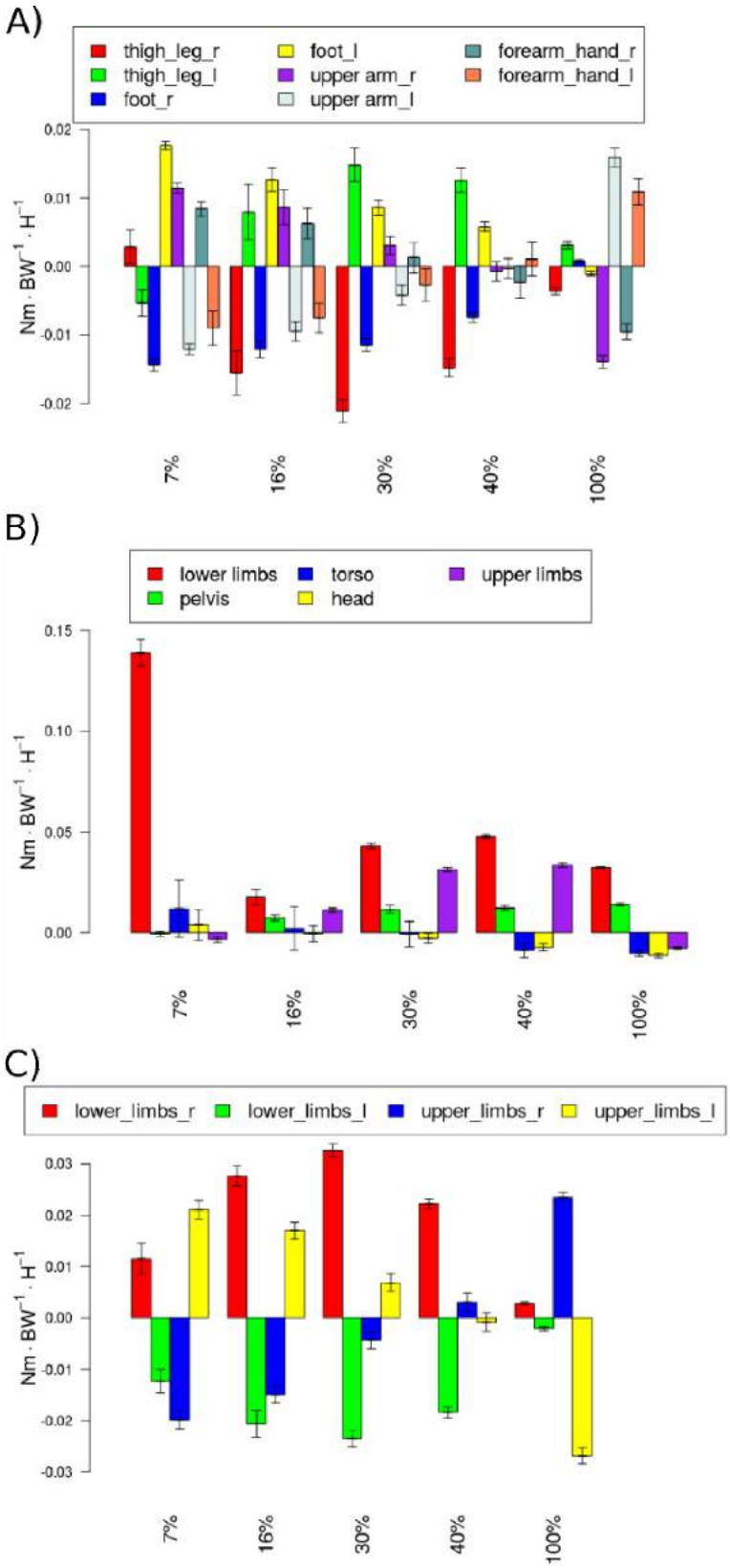

Figure 2.22: Segment groups contribution to total *AMD*. In (**A**), contributions to FAMD. In (**B**), contribution to SAMD. In (**C**), contributions to TAMD. Angular momentum derivative is normalized by the height and body weight. The time is normalized from 0% to 100%

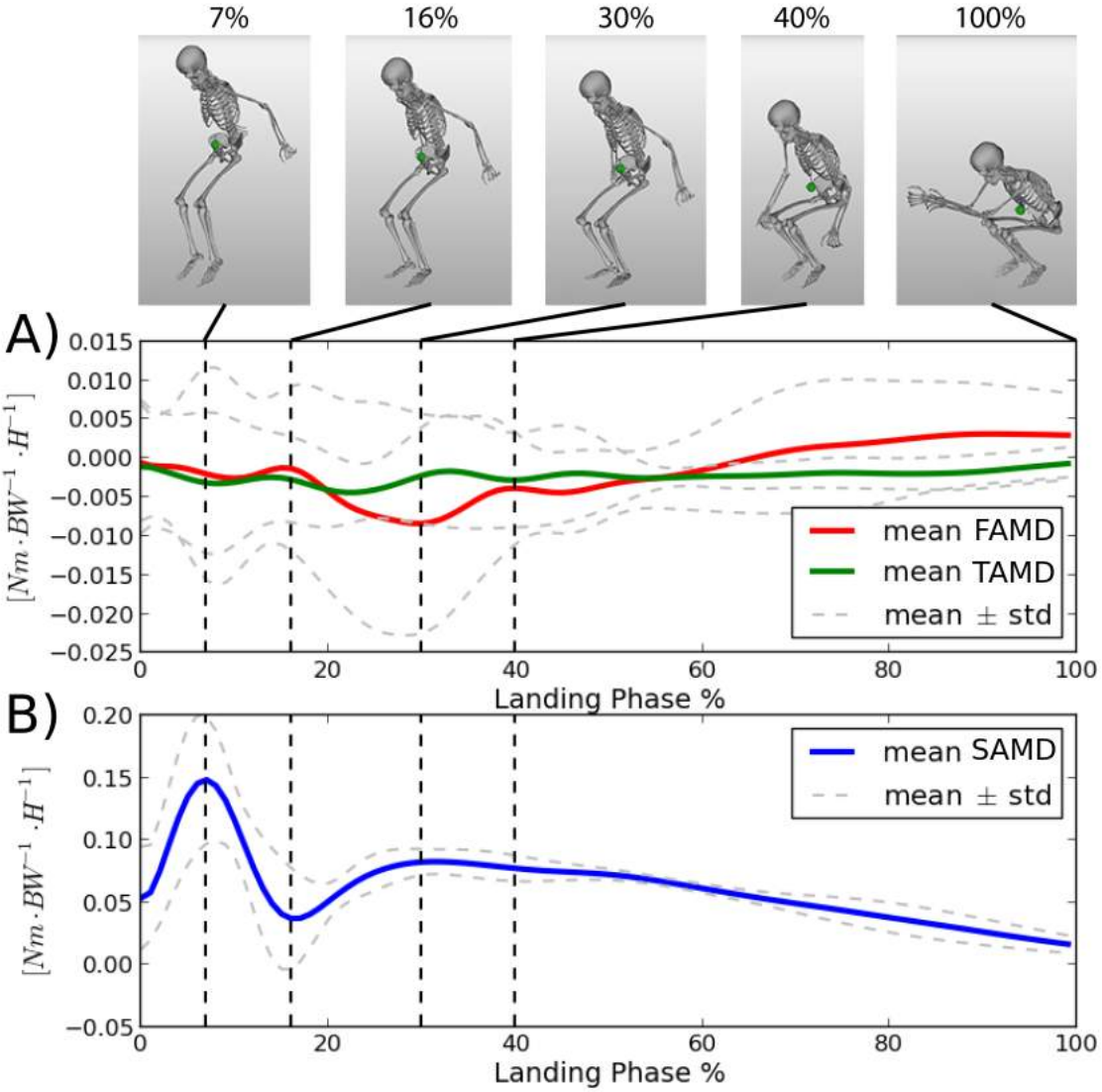

Figure 2.23: Mean (±std) of the *AMD*. In (**A**, red), the frontal *AMD* around A-P axis "FAMD". In (**A**, green), the transversal *AMD* around vertical axis "TAMD". In (**B**, blue), sagittal *AMD* around M-L axis "SAMD". In the top, snapshots of representative configurations extracted from the inverse kinematics computation, of a participant executing the precision landing technique.

2.5.4 Discussion

The derivative of angular momentum (*AMD*) appears to be minimized by the mechanical actions of whole-body segments during parkour precision landing (Fig. 2.23B). This make sense as the *AMD* expressed at the CoM is directly linked to the body's angular acceleration, according to Newton's law. Our study also reveals complex strategies of traceurs such as opposed segment cancellations and temporal

organization of the motion.

2.5.4.1 Frontal AMD around A-P axis "FAMD"

FAMD is regulated around zero with small variations ($\pm 0.01 Nm \cdot BW^{-1} \cdot H^{-1}$). A strategy of right and left segments cancellation is observed (Fig. 2.22) which contributes to minimize the FAMD. In the beginning of the landing phase (up to 40 %), the control comes from lower limbs contribution especially. This might be a strategy of the jumper to prevent injuries such as ACL or sprains by avoiding excessive varus-valgus motions. Furthermore, an important segment cancellation of the arms at the end of the motion phase is observed. It seems that this is a potential error correction strategy that insures the final regulation to zero of the FAMD. This might be linked to the fact that the traceur has almost reached the lower limb's joint limits and therefore needs another strategy to control FAMD. This is why the traceur chooses to use the arms which are free to move to compensate the small deviation.

2.5.4.2 Sagittal AMD around M-L axis "SAMD"

Fig. 2.23 reveals a perturbation rejection profile of the SAMD (up to 40% of the movement) where the lower limbs contribution at the beginning of the landing phase is considerable. This is not surprising as the main tipping effects occur in the sagittal plane after a standing long jump.

2.5.4.3 Transversal AMD around vertical axis "TAMD"

TAMD is regulated around zero with small variations ($\pm 0.02 Nm \cdot BW^{-1} \cdot H^{-1}$). The same segment cancellation strategy as in FAMD is used to minimize the *AMD* in the transversal plane. The upper limbs segment cancellation is important at the end of the phase and the same reasoning as for FAMD applies.

2.5.4.4 Segment cancellation interpretation

At first glance, inter-segment cancellation does not contribute to *AMD* of angular momentum. We interpret it in terms of an energy storing strategy for potential mechanical action to control stability. Potential, because if the motion stays symmetrical, the contribution is null, otherwise, the inter-segment difference generates the required torque at the CoM. In this way, the mechanical action can be generated precisely and instantaneously (by making profit of the motion dynamics) instead of producing it from scratch.

2.5.5 Conclusions

In this study, a whole-body analysis of angular momentum during parkour precision landing was presented. It is interesting to highlight that whole-body dynamic strategies to regulate the *AMD* at the CoM to zero were observed. This might serve

as a starting point to test if performance variables linked to angular momentum are being controlled steadily by the brain. This study provides also a basis for controlling dynamic landing performances and for generating such motion using the robotic framework (human-inspired motion).

2.6 Additional Movements

During this work, an extensive database of parkour movements were collected and processed. The database includes jumps, landings, vaultings and climbing motions that were not further analyzed during this thesis. The database contains more than 700 trials divided as follows:

- 108 motions were processed for the lower limb motion study of parkour landings.
- 56 motions including take-off, flight and landing motions were processed for the whole-body motion study of parkour landings.
- 176 parkour vaulting motions including the safety vault and kong vault techniques were processed and not yet reported (Fig. 2.24).
- 88 motions of techniques used to train for parkour climbings including the pull-up and muscle-up techniques were processed and not yet reported (Fig. 2.25).
- More than 110 motions of a fatigue protocol of muscle-up technique were recorded and partially processed.

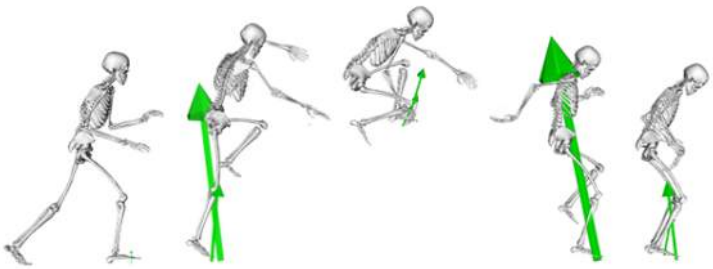

(a) Safety vault

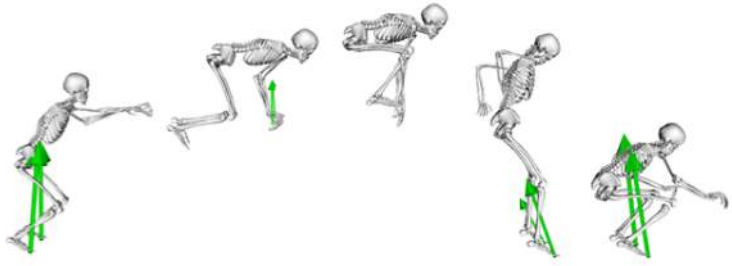

(b) Kong vault

Figure 2.24: Vaulting techniques

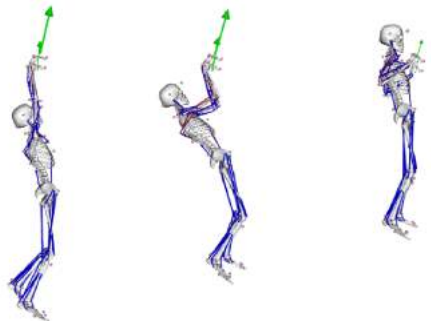

(a) Pull-up

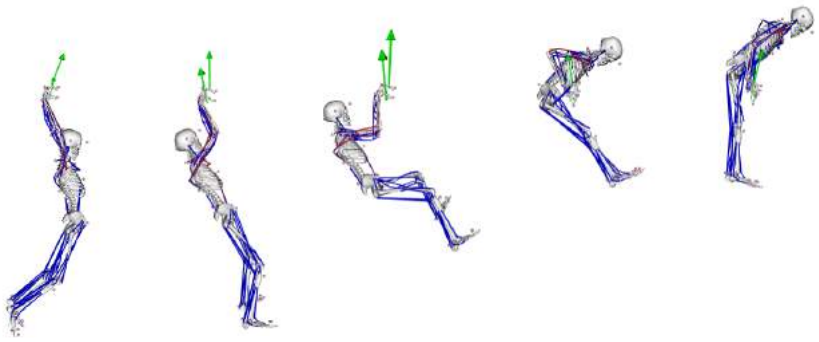

(b) Muscle-up

Figure 2.25: Climbing techniques

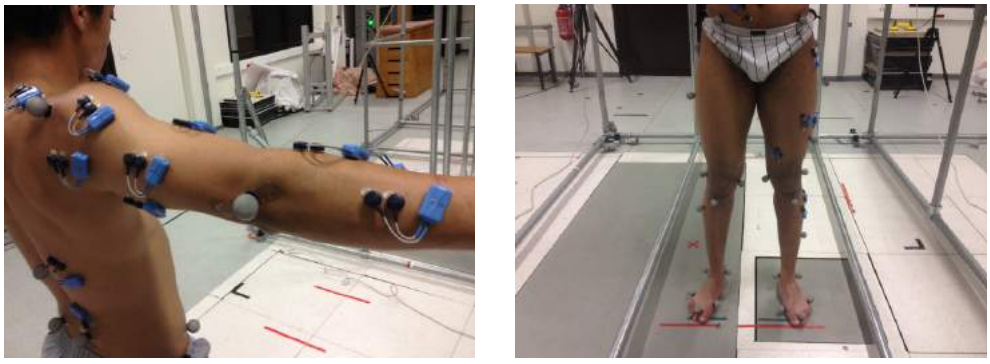

(a) **(b)**

Figure 2.26: Wireless EMG sensors placed on the upper limbs (**a**) and lower limbs (**b**) of a recorded participant. EMG recording included also the trunk and neck muscles.

In this manuscript, only jump and landing strategies have been presented to illustrate the interdisciplinary approach proposed in this thesis. Unfortunately, the biomechanical analysis of the remaining movements was not exploited in this thesis because of the lack of time. Moreover, as described in this chapter, a whole-body model including the principal stabilizer muscles for executing the parkour motions

was built. During our recording sessions, we also collected muscular activity of lower limbs, upper limbs, trunk and neck muscles through surface EMG sensors as shown in Fig. 2.26. These studies will be done in a near future.

2.7 Conclusion and Perspectives

In this chapter, an epidemiological study of parkour in France, a musculoskeletal model for analyzing and generating parkour movements and several biomechanical studies of the parkour precision landing technique were presented. For the continuation of our research, the key information extracted from this chapter can be summarized as follows:

- Whole-body strategies were observed when regulating the derivative of angular momentum expressed at the CoM in parkour landings.
- Ground reaction forces, joint torques and joint mechanical power are lowered by parkour practitioners.
- Time and energy expenditure is increased in parkour landings.
- Motion is smooth and stable.

From these conclusions, we decide to chose the derivative of angular momentum expressed at the CoM and the control of net GRFs (which corresponds to the derivative of linear momentum according to Newton-Euler laws of motion) as performance variables of the motion. In next chapter, this discussion is extended and a method to test whether these variables are being controlled steadily by the brain is presented.

Finally, it is important to recall that though the biomechanical methodology provides an efficient tool for analyzing human movement, it is known to have some limitations. Sources of errors are the simplifications made when modeling the human body (e.g. modeling segments as rigid bodies, number of degrees of freedom of the model, or simplifications when modeling complex human articulations), the estimation of anthropomorphic parameters and the data processing (e.g. motion reconstruction, filtering of the noise, soft tissue artifacts). Future works may assess the additional movements presented in the previous chapter. Moreover, more rigorous epidemiological studies are needed including longitudinal studies. In this direction it will be interesting to consider other factors such as biological, sociological and psychological ones to better understand the injuries mechanisms in parkour.

Chapter 3

Identification of Motor Tasks in Parkour Motion: An Extension of the UCM Theory

"Repetition without repetition" [Bernstein 1967].

Contents

Performance task variables extracted from the previous biomechanical study allowed for describing the mechanical behavior of traceurs executing parkour landing motions. Particularly, in the whole-body study of the parkour precision landing technique, strategies that contribute to regulate angular momentum at the CoM were observed. In this chapter, we extend this observation and propose hypotheses about how the brain coordinates this motion. To this end, we base our analysis on the uncontrolled manifold theory (UCM) to assess if key hypothetical performance

variables (tasks) are being controlled steadily [Hasan 2005] by the brain. In this chapter, we will use the definition of motor task stability as reduced variability of hypothetical performance variable across repetitions as it is used in the motor control community [Latash 2016]. The term mechanical stability will be used when analyzing the motion in the context of robotics or biomechanics [Sardain 2004].

The chapter is organized as follows:

- First, the most relevant theories of motor control in the context of this thesis are presented. At the end of this section, we present the mathematical framework of the UCM theory.
- Secondly, a mathematical framework derived from robotics to formulate motor tasks in human motions is introduced.
- Afterwards, we propose an extension of the UCM theory for studying human dynamic motions.
- At the end, we show a case study of the parkour take-off and landing techniques where the task formulation and the extension of the UCM theory are applied.

3.1 Motor Control

Motor control aims at investigating how the CNS produces coordinate movements in a purposeful manner. To this end, hypotheses about precise variables of physical and physiological processes that are involved in the generation of human movement have been formally proposed as theories for motor control. These theories are split into two principal approaches: computational and physiological. Common to both approaches is the concept of redundancy in human motion. In this section, the question of redundancy in human motion science is briefly introduced. Then, a brief review of computational and physiological approaches to study redundancy in human motion is presented. The notion of synergies, the Uncontrolled Manifold theory (UCM) and the equilibrium point theory (E-P) are then introduced.

3.1.1 Redundancy in human motion

The problem of motor redundancy [Bernstein 1967] is related to the fact that more degrees of freedom than the minimum needed for generating a given movement, are available to the central nervous system (CNS). This implies that a movement can be realized through different combinations of motor-neurons, muscles and joints activity patterns. Consider for example the upper limbs of the human body. If we model the upper limb motion with 3 degrees of freedom at the shoulder joint (or glenohumeral joint), 2 degrees of freedom at the elbow joint and 2 degrees of freedom at the writs joint, we have at least 7 seven degrees of freedom available. Note that in order to describe the position and orientation of a solid in the 3D space,

6 degrees of freedom are necessary. Thus, in our example, there will be at least one kinematic degree of freedom redundant in the execution of a given geometric task with the upper limbs. This is a simplified case. In fact, redundancy in human motion increases if we model whole-body joints, if we consider the organization of the motion at the level of muscles (many muscles for one joint and bi-articulated muscles) and at the level of motor units (number of muscular fibers innervated by an neuron axon). Redundancy in human motion is investigated to better understand how the CNS chooses a particular strategy from many possible ones in order to achieve a given motion objective.

Theories of motor control addressing redundancy can be split into a computational and physiological approaches. Computational approaches provide a theoretical framework for studying motor control by specifying the desired states and the outputs of the system with a computational process related to a given task goal. The solution is unique and relies on the assumption that the CNS models interactions between body segments and between the body and the environment. These approaches are principally based on motor primitives [Tresch 2006, Flash 2005] and optimization [Nelson 1983, Todorov 2002]. Physiological approaches provide a theoretical framework for studying motor control as a physiological process linked to the physics of the system. These approaches consider redundancy not as a problem, but rather as a benefit for the CNS [Gera 2010]. According to the motor abundance principle [Gelfand 1998], redundant degrees of freedom improve the capacity of the central nervous system "CNS" to find a stable motor task solution. In motor control, stability is defined in terms of reduced inter-trial variability of a task across repetitions. This problem is not solved by finding a unique optimal solution, but by facilitating families of solutions that are capable of solving the task. This is achieved by co-varying elemental variables (e.g. joint patterns or muscular activity) in such a way that the overall output remains close to a required value (Uncontrolled Manifold Theory [Scholz 1999]). Apart from explaining redundancy, physiological approaches provide a framework to describe how physiological variables might be used by the brain to control muscles (Equilibrium-Point Theory [Feldman 1966]).

3.1.2 Motor synergies

Synergies in human motion have been studied to analyze the synergetic action of elements of the motor system such as joints, muscles, or motor units, in order to generate motion. According to the definition in human motion, a synergy means that elements of the motor system work together to accomplish a goal.

In the literature, three types of motor synergies have been proposed:

- Synergies where parallel changes in activity are observed, even if no obvious tasks is being accomplished. These synergies can be observed for example in clinical cases, where patients show stereotypical muscle activation patterns.

- Synergies where parallel changes in activity are linked to a task. Studies of this type of synergies are based on matrix factorization techniques such as principal

component analysis (PCA), independent component analysis (ICA) and non-negative matrix factorization (NNMF) [Tresch 2006]. Motor primitives are an example of these synergies.

- Synergies where parallel changes in activity are linked to the stabilization of a task. The Uncontrolled Manifold theory, which is introduced in the next subsection, is an approach to study this synergy type.

3.1.3 Uncontrolled manifold theory

The uncontrolled manifold theory (UCM) [Scholz 1999] is a task-based approach that studies the variability between two vectors that are orthogonal to each other, to identify tasks that are being controlled steadily by the CNS. The deviation of elemental variables (e.g. joints configuration) from a mean behaviour (e.g. the mean joint configuration) across repetitions is projected onto the null space of the task Jacobian. Any variation in this null space does not affects the task execution while any variation in its orthogonal space affects it. The UCM theory states that when the variability of the deviation projected in the null space (UCM) is greater than the variability of its orthogonal space, the motor task is being controlled steadily by the CNS.

The UCM theory is one of the most used approaches to explain one of the most important characteristics of human motion: variability (or "repetition without repetition" [Bernstein 1967] as it was pointed out half a century ago by Nicolas Bernstein when describing the process of practice in human motion). The UCM theory assesses the variability of the space of performance variables compared to the space of elemental variables (e.g. joints, muscles) that are coordinated for the execution of the movement. Motor tasks can be defined as performance variables used by the CNS to plan, time and control the movement execution. The UCM theory is linked to the principle of motor abundance [Latash 2000] that considers motor redundancy as a positive benefit for the CNS rather than being treated as a problem. More specifically, motor abundance principle allows for different combinations of joint and muscle coordinated strategies to purposefully achieve a given task performance. In this sense, multiple motor solutions might exist rather than a single optimal solution, and reduction of degrees of freedom is not a requisite to explain human motion (Subsection 3.1.4). In the context of the UCM theory, it implies that degrees of freedom (DoF) are purposely used by the brain for providing motor task solutions that are stable across repetitions. Motor abundance guarantees the achievement of a task in case of external (e.g. forces) or internal (e.g. muscle fatigue) perturbations that affect the task goal. This implies that abundant DoF, which are not controlled steadily by the brain for the task achievement, can be utilized to guarantee the task execution.

The UCM theory has been applied to the study of various motor tasks. Postural tasks have been studied through muscles modes [Danna-dos Santos 2007] and joint coordination [Hsu 2007]. Tasks such as pointing [Domkin 2005], reaching and

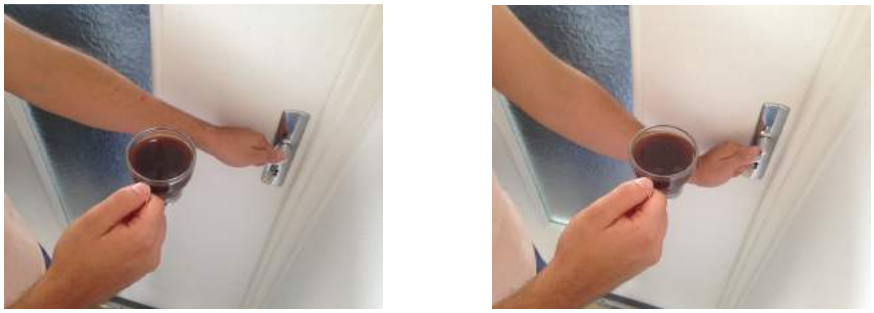

(a) (b)

Figure 3.1: Two tasks executed in parallel: holding the filled coffee cup while avoiding to spill out the coffee and opening the door.

grasping [Fan 2006], sit-to-stand [Scholz 2001], and drawing [Tseng 2006] have also been studied through joint coordination. Force production tasks have been investigated by considering finger forces [Latash 2001] and joint torques [Yen 2009]. Most of these studies only accounted for quasi-static motor tasks, although most of human movements are inherently dynamic. In this chapter, we propose a general framework to extend the formalism of the UCM theory [Scholz 1999] to dynamic movements that requires to consider higher order derivatives of the joint variables (Section 3.3).

3.1.4 Hierarchies of Motor Tasks

The principle of motor abundance is linked to a hierarchical organization of motor tasks. Redundancy is then purposely used to execute more than one task at the same time. A hierarchical structure of motor tasks allows for executing secondary tasks without interfering with the execution of a more important task. For example, let us imagine that we try to open a door while holding a cup filled of coffee. At least, there are two tasks which are likely to be controlled steadily by the CNS: turning the handle of the door and not spilling the coffee (Fig. 3.1). In this case, the door should be opened (secondary task) only if the coffee is not spilled out (primary task). To deal with multiple tasks at the same time, it has been proposed that the human brain could favour a hierarchical organization of motor tasks which are used to accomplish the motion purpose. In fact, it has been suggested that hierarchical organization not only exists at the neuromotor level [Latash 2008], but also at the level of the tasks execution [Todorov 2005, Gera 2010]. Hierarchies in human movement have been supported by studies of motor synergies. As it has been mentioned in the introduction of this chapter, the definition of the UCM theory is linked to the notion of a purposely stabilizing synergy [Latash 2010]. From this, it could be said that the existence of a synergy linked to the steady execution of a task implies that there must be more good than bad variability. From this reasoning, we can deduce that a large amount of good variability is important. However, why should the CNS facilitate large good variability, which does not affect variance of

the performance?

In fact, it has been suggested that good variability is not irrelevant because it favours the CNS to perform different tasks simultaneously (Fig. 3.1) and to deal with unexpected perturbations (e.g. external forces affecting the accomplishment of the task). For example, in [Zhang 2008], participants were asked to produce several levels of a force by pressing with the four fingers on force sensors under stable and unstable conditions. In the unstable condition, moment of force was needed because of the experimental conditions. Results shown that moment of force stabilization was accomplished by participants without adversely affecting the total force stabilization task. These observations show that participants converge on similar solutions when an additional constraint is introduced. The authors suggested that the use of variable solutions allows for avoiding a loss in accuracy of performance when the same elements get involved in another task. Similarly, in [Gera 2010], it was suggested that that a major advantage of motor abundance is that it facilitates simultaneous solutions of multiple task constraints, with minimal interference among tasks or among components of a given task. This study was conducted by examining the effect of manipulating one task constraint on the stability of another. Moreover, notice that there might be tasks which need to be more stabilized than others. In the example shown in Fig. 3.1 it might be possible that not spilling out the coffee is a more important task than opening the door.

3.1.5 Equilibrium-Point hypothesis

Before finishing with the theoretical framework of this section, let us introduce the equilibrium point hypothesis (EP) [Feldman 1966] which supports the UCM theory. The (EP) hypothesis is formulated in terms of position control of reference configurations (RC) [Feldman 1995]. Reference configurations can be observed at the level of the task (e.g. the placement of the hand in the space), at the level of joint (desired joint configuration), at the level of muscles (λ), at the level of motor units and even deeper. Each of these levels is abundant (redundant) and a transformation is needed to go from one level to the other.

In the EP hypothesis, RC of muscles are reached through neural control signals that are supposed to shift the equilibrium state of the motor system. This means that muscle activations and hence the force, vary through tonic stretch reflexes (λ) in relation to the difference between the actual and the threshold muscle lengths, the rate of the muscle length change and the external load. The variation of muscular actions describes an equilibrium trajectory (virtual trajectory) generated by the CNS (as a descending command to muscles) and no complex inverse dynamics calculation is needed. The EP hypothesis has been shown to be adapted for explaining the neurophysiological mechanisms of different movements including multi-joint arm motion [Feldman 1990], eye movement [Feldman 1981], human jaw movement during speech [Flanagan 1990] or arm movement in impaired motor control [Levin 1994]. The EP hypothesis is related to the UCM theory which is at the heart of this chapter if we consider that muscle control is hypothesized to stabilize

final equilibrium states of muscles by using referent configurations. In consequence, EP hypothesis is related to synergies stabilizing task-specific variables.

In the next section, we start presenting our contributions. To this end, we begin by introducing a generalized framework that can be used for expressing dynamic motor tasks in humans and humanoids.

3.2 Tasks Function Formalism in Robotics and the UCM Theory

The task function formalism [Samson 1991] in robotics [Nakamura 1991] can be applied to express motor tasks of anthropomorphic systems. We start this subsection by introducing the task function approach and by drawing the link with the UCM theory.

3.2.1 Task function approach

Let $n = k + 6$ be the total number of degrees of freedom "DoF" of the body, and $\mathcal{Q}$ the configuration space formed by k elemental variables describing the values of the joints plus 6 parameters describing the pose (position and orientation) of a reference frame usually called root frame. The space $\mathcal{Q}$ is a $n-$dimensional manifold which can be locally identified to $\mathbb{R}^n$. In order to express behaviors of humans at the kinematic level, motor tasks can be expressed in terms of positioning specific body segments. Let us denote by $\boldsymbol{q}(t) \in \mathcal{Q}$ a configuration of the body at time t. For notational convenience we will omit to express the dependence on t, except when necessary. Let $\mathcal{M}$ be the space of the task and let us denote by $\boldsymbol{e}(\boldsymbol{q}) \in \mathcal{M}$ a task function. $\mathcal{M}$ is a $m-$dimensional manifold which can be locally identified to $\mathbb{R}^m$. A task function comes down to an output error function whose regulation to zero corresponds to the execution of the task. For instance, a pointing task can be defined by the task function $\boldsymbol{e}(\boldsymbol{q}) = hand(\boldsymbol{q}) - hand_{target}$, which describes the gap between the current hand position $hand(\boldsymbol{q})$ when the body is at configuration $\boldsymbol{q}$ and the expected hand position $hand_{target}$. In order to compute how the task function varies with respect to the body configuration, roboticists use the so called task Jacobian $J_e = \frac{de}{dq}$. It is a m by n matrix whose entries are defined as:

$$\forall i \in 1, \cdots, m \qquad \forall j \in 1, \cdots, n \qquad J_e(\boldsymbol{q}) = \frac{\partial e_i}{\partial q_j}. \tag{3.1}$$

This leads to the UCM theory formulation developed in [Scholz 1999] that is briefly recalled in the sequel.

3.2.2 Mathematical formulation of the UCM theory

Consider that N_r repetitions of a studied movement have been recorded with one participant. For $r = 1, ..., N_r$, let us define by $\boldsymbol{q}_r(t)$ and $\boldsymbol{e}(\boldsymbol{q}_r(t))$ the joint configuration trajectory and a task function trajectory of the r^{th} repetition respectively. Let us denote by $\bar{\mathbf{q}}(t)$ the mean value of the joints configuration trajectory across the N_r repetitions. At each time t, given the definition of the task Jacobian, the first order Taylor expansion of a task $\boldsymbol{e}(\boldsymbol{q})$ around the mean configuration $\bar{\boldsymbol{q}}$ yields:

$$\forall r = 1, ..., N_r, \quad \boldsymbol{e}(\boldsymbol{q}_r) - \mathbf{e}(\bar{\boldsymbol{q}}) = J_e(\bar{\boldsymbol{q}})(\boldsymbol{q}_r - \bar{\boldsymbol{q}}) + \boldsymbol{\varepsilon}(\boldsymbol{q}_r), \tag{3.2}$$

where $\boldsymbol{\varepsilon}(\boldsymbol{q}_r)$ contains higher order terms of the expansion and it is known as a residual. Considering the residual as negligible, one can compute for each repetition r the deviation of the joint configuration $\boldsymbol{q}_r - \bar{\boldsymbol{q}}$ projected onto the nulls pace of the Jacobian matrix $J_e(\bar{\boldsymbol{q}})$ and the deviation in its orthogonal space at each time t as:

$$\boldsymbol{ucm}_r = P_e(\boldsymbol{q}_r - \bar{\boldsymbol{q}}), \tag{3.3a}$$

$$\boldsymbol{ucm}_{\perp r} = (\boldsymbol{q}_r - \bar{\boldsymbol{q}}) - \boldsymbol{ucm}_r, \tag{3.3b}$$

where $\boldsymbol{ucm}_r$ and $\boldsymbol{ucm}_{\perp r} \in \mathbb{R}^n$ are the two projections of the deviation from the reference behavior. $P_e = \mathbb{1} - J_e^{\#} J_e$ is the projector onto the null space of J_e (i.e. $P_e J_e = 0$ and $P_e P_e = P_e$). The inter-trial variance of $ucm_{r=1,\ldots,N_r}$ and $ucm_{\perp r=1,\ldots,N_r}$ respectively denoted by $V_{ucm} \in \mathbb{R}$ and $V_{ucm_\perp} \in \mathbb{R}$, are then normalized by the dimension of each space with $N_{UCM} = \dim(\mathcal{Q}) - \dim(\mathcal{M})$ and $N_{UCM_\perp} = \dim(\mathcal{M})$. Note that in order to report the variability of $\boldsymbol{ucm}_r$ and $\boldsymbol{ucm}_{\perp r}$ independently, one should also normalize by the number of repetitions. Then, an index of motor task control "ITC" can be calculated as the ratio between both variances:

$$V_{ucm} = \sum_{r=1}^{N_r} \frac{1}{n} ||\boldsymbol{ucm}_r||_2^2, \tag{3.4}$$

$$V_{ucm_\perp} = \sum_{r=1}^{N_r} \frac{1}{n} ||\boldsymbol{ucm}_{\perp r}||_2^2, \tag{3.5}$$

$$ITC = \ln\left(\frac{V_{UCM} \cdot N_{UCM_\perp}}{V_{UCM_\perp} \cdot N_{UCM}}\right). \tag{3.6}$$

According to the UCM theory, when the ITC is greater than 0, the motor task is considered to be steadily controlled by the CNS [Nisky 2014, Scholz 1999]. In its current form, the UCM theory proposes to deduce, from the variability of task-relevant variables, which geometrical tasks are steadily controlled by the brain. To this end, the considered task function $\boldsymbol{e}_r(\boldsymbol{q})$ is expressed as joint position error between the current trial configuration of the joints and a mean reference behavior. In order to extend this approach to dynamic motions, we propose to consider candidate task functions that depend on higher order derivatives of the elemental variables. In the next section, we introduce the generalized framework for expressing dynamic motor tasks.

3.3 Extending the UCM Theory to Dynamic Tasks

The task Jacobian (Eq. (3.1)) is also the linear mapping between the time derivative of the task and the velocity of the elemental variables :

$$\dot{\boldsymbol{e}}(\boldsymbol{q}, \dot{\boldsymbol{q}}) = J_e(\boldsymbol{q})\dot{\boldsymbol{q}}. \tag{3.7}$$

In turn, $\dot{\boldsymbol{e}}(\boldsymbol{q}, \dot{\boldsymbol{q}})$ can be viewed as a new task function depending on $\boldsymbol{q}$ but also on $\dot{\boldsymbol{q}}$. This task function is well suited for describing differential behaviors as speed tracking tasks for instance. This representation of motion is still decoupled from the dynamics of the system and thus does not take into account inertial effects that are essential for analyzing most mechanical motions. Now, if one wants to express the motion at the level of the dynamics, task functions need to be related to higher order derivative of the configuration variables. Indeed, it is well-known that rigid body dynamics is expressed as a function of the second order derivative of the joints variables [Saab 2011]. In order to express the system dynamics in the task space, Eq. (3.7) must be differentiated with respect to time:

$$\ddot{\boldsymbol{e}}(\boldsymbol{q}, \dot{\boldsymbol{q}}, \ddot{\boldsymbol{q}}) = \dot{J}_e(\boldsymbol{q}, \dot{\boldsymbol{q}})\dot{\boldsymbol{q}} + J_e(\boldsymbol{q})\ddot{\boldsymbol{q}}, \tag{3.8}$$

where $\dot{J}(\boldsymbol{q}, \dot{\boldsymbol{q}})\dot{\boldsymbol{q}}$ can be viewed as a dynamic drift of the task corresponding to nonlinear effects.

In the sequel, we propose to extend the UCM theory to task functions of the form of Eq. (3.7) and Eq. (3.8). As expressed in Eq. (3.7), $\dot{\boldsymbol{e}}$ is a function of $\boldsymbol{q}$ and $\dot{\boldsymbol{q}}$. We can write down an approximation of $\dot{\boldsymbol{e}}$ around a particular mean behavior of the participant across trials $(\bar{\boldsymbol{q}}, \bar{\dot{\boldsymbol{q}}})$, by computing a first order Taylor expansion as in Eq. (3.2). To this end, the partial derivatives of $\dot{\boldsymbol{e}}$ need to be computed with respect to $\boldsymbol{q}$ and $\dot{\boldsymbol{q}}$:

$$\left.\frac{\partial \dot{\boldsymbol{e}}}{\partial \dot{\boldsymbol{q}}}\right|_{\boldsymbol{q}=\bar{\boldsymbol{q}}} \hat{=}\ A(\bar{\boldsymbol{q}}, \dot{\boldsymbol{q}}), \tag{3.9a}$$

$$\left.\frac{\partial \dot{\boldsymbol{e}}}{\partial \boldsymbol{q}}\right|_{\dot{\boldsymbol{q}}=\bar{\dot{\boldsymbol{q}}}} \hat{=}\ B(\boldsymbol{q}, \bar{\dot{\boldsymbol{q}}}). \tag{3.9b}$$

It is straightforward that $A(\bar{\boldsymbol{q}}, \dot{\boldsymbol{q}})$ does not depend on $\bar{\dot{\boldsymbol{q}}}$: $A(\bar{\boldsymbol{q}}, \dot{\boldsymbol{q}}) = J_e(\bar{\boldsymbol{q}})$. The calculation details for B are given in Appendix A.1:

$$B_{ij} = \sum_{k=0}^{n} \frac{\partial (J_e(\boldsymbol{q}))_{ik}}{\partial q_j} \bar{\dot{q}}_k. \tag{3.10}$$

This leads to the first order Taylor expansion of $\dot{\boldsymbol{e}}$ around $(\bar{\boldsymbol{q}}, \bar{\dot{\boldsymbol{q}}})$:

$$\dot{\boldsymbol{e}}(\boldsymbol{q},\dot{\boldsymbol{q}}) - \dot{\boldsymbol{e}}(\bar{\boldsymbol{q}},\bar{\dot{\boldsymbol{q}}}) = \underbrace{\left[\begin{array}{c|c} B(\bar{\boldsymbol{q}},\bar{\dot{\boldsymbol{q}}}) & A(\bar{\boldsymbol{q}},\bar{\dot{\boldsymbol{q}}}) \end{array}\right]}_{J_{\dot{e}}} \left[\begin{array}{c} \boldsymbol{q}-\bar{\boldsymbol{q}} \\ \dot{\boldsymbol{q}}-\bar{\dot{\boldsymbol{q}}} \end{array}\right] + \boldsymbol{\varepsilon}(\boldsymbol{q},\dot{\boldsymbol{q}}). \tag{3.11}$$

Similarly, $\ddot{\boldsymbol{e}}$ is a function of $\boldsymbol{q}$, $\dot{\boldsymbol{q}}$ and $\ddot{\boldsymbol{q}}$ (Eq. (3.8)). To express its first order Taylor expansion around the mean behavior of the participant ($\bar{\boldsymbol{q}}$, $\bar{\dot{\boldsymbol{q}}}$, $\bar{\ddot{\boldsymbol{q}}}$), the partial derivatives of $\ddot{\boldsymbol{e}}$ need to be computed with respect to $\boldsymbol{q}$, $\dot{\boldsymbol{q}}$ and $\ddot{\boldsymbol{q}}$:

$$\left.\frac{\partial \ddot{\boldsymbol{e}}}{\partial \ddot{\boldsymbol{q}}}\right|_{\substack{\boldsymbol{q}=\bar{\boldsymbol{q}} \\ \dot{\boldsymbol{q}}=\bar{\dot{\boldsymbol{q}}}}} \hat{=}\, C(\bar{\boldsymbol{q}},\bar{\dot{\boldsymbol{q}}},\bar{\ddot{\boldsymbol{q}}}), \tag{3.12a}$$

$$\left.\frac{\partial \ddot{\boldsymbol{e}}}{\partial \dot{\boldsymbol{q}}}\right|_{\substack{\boldsymbol{q}=\bar{\boldsymbol{q}} \\ \ddot{\boldsymbol{q}}=\bar{\ddot{\boldsymbol{q}}}}} \hat{=}\, D(\bar{\boldsymbol{q}},\dot{\boldsymbol{q}},\bar{\ddot{\boldsymbol{q}}}), \tag{3.12b}$$

$$\left.\frac{\partial \ddot{\boldsymbol{e}}}{\partial \boldsymbol{q}}\right|_{\substack{\dot{\boldsymbol{q}}=\bar{\dot{\boldsymbol{q}}} \\ \ddot{\boldsymbol{q}}=\bar{\ddot{\boldsymbol{q}}}}} \hat{=}\, E(\boldsymbol{q},\bar{\dot{\boldsymbol{q}}},\bar{\ddot{\boldsymbol{q}}}). \tag{3.12c}$$

It is straightforward that $C(\bar{\boldsymbol{q}},\bar{\dot{\boldsymbol{q}}},\ddot{\boldsymbol{q}})$ does not depend neither on $\bar{\dot{\boldsymbol{q}}}$ nor on $\ddot{\boldsymbol{q}}$: $C(\bar{\boldsymbol{q}},\bar{\dot{\boldsymbol{q}}},\ddot{\boldsymbol{q}}) = J_e(\bar{\boldsymbol{q}})$. The calculation details for D and E are given in Appendices A.2.1 and A.2.2.

$$D_{ij} = \sum_{k=0}^{n} \frac{\partial(\dot{J}_e(\bar{\boldsymbol{q}},\dot{\boldsymbol{q}}))_{ik}}{\partial \dot{q}_j}\dot{q}_k + \delta_{jk}(\dot{J}_e(\bar{\boldsymbol{q}},\dot{\boldsymbol{q}}))_{ik}, \tag{3.13}$$

$$E_{ij} = \sum_{k=0}^{n} \frac{\partial(\dot{J}_e(\boldsymbol{q},\bar{\dot{\boldsymbol{q}}}))_{ik}}{\partial q_j}\bar{\dot{q}}_k + \sum_{k=0}^{n} \frac{\partial(J_e(\boldsymbol{q}))_{ik}}{\partial q_j}\bar{\ddot{q}}_k, \tag{3.14}$$

with δ, the Kronecker delta. This leads to the first order Taylor expansion of $\ddot{\boldsymbol{e}}$ around $\bar{\boldsymbol{q}}$, $\bar{\dot{\boldsymbol{q}}}$ and $\bar{\ddot{\boldsymbol{q}}}$:

$$\ddot{\boldsymbol{e}}(\boldsymbol{q},\dot{\boldsymbol{q}},\ddot{\boldsymbol{q}}) - \ddot{\boldsymbol{e}}(\bar{\boldsymbol{q}},\bar{\dot{\boldsymbol{q}}},\bar{\ddot{\boldsymbol{q}}}) =$$

$$\underbrace{\left[\begin{array}{c|c|c} E(\bar{\boldsymbol{q}},\bar{\dot{\boldsymbol{q}}},\bar{\ddot{\boldsymbol{q}}}) & D(\bar{\boldsymbol{q}},\bar{\dot{\boldsymbol{q}}},\bar{\ddot{\boldsymbol{q}}}) & C(\bar{\boldsymbol{q}},\bar{\dot{\boldsymbol{q}}},\bar{\ddot{\boldsymbol{q}}}) \end{array}\right]}_{J_{\ddot{e}}} \left[\begin{array}{c} \boldsymbol{q}-\bar{\boldsymbol{q}} \\ \dot{\boldsymbol{q}}-\bar{\dot{\boldsymbol{q}}} \\ \ddot{\boldsymbol{q}}-\bar{\ddot{\boldsymbol{q}}} \end{array}\right] + \boldsymbol{\varepsilon}(\boldsymbol{q},\dot{\boldsymbol{q}},\ddot{\boldsymbol{q}}). \tag{3.15}$$

From these matrix formulations of the first order Taylor expansions of $\dot{\boldsymbol{e}}$ and $\ddot{\boldsymbol{e}}$ (Eqs. (3.11) and (3.15)), one can directly apply the UCM approach previously recalled, by computing the nulls pace of $J_{\dot{e}}$ and $J_{\ddot{e}}$ respectively. Then, by projecting the variation of elemental variables with regard to the mean reference behavior onto the null space and its orthogonal, one can compute $\boldsymbol{ucm}_r$ and $\boldsymbol{ucm}_{\perp r}$, as in Eqs.

(3.3a) and (3.3b). The computation of the ITC is then performed to conclude whether the task under study is steadily controlled by the participant or not.

3.3.1 Using the extension of the UCM with dynamic motor tasks

The described formalism can be directly applied to placement tasks. Without loss of generality, the same approach as before can be applied to formulate other tasks. In robotics, this expression was used to formulate CoM trajectory tasks (Mansard, Kathib & Kheddar, 2009), visual servoing tasks (Chaumette & Hutchinson, 2006) or momentum tasks [Orin 2013]. In the sequel we show how to express dynamic tasks in terms of CoM, vision and momentum.

Center of mass (CoM) task

For writing a motor task in terms of the CoM trajectory, the position of the CoM (see Chapter 2) and the differential mapping J_c that relates joints velocities $\dot{\boldsymbol{q}}$ to the center of mass velocity $\dot{\boldsymbol{c}}(\boldsymbol{q}, \dot{\boldsymbol{q}})$ need to be computed. In this way, the CoM task can be expressed in the form of Eq. (3.7) or Eq. (3.8). Moreover, the application of the UCM extension to CoM tasks is similar to placement tasks.

Gazing task

To model a gazing task, a motion objective could be to move the head in such a way that the gaze is focused at a certain point $\boldsymbol{p}_i \in \mathbb{R}^3$ during motion. This point is projected from 3D space to a certain position $\boldsymbol{p}_i \in \mathbb{R}^2$ in a 2D image. The task Jacobian is given by $J_{gaze} = L\ J_{vis}$, where L represents the interaction matrix [Chaumette 2006] which describes the relation between the velocity of the visual frame and the velocity of the 2D image point, and J_{vis} is the Jacobian of the kinematic chain linking the visual frame so:

$$\dot{\boldsymbol{e}}(\boldsymbol{q}, \dot{\boldsymbol{q}}) = J_{gaze}(\boldsymbol{q})\dot{\boldsymbol{q}}, \tag{3.16}$$

which can be differentiated and mapped directly to the generic formulation of dynamic tasks Eq. 3.8 as:

$$\ddot{\boldsymbol{e}} = J_{gaze}\ddot{\boldsymbol{q}} + \dot{J}_{gaze}(t)\dot{\boldsymbol{q}}. \tag{3.17}$$

The application of the UCM extension to gaze tasks is similar to placement and center of mass tasks.

Linear and angular momenta tasks

Dynamic tasks can also be expressed in terms of momenta which allows for considering the inertial effects in the movement. Momenta tasks can be computed based on the centroidal dynamics: the dynamics computed at the CoM of the system [Orin 2013]. A momenta task can be formulated by using the centroidal momentum matrix $A_c(\boldsymbol{q})$ which is the product of the inertia matrix of the system and the

Jacobian matrix of the system ($A_c(\boldsymbol{q}) = X_c\ I_{sys}\ J_{sys}$) with X_c a matrix which expresses the momenta at the center of mass of the system, as defined in [Orin 2008]. The centroidal momenta matrix maps the joint velocities $\dot{\boldsymbol{q}}$ to the the centroidal momenta $\boldsymbol{h}_c$ as follows:

$$\boldsymbol{h}_c = A_c(\boldsymbol{q})\dot{\boldsymbol{q}}. \tag{3.18}$$

This relation has the form of Eq. (3.7). Moreover Eq. (3.18) can be differentiated with respect to time as:

$$\dot{\boldsymbol{h}}_c = A_c(\boldsymbol{q})\ddot{\boldsymbol{q}} + \dot{A}_c(\boldsymbol{q}, \dot{\boldsymbol{q}})\dot{\boldsymbol{q}}, \tag{3.19}$$

where $\dot{\boldsymbol{h}}_c = \begin{bmatrix} \dot{\boldsymbol{p}} & \dot{\mathcal{L}}_c \end{bmatrix}^T$ represents the derivative of the centroidal momenta expressed at the CoM position. This notation is a compact formulation that embeds the three components of the linear momentum derivative (LMD(x), LMD(y) and LMD(z)) and the three components of the angular momentum derivative (AMD(x), AMD(y) and AMD(z)).

Note that Eq. (4.14) which matches the pattern of Eq. (3.8) and thus can be used as a task function under the presented formalism. Hence, the application of the UCM theory to Eq. (4.14) requires to compute its partial differentiations which are really similar to the ones of Eq. (3.8) (Eqs. (3.12a), (3.12b) and (3.12c)) and that are developed in Appendix A.2.3. Note also that the previously defined *ITC*, or the ratio between good and bad variability, could be used to quantify a hierarchical structure of motor tasks according to their apparent importance in the generation of human movement (Subsection 3.1.4). This implies that a larger value of *ITC* might implies that one motor task is more important for the brain than other with a lower *ITC* value [Latash 2008]. In the following, a direct application to linear and angular momenta derivative task functions is presented, for investigating the control of these quantities by the CNS during jumping and landing motions in parkour.

3.4 Application to Take-off and Landing Motions in Parkour

In this section, we show how the proposed formalism can be applied to the study of a dynamic movement. For this purpose, we develop a practical case of application to highly dynamic and complex parkour motions, referred to as precision jump and precision landing techniques (Introduced in Chapter 2).

3.4.1 Hypothesized steadily controlled tasks

Hypothesized tasks of the parkour technique were chosen according to the previous whole-body motion study (Chapter 2) and the scientific literature. In this context, we expressed motor tasks in terms of linear and angular momenta. Besides testing whether these tasks are steadily controlled by the brain or not, we also check for the existence of a hierarchical structure of tasks that could describe the motion organization. This hypothesis is motivated by the fact that in the execution of these motions, the brain might have to organize several motor tasks simultaneously to guarantee the achievement of the motion goal (e.g. perform a precise landing without tipping over or breaking a bone).

3.4.1.1 Motion slicing into sub-motions

The motion is divided into three sub-motions: take-off, flight and landing. As our goal was to focus on momenta tasks, which are conserved quantities during the flight, we decided to exclude the flight motion from our analysis. The take-off phase is defined between the time at which the vertical position of the CoM is minimal and the last foot contact instant. The flying phase was defined between the end of the take-off phase and the initial contact with the ground “IC", defined as the time at which the vertical ground reaction force reaches 50 [N]. The landing phase was defined between IC and the time at which the vertical position of the CoM becomes minimal. The phases were normalized by time duration from 0% to 100% (Fig. 3.2).

3.4.1.2 Motor tasks during take-off

Research on the standing long jump motion, which is similar to the parkour motion in this study, have shown that during take-off, the impulse profile which modifies the take-off velocity of the CoM constitutes the principal performance factor [Wakai 2005]. In order to produce the desired impulse profile, the jumper has to generate the necessary forces against the ground which provide the CoM ballistic motion. Moreover, it has been shown that arms swing contribute to increase the impulsion, and therefore the CoM velocity, through joint torque augmentation [Cheng 2008, Hara 2006]. It has also been demonstrated that arm swinging improves the performance by alleviating excessive forward rotation [Ashby 2002] and contributing to position the body segments properly for landing [Ashby 2006].

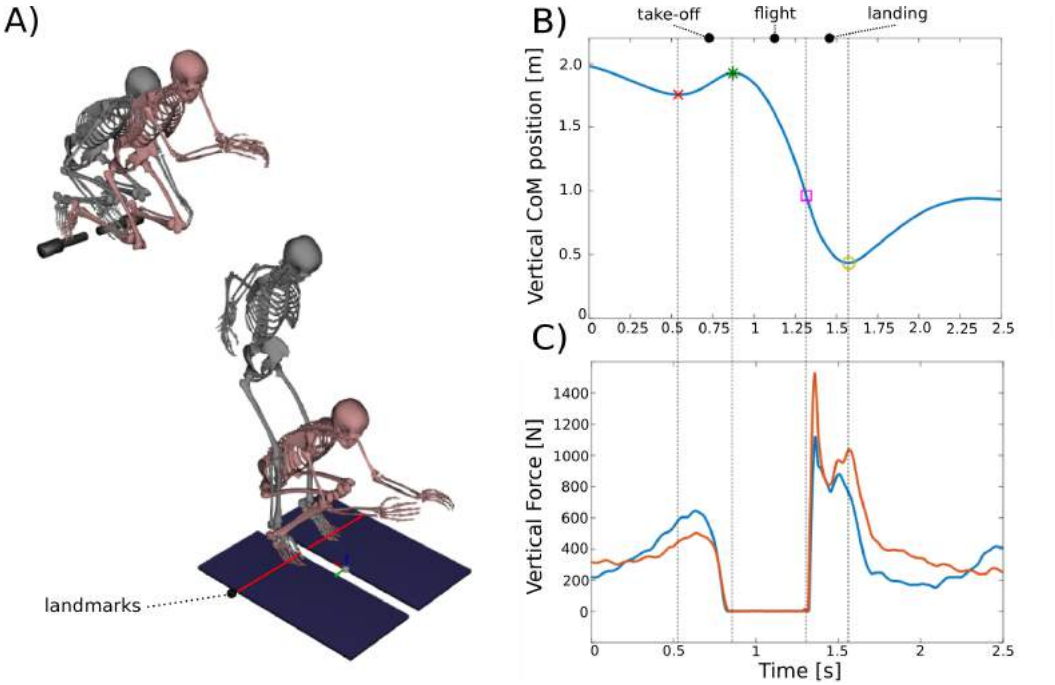

Figure 3.2: Parkour motion analysis. **(A)** The first two skeletons illustrate the beginning and the end of the take-off motion while the last two skeletons show the beginning and the end of the landing. In **(B)**, the center of mass vertical trajectory. In **(C)** the vertical reaction force profile. The CoM kinematics and the ground reaction forces allow for slicing the parkour technique into three sub-motions: take-off, flight and landing.

Controlling the ground reaction forces and the arms swing during impulse, appears to be the most relevant action for generating an optimal ballistic motion of the CoM. On the other hand, momenta derivatives expressed at the CoM are equal to net external forces and torques according to Newton-Euler equations. Accordingly, we suggest that linear and angular momentum derivatives expressed at the CoM should be steadily controlled by the brain during the take-off motion through the following tasks:

- "LMD(y,z)": A task that reflects the control of the forces to generate the required CoM velocity expressed in terms of the antero-posterior (A-P) and vertical components of the linear momentum derivative "LMD".

- "AMD(y)": A task that enhances the jumper's performance when jumping, and that contributes to prepare the body posture for landing in terms of the A-P component of the angular momentum derivative "AMD" expressed at the CoM.

3.4.1.3 Motor tasks during landing

During landing, reducing the vertical ground reaction forces "GRF" (which is the same as reducing the vertical linear momentum derivative) and lowering the loading rate (which is equivalent to control the time to the vertical GRF peak) contribute to prevent pain and injury [Gittoes 2012]. It has been shown that traceurs are able to reduce these quantities [Standing 2015]. Moreover, traceurs are able not only to land safer but also to better control they posture. A study of the center of pressure "CoP" control through the modulation of A-P and medial-lateral (M-L) components of the GRFs provided this evidence [Maldonado 2015](See also Chapter 2). Lastly, during our pre-tests, we noticed a rapid swing of the arms in the three dimensions during landing that could regulate the CoM trajectory. This observation was verified by calculating the contribution of each body segment to the total AMD during landing expressed at the CoM (See previous chapter).

Based on these elements, we made the following hypotheses regarding the tasks that are likely to be controlled by the CNS during landing:

- "LMD(z)": A task that reflects a strategy to guaranty a safe landing execution by lowering the vertical reaction forces and the loading rate. This task is expressed in terms of the vertical component of the LMD.
- "LMD(x,y)": A task that reflects a strategy of postural control in terms of the medial-lateral and antero-posterior components of the LMD.
- "AMD(x,y,z)": A task that reflects a falling-down avoidance strategy through rotational motions around the body principal axes expressed in terms of the AMD. This task might also reflect an injury prevention strategy by decreasing the varus-valgus motion of the knees.

Before contact with the ground, participants pre-activate their muscles in preparation for landing [Yeadon 2010] and pre-programmed stretch reflexes are likely to happen at initial contact with the ground [Kamibayashi 2006]. Thus, landing was analyzed from 4% of the motion to ensure consistency of our interpretations.

3.4.2 Methodology

3.4.2.1 Participants, experimental protocol and data treatment

The same participants, experimental protocol and data acquisition methods explained in Chapter 2 for the whole-body angular momentum study was used (including the whole-body model) to record and process biomechanics data. Results were used to apply the proposed extension of the UCM later. For this, computations were performed using a custom made program with the described whole-body model and a physics engine developed in the Gepetto team [Carpentier 2015]. The free-flyer joint (root frame) was not considered in this study because this joint is under-actuated according to the dynamic equations of poly-articulated systems (see Chapter 4).

3.4.3 Statistical analysis

Individual statistical studies were conducted for the take-off and landing techniques. All data are presented as the mean ± the confidence interval. The normality of the data was assessed thanks to the Shapiro–Wilk test. The $p-$value for determining statistical significance of hypotheses was $p = .05$. To statistically verify if motor tasks are steadily controlled by the CNS, unpaired $t-$tests comparing variability of normalized orthogonal spaces (V_{ucm} vs $V_{ucm\perp}$) were performed. To investigate if task hierarchies can be identified in the organization of the motion and to assess the temporal evolution of tasks during each motion, a repeated measures ANOVA ($task \times phase$) with the phases as within-subjects factors, and the task as between-subjects factor was performed. Paired $t-$tests with the Bonferroni correction were then carried out to assess main effects. Finally, the eta-squared method was used to test the effect size on the measures and the power of the statistics. All statistics were computed using R [R Development Core Team 2008].

3.4.4 Results

3.4.4.1 Take-off

Each of the two hypothesized tasks turned out to be significantly controlled at each motion phase ($p < .001$). A repeated measures analysis of variance of the ITC emphasized a main effect for the task factor ($F(1,6) = 36.77,\ p < .001,\ \eta^2 = .86,\ f = 2.47$). No significant effect was observed for the phase factor ($F(3,18) = 2.74,\ p = .071,\ \eta^2 = .31,\ f = 2.47$). Post-hoc comparisons using paired t-tests with the Bonferroni correction ($p/4$) indicated that tasks ITCs were significantly different at the the beginning ($p = .005$), at 40% ($p = .002$) and at 100% of the motion ($p = 0.042$). The AMD(y) ITC was statistically more important than LMD(y,z)'s one (Fig. 3.3 and Table 3.1).

Table 3.1: Hierarchical organization of the take-off motion in terms of tasks.

	Phases			
	1%	**40%**	**70%**	**100%**
1	AMD(y) ∗	AMD(y) ∗	AMD(y)	AMD(y) ∗
2	LMD(y,z)	LMD(y,z)	LMD(y,z)	LMD(y,z)

Note. ∗, significantly different from LMD(y,z);

3.4.4.2 Landing

Again, each of the hypothesized tasks were significantly controlled steadily at each motion phase ($p < .001$). A repeated measures analysis of variance of the ITC indicated a main effect for the task factor ($F(2,12) = 14.23,\ p < 0.001,\ \eta 2 = 0.70,\ f = 1.54$) and for the phase factor ($F(4,24) = 67.4, p < 0.001, \eta 2 = 0.91, f = 3.35$). Post-hoc comparisons using paired t-tests with Bonferroni correction corroborated that tasks ($p/15$) were significantly different ($p < 0.001$) and that ITC values of the

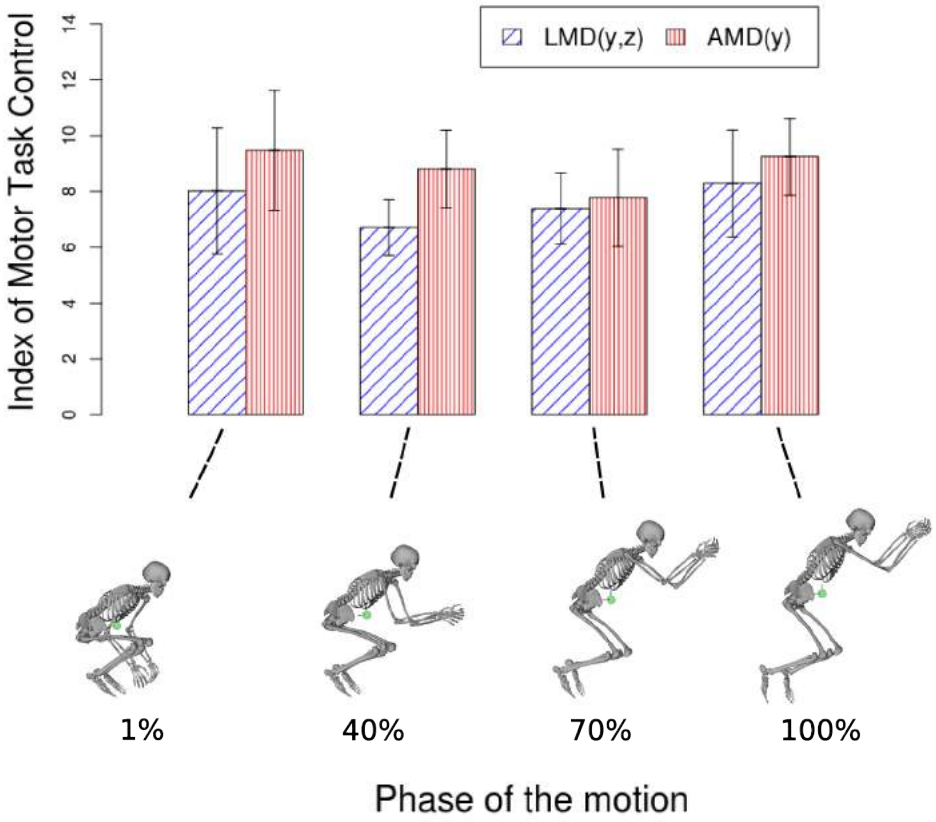

Figure 3.3: On bottom: snapshots of the reconstructed motion taken at each phase of the motion (1, 40, 70 and 100%). On top: the corresponding mean (± confidence intervals) values of the indexes of motor task control (ITC) during the take-off motion for the LMD(y,z) and the AMD(y) task.

phases ($p/10$) evolved differently with time (Table 3.2). A hierarchical organization of the tasks regarding the ITC value was observed (Table 3.3).

Table 3.2: Pairwise comparisons using paired t-tests for the task factor in the landing phases. The $p-$values were adjusted with the Bonferroni correction.

	Phases				
Task Comparison	**4%**	**13%**	**20%**	**40%**	**97%**
LMD(z) & LMD(x,y)	1	1	1	1	1
LMD(x,y) & AMD(x,y,z)	0.94	.59	.044	.0033	<.001
LMD(z) & AMD(x,y,z)	1	.011	.275	.0046	.0042

Table 3.3: Hierarchical organization of the landing motion in terms of tasks.

	Phases				
	4%	**13%**	**20%**	**40%**	**97%**
1	LMD(x,y)	LMD(z)†	AMD(x,y,z) ∗	AMD(x,y,z) ∗‡	AMD(x,y,z) ∗‡
2	LMD(z)	LMD(x,y)	LMD(x,y)	LMD(z)	LMD(x,y)
3	AMD(x,y,z)	AMD(x,y,z)	LMD(z)	LMD(x,y)	LMD(z)

Note. ∗, significantly different from LMD(x,y); †, significantly different from AMD(x,y,z); ‡ significantly different from LMD(z).

Table 3.4: Pairwise comparisons using paired t-tests for the phase factor in the landing phases. The $p-$values were adjusted with the Bonferroni correction.

	LMD(z)				**LMD(x,y)**				**AMD(x,y,z)**			
Phase	**4%**	**13%**	**20%**	**40%**	**4%**	**13%**	**20%**	**40%**	**4%**	**13%**	**20%**	**40%**
13%	.674	-	-	-	1	-	-	-	1	-	-	-
20%	.284	.092	-	-	.102	.005	-	-	1	.05	-	-
40%	.007	.001	.592	-	.008	<.001	.005	-	.064	.002	.065	-
97%	.002	<.001	.079	.088	<.001	<.001	<0.0011	.041	.005	<.001	.024	0.067

3.4.5 Discussion

The hypothesized motor tasks in this study were chosen accordingly to the physics of the motion and the literature. Results reveal complex whole-body motion strategies which lead to the stable control of the hypothesized tasks, supporting motor abundance [Latash 2000]. The time decomposition of the motion phases reveals that the amount of control dedicated to a task might not only depend on the task but also on the phase of the motion. This might be interpreted as a strategy of the CNS to organize motor tasks in terms of temporal and inter-tasks priorities. In the sequel, we discuss the results obtained by analyzing the proposed extension of the UCM theory to take-off and landing motions in parkour.

3.4.5.1 Take-off

The *ITC* of the LMD(y,z) reveals that this task is steadily controlled during the take-off motion. This is consistent with the physics of the problem: the traceur has to induce a certain velocity to his CoM in order to precisely determine the ballistic motion that the body will be subject to during the flight phase [Wakai 2005]. This velocity is obtained by integrating over time the acceleration of the CoM, which is the result of the forces applied by the participant on the ground (Newton's second law). The time integration of the forces exerted on the ground must therefore be precisely controlled at each time step during the take-off.

The AMD(y,z) task appears to be also steadily controlled by the brain during the take-off phase. Its *ITC* value turns out to be greater throughout the take-off motion. This result makes sense with regard to Euler's law of motion and the conservation of angular momentum in the sense that, after the very moment of contact loss and

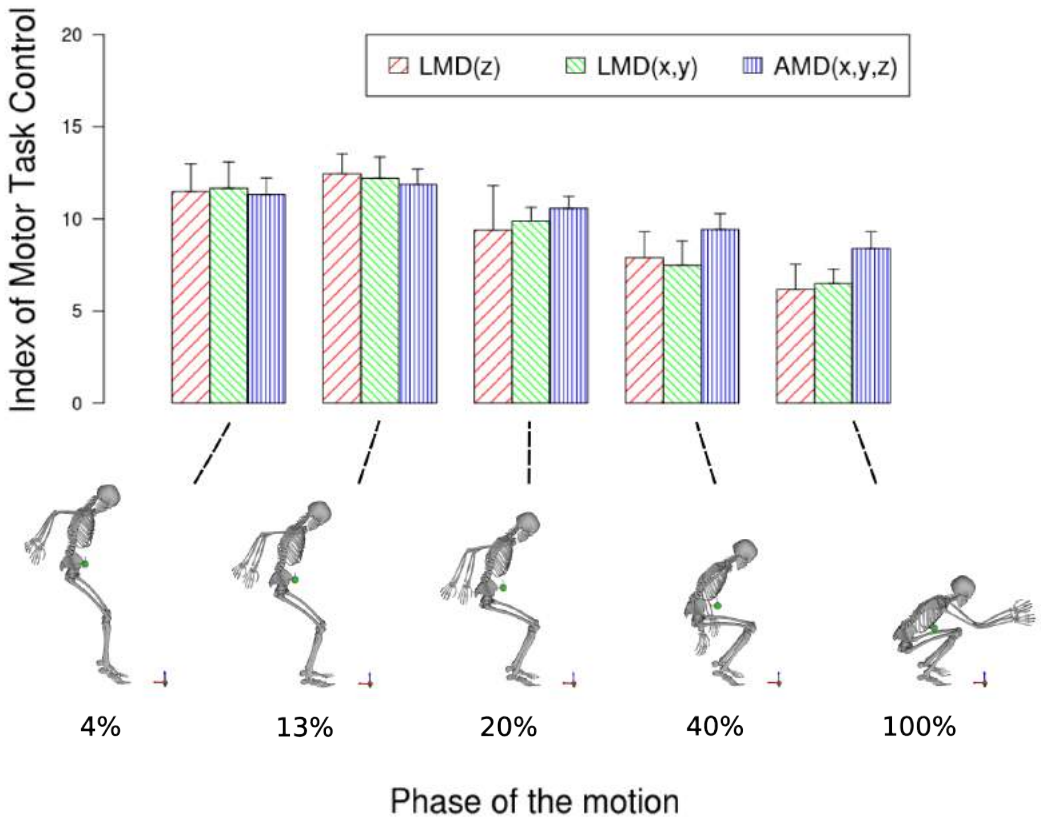

Figure 3.4: On bottom: snapshots of the reconstructed motion taken at each phase of the motion (4, 13, 20, 40 and 100%). On top: the corresponding mean (± confidence intervals) values of the indexes of motor task control (ITC) during the landing motion for the LMD(z), the LMD(x,y) and the AMD(x,y,z) task.

during the whole flight, traceurs will not be able to change their angular momentum. As a consequence, for the type of motions participants were instructed to perform, excessive rotational motions must be avoided. Another reason for traceurs to control the AMD(y) before flying is to ensure they can reach an appropriate posture in preparation for landing [Ashby 2006]. The leaning forward position of the traceur (Fig. 3.3) and the gravity force, are used to generate a net torque at the CoM which has to be counteracted throughout the take-off in order to reach the desired angular momentum. To this end, the observed strategy of the arms, pelvis, trunk and head swings contributes to counterbalance the forward sagittal angular momentum [Ashby 2002]. This upper body strategy allows lower limbs to be more involved in the production of the impulsion torques without having to compensate for the forward momentum [Ashby 2002]. This complex inter-limb coordination highlights the importance of controlling the AMD(y) task as corroborated by our results.

Task AMD(y,z) appeared to be significantly more controlled at the beginning and end of the take-off. This might reflect that for guaranteeing a correct body posture before landing is more important than generating the desired ballistic tra-

jectory of the CoM. Not controlling properly the angular momentum during the take-off might imply to fall down and getting injured after landing (in the next chapter there is an example of how not properly controlling this task might imply falling down).

3.4.5.2 Landing

The LMD(z) task appears to be controlled throughout the landing motion. From the beginning and up to 20% of the motion, the vertical force is controlled so that the peak loading rate and the peak forces can be reduced [Standing 2015]. This contributes to prevent pain and injuries [Gittoes 2012]. During the remaining of the landing, this task is kept controlled. This is not surprising when considering that the time integration of this force provides the vertical deceleration of the CoM.

The LMD(x,y) task is also controlled during the whole landing. This is expected during this process because the resulting GRF direction, which depends on the amount of medial-lateral and antero-posterior forces with regard to the normal force must remain inside the friction cones of contact in order to avoid slipping. Moreover, the LMD(x,y) task affects the center of pressure (CoP) position, which reflects the neuromuscular postural control. Note that, in order to reach static equilibrium — which is the final goal of the parkour technique —, the CoP must finally coincide with the projection of the CoM on the ground. The LMD(x,y) task is also linked to the forward deceleration of the CoM.

The AMD(x,y,z) task is also controlled during landing. Due to the conservation of angular momentum principle, the value of the AMD before the impact is zero. Right after it, because of external forces and torques, the AMD increases. One way to compensate this augmentation in order to keep balance, is to limit the derivative of joint torques during the landing phase. One can note that the pre-activation of muscles in preparation for landing [Yeadon 2010] contributes to keep the derivative of joint torques into reasonable bounds. This strategy is also responsible for the visual smoothness of the motion in terms of compliance and style (see minimum jerk and torque change in Chapter 2). Furthermore, controlling the AMD(x,y,z) around the vertical axis contributes to reduce the varus-valgus motion and can be an injury prevention mechanism.

Two hierarchies of tasks and a temporal evolution of the *ITC* value were observed during the landing phase. At 13% beginning of the motion, traceurs appear to control more the LMD(z) task. The AMD(x,y,z) task is significantly more controlled throughout the end of landing (from 20% to 100%). Note that after 20% of the landing, the vertical force is lowered. This control might be used to perform small postural adjustments thanks to the observed segment cancellation strategy (Chapter 2).

3.5 Conclusion and Perspectives

In this chapter, we first presented a theoretical framework for the identification of motor tasks based on the task function formalism used in robotics. Then, we proposed an extension of the UCM theory to dynamic tasks, illustrated by the study of a parkour motion for which tasks were formulated in terms of the derivatives of linear and angular momenta. By making reasonable assumptions about which physical quantities humans might control during parkour precision jump, we were able to provide consistent computational arguments about which ones could be actually steadily controlled by the brain during the successive phases of the motion. This study also revealed that the hypothesis of a hierarchical organization of tasks in human motion control is consistent. This organization could be used by the CNS to generate precise, highly dynamic, stable and injury-free motions. Such results might be of great interest in the fields of computer animation and humanoid robotics to generate human-inspired motions. A limitation of this work is the inherent errors of biomechanical methods that we are subject to when analyzing human motion (experimental protocol, scaling of anthropomorphic data, inverse kinematics,...). The UCM analysis of highly dynamic human motions is also promising for the study of dynamic motion generation in humans.

Chapter 4

Motion Generation With the Robotics Formalism: Application to Parkour

Contents

In this chapter, we recall the motion generation tools in robotics based on the task-space formalism. Then, based on the performance variables identified in the biomechanical (Chapter 2) and motor control (Chapter 3) studies, and by using the whole-body skeletal model introduced in Chapter 2, we consider the problem of parkour motion generation. We apply the methodology to generate the parkour precision jump and landing technique. At the end of the chapter, we provide a summary of the method and we discuss how our interdisciplinary approach based on biomechanics, motor control and robotics can be utilized to generate and understand human movement.

4.1 Whole-body Motion Generation of Anthropomorphic Systems

Whole-body motion generation of anthropomorphic systems, such as humanoid robots or skeletal systems, requires to model the system dynamics. To this end, in this section, the framework of the task function approach [Samson 1991, Nakamura 1991] and the formalism of poly-articulated systems are recalled. The inverse kinematics and inverse dynamics formulations for solving the equations of motion in robotics are briefly introduced. Finally, a hierarchical task controller which allows for solving strict hierarchy problems is also reviewed.

4.1.1 Dynamic model

The dynamic model of poly-articulated systems can be written by using the Euler-Lagrange equation. The robotic system is modeled as an under-actuated kinematic-tree chain composed of rigid bodies with a free-floating base (also called root frame) subject to external contact forces as follows:

$$M(\boldsymbol{q})\ddot{\boldsymbol{q}} + \boldsymbol{b}(\mathbf{q}, \dot{\boldsymbol{q}}) = S^T \boldsymbol{\eta}_{int} + \sum_{k=1}^{K} J_k^T(\boldsymbol{q}) \boldsymbol{\phi}_k, \tag{4.1}$$

where $M(\boldsymbol{q})$ is the inertia matrix, $\boldsymbol{b}(\boldsymbol{q}, \dot{\boldsymbol{q}})$ contains gravitational, centrifugal and Coriolis forces, $\boldsymbol{S} = \begin{bmatrix} \boldsymbol{0}_{n\times 6} & \boldsymbol{I}_{n\times n} \end{bmatrix}$ is a matrix that selects the internal joint torques $\boldsymbol{\eta}_{int}$ of the actuated part of Eq. (4.1), $J_k(\boldsymbol{q})$ is the Jacobian matrix of the k^{th} external contact and $\boldsymbol{\phi}_k = \begin{bmatrix} \boldsymbol{f}_{ext_k} & \boldsymbol{\eta}_{ext_k} \end{bmatrix}^T$ is the vector of the external forces and torques induced by the k^{th} contact.

Eq. (4.1) can be split into two parts: the under-actuated dynamics and the dynamics of the actuated segments as follows:

$$\begin{bmatrix} M_u(\boldsymbol{q}) \\ M_a(\boldsymbol{q}) \end{bmatrix} \ddot{\boldsymbol{q}} + \begin{bmatrix} \boldsymbol{b}_u(\boldsymbol{q}, \dot{\boldsymbol{q}}) \\ \boldsymbol{b}_a(\boldsymbol{q}, \dot{\boldsymbol{q}}) \end{bmatrix} = \begin{bmatrix} \boldsymbol{0}_6 \\ \boldsymbol{\eta}_{int} \end{bmatrix} + \sum_{k=1}^{K} \begin{bmatrix} J_{k,u}^T(\boldsymbol{q}) \\ J_{k,a}^T(\boldsymbol{q}) \end{bmatrix} \boldsymbol{\phi}_k, \tag{4.2}$$

where the sub-index u denotes the under-actuated part and the sub-index a denotes the actuated part. The first 6 rows of Eq. (4.2) represents the dynamics of the free-floating base (under-actuated part), also called the centroidal dynamic [Orin 2013] which coincides with the Newton-Euler equations of motion and links the variation of the linear momentum and the angular momentum of the whole system expressed around its CoM to the contact forces. These equations can be rewritten using the Newton-Euler equations as follows:

$$\dot{\boldsymbol{p}} = \sum_{k=1}^{K} \boldsymbol{f_k} - m\boldsymbol{g}, \tag{4.3}$$

$$\dot{\boldsymbol{\mathcal{L}}}_c = \sum_{k=1}^{K} (\boldsymbol{k}_k - \boldsymbol{c}) \times \boldsymbol{f}_k + \boldsymbol{\eta}_k, \tag{4.4}$$

where $\dot{\boldsymbol{p}}$ is the linear momentum derivative, $\boldsymbol{f}$ the external forces, m the mass of the poly-articulated system, $\boldsymbol{g}$ the gravity vector, $\dot{\boldsymbol{\mathcal{L}}}_c$ the angular momentum derivative, $\boldsymbol{k}_k$ is the position of the k^{th} contact point relative to the inertial frame, $\boldsymbol{c}$ is a position with respect to the inertial frame which is the center of mass of the system and $\boldsymbol{\eta}_k$ is the torque at the k^{th} contact point.

4.1.2 Task formalism for motion generation

The task formalism used in robotics, which was presented in the previous chapter for expressing human motor tasks, can be used to generate motions with robots. Let us recall the first and second order kinematic equations which are written as:

$$\dot{\boldsymbol{e}}(\boldsymbol{q}, \dot{\boldsymbol{q}}) = J_e(\boldsymbol{q})\dot{\boldsymbol{q}}, \tag{4.5}$$

$$\ddot{\boldsymbol{e}}(\boldsymbol{q}, \dot{\boldsymbol{q}}, \ddot{\boldsymbol{q}}) = J_e(\boldsymbol{q})\ddot{\boldsymbol{q}} + \dot{J}_e(\boldsymbol{q}, \dot{\boldsymbol{q}})\dot{\boldsymbol{q}}. \tag{4.6}$$

As it has been mentioned in the previous chapter, a task function (e.g. $\boldsymbol{e}(\boldsymbol{q})$, $\dot{\boldsymbol{e}}(\boldsymbol{q}, \dot{\boldsymbol{q}})$ or $\ddot{\boldsymbol{e}}(\boldsymbol{q}, \dot{\boldsymbol{q}}, \ddot{\boldsymbol{q}})$) comes down to an output error function whose regulation to zero corresponds to the execution of the task. For controlling the convergence of the task function to zero, a control law can be specified in order to ensure a reference behavior of the task function ($\boldsymbol{e}^*$, $\dot{\boldsymbol{e}}^*$, $\ddot{\boldsymbol{e}}^*$). For example, the expected behavior can be specified with a proportional derivative (PD) control law. The gains of the proportional derivative task can be tuned to obtain different reference behaviors such as exponential decays or adaptive gains of the task. Exponential decays control laws of the form $\dot{\boldsymbol{e}}^* = -\lambda_e \boldsymbol{e}$ are commonly used in robotics to make the task error converge quickly to a desired value. If reference behaviors can be extracted from human studies in terms of performance variables (tasks), then it is possible to set human-inspired reference behaviors. For example, the minimum jerk criterion observed in human motions [Flash 1985], has been used in the control of reaching tasks [Hoff 1992].

Note that, apart from tasks introduced in the previous chapter, a task can also be expressed directly in the configuration space to control the posture of the robot (posture task). Instead of the task Jacobian matrix, a selection matrix is used to select the joints that are aimed to be controlled.

4.1.3 Inverse kinematics control

The inverse kinematics problem consists in finding the joint kinematics that allows the robot to accomplish a reference kinematic task behavior. In the next subsections we show how to control the execution of tasks expressed in terms of velocities (first order kinematics) and accelerations (second order kinematics).

4.1.3.1 First order kinematics

The first order kinematics formulation consists in finding the joint velocities that produces the desired task velocity (the time derivative of some task function $\boldsymbol{e}(\boldsymbol{q})$) using the relationship obtained in Eq. (4.5). In order to control the task performance, a reference task behavior $\boldsymbol{e}^*$ is provided as input and the control problem can be expressed as the solution to the following unconstrained minimization problem:

$$\min_{\dot{\boldsymbol{q}}^*} \|\dot{\boldsymbol{e}}^* - J_e(\boldsymbol{q})\dot{\boldsymbol{q}}^*\|_2^2 . \tag{4.7}$$

The solution to this problem provides the control law of the system.

$$\dot{\boldsymbol{q}}^* = J_e^{\#}(\boldsymbol{q})\dot{\boldsymbol{e}}^* + P_{J_e}\dot{\boldsymbol{q}}_2, \tag{4.8}$$

where $\{.\}^{\#}$ represents the generalized inverse, P_{J_e} is the projector onto the null space of $J_e(\boldsymbol{q})$, and $\dot{\boldsymbol{q}}_2$ is a secondary control input that can be used to exploit the systems redundancy with respect to the task.

4.1.3.2 Second order kinematics

In the second order kinematics problem, the relationship between task acceleration and joints acceleration provided by Eq. (4.6) is used. The control problem consists in finding the joint accelerations that generate the task reference behavior:

$$\min_{\ddot{\boldsymbol{q}}^*} \left\| \ddot{\boldsymbol{e}}^* - J_e(\boldsymbol{q})\ddot{\boldsymbol{q}}^* - \dot{J}_e(\boldsymbol{q})\dot{\boldsymbol{q}} \right\|_2^2 . \tag{4.9}$$

Using the same notation as before, the control law expressed in terms of the joint accelerations is then written as:

$$\ddot{\boldsymbol{q}}^* = J_e^{\#}(\boldsymbol{q})(\ddot{\boldsymbol{e}}^* - \dot{J}_e(\boldsymbol{q})\dot{\boldsymbol{q}}) + P_{J_e}\ddot{\boldsymbol{q}}_2. \tag{4.10}$$

4.1.4 Inverse dynamics control

The inverse dynamics problem consists in finding the joint torques that will generate a reference task acceleration behavior $\ddot{\boldsymbol{e}}^*$. By multiplying the actuated part of Eq. (4.1) with JM^{-1} and replacing Eq. (4.6) in Eq. (4.1) we obtain the following relation:

$$\ddot{\boldsymbol{e}} + J_e(\boldsymbol{q})M^{-1}\boldsymbol{b} - \dot{J}_e(\boldsymbol{q},\dot{\boldsymbol{q}})\dot{\boldsymbol{q}} = J_e(\boldsymbol{q})M^{-1}\boldsymbol{\eta}. \tag{4.11}$$

The inverse dynamics control law can be written as:

$$\boldsymbol{\eta}^* = \left(J_e(\boldsymbol{q})M^{-1}\right)^{\#}\left(\ddot{\boldsymbol{e}}^* + J_e(\boldsymbol{q})M^{-1}\boldsymbol{b} - \dot{J}_e(\boldsymbol{q},\dot{\boldsymbol{q}})\dot{\boldsymbol{q}}\right) + P_{J_eM^{-1}}\,\boldsymbol{\eta}_2, \tag{4.12}$$

where $(P_{J_eM^{-1}})$ is the projector onto the null space of $J_e(\boldsymbol{q})M^{-1}$ and $\boldsymbol{\eta}_2$ is an arbitrary vector that can be used to control other tasks. Eq. (4.12) can be extended to include rigid contact constraints [Saab 2013]. The control of humanoid robots

interacting with the environment has to take into account external forces. Thus, the control problem consists in finding a control law that achieves a desired task behavior while respecting the dynamic model of the system and additional constraints that ensure the feasibility of the motion. This problem can be solved by setting a minimization problem under equality and inequality constraints as in [Saab 2011]:

$$\begin{aligned} & \min_{\ddot{\boldsymbol{q}},\, \boldsymbol{\eta},\, \boldsymbol{\lambda}} \|\ddot{\boldsymbol{e}}^* - \ddot{\boldsymbol{e}}(\boldsymbol{q}, \dot{\boldsymbol{q}}, \ddot{\boldsymbol{q}})\|_N^2 \\ s.t. \quad & M(\boldsymbol{q})\ddot{\boldsymbol{q}} + \boldsymbol{b}(\boldsymbol{q}, \dot{\boldsymbol{q}}) - \boldsymbol{g}(\boldsymbol{q}) - \sum_{k=1}^{K} J_k^T(\boldsymbol{q})\boldsymbol{\lambda}_k = S^T\boldsymbol{\eta}_{int} \\ & J_k\ddot{\boldsymbol{q}} + \dot{J}_k\dot{\boldsymbol{q}} = 0 \\ & \boldsymbol{\lambda}_k^{\perp} \geq 0, \end{aligned} \tag{4.13}$$

where J_k is the contact Jacobian associated to the k^{th} contact point. The first equality of Eq. (4.13) ensures the respect of the dynamical model of the system. The inequality constraint $\boldsymbol{\lambda}_k^{\perp} \geq 0$ guarantees that the contact forces are correctly oriented and that there is no interpenetration (rigid contact). In the same manner, other inequality constraints can be added such as joint limits ($\underline{\boldsymbol{q}} \geq \boldsymbol{q} \geq \overline{\boldsymbol{q}}$), torque limits ($\underline{\boldsymbol{\eta}} \geq \boldsymbol{\eta} \geq \overline{\boldsymbol{\eta}}$) or other tasks (as given in Subsection 4.1.2).

4.1.5 Hierarchical control

Solutions to problems in the form of Eq. (4.13) can be formulated based on null space projections or optimization methods. Prioritization schemes are based on projections onto the null space of higher order priority tasks in the form of Eq. (4.8) and Eq. (4.10) [Nakamura 1987, Siciliano 1991, Mansard 2009]. On the other hand, optimization techniques can be used to solve problems of the form of Eq. (4.13) which can also handle inequality constraints. A typical method is to use Hierarchical Quadratic Programming (HQP) [Kanoun 2009, Escande 2010, Escande 2014].

4.2 From Biomechanics and Motor Control to Robotics

4.2.1 Motion generation of parkour precision jumps and landings

In order to generate the motion, we utilized the model introduced in Chapter 2 for human motion analysis. The robotics framework of hierarchical task control was also considered although the strict task hierarchy observed in the motor control study (Chapter 3) was not used for this study. Tasks were parameterized based on the biomechanical study made Chapter 2. The rigid body dynamics computations were done using the Pinocchio library developed by the Gepetto team of LAAS-CNRS [Carpentier 2015]. The motion was generated using the method of null space projections and second order kinematics previously introduced based on basis multiplications [Escande 2010] (See Appendix B.1 for computational details).

4.2.1.1 Description of the tasks

As for motion analysis in the whole-body study, the motion generation is divided into three phases: take-off, flight and landing. In order to apply the hierarchical control framework, tasks are stacked in a hierarchical manner for each motion phase. The selection of the tasks and their hierarchy are based on the previous biomechanical and motor control study using mainly linear and angular momenta tasks. Only desired values of momenta tasks were used to set the tasks at key points (beginning and end of motion phases), and not the whole momenta trajectory. The behaviour of the tasks was controlled using exponential decay control laws. Additional tasks for foot placement, CoM position and posture at key points (beginning/end of each motion phase) were also considered to better specify the motion. The desired values for parametrizing the controller were deduced from the biomechanical study. The motion was controlled using joint accelerations according to Eq. (4.14) which was described in Chapter 3.

$$\dot{\boldsymbol{h}}_c = A_c(\boldsymbol{q})\ddot{\boldsymbol{q}} + \dot{A}_c(\boldsymbol{q}, \dot{\boldsymbol{q}})\dot{\boldsymbol{q}}. \tag{4.14}$$

Preparation phase

A preparation phase was added before the take-off phase. The motion is generated through the control of a hierarchy of the tasks organized as follows:

- At the highest priority we set a 3D foot placement task. This task was used to control the 3D position of each forefoot so that contact with the handle-bars is maintained during the phase. The orientation components of this tasks are not constrained. The 3D position was set according to the experimental protocol described in Chapter 2 in the angular momentum study. This includes a jump height of 75% of the height of the skeletal model.

- At the second level of the hierarchy, we set a task specifying a desired 3D position of the CoM. The desired position of the CoM was deduced from the motion analysis.

- The remaining of degrees of freedom are used to control the whole-body posture which was also extracted from the motion analysis.

Take-off phase

The take-off phase follows the preparation phase. The motion generated during this phase is organized in terms of tasks as follows:

- At the highest priority level, the 3D foot placement task of the preparation phase is kept.

- To generate the ballistic trajectory of the CoM, a linear momentum task is added at the second level of the hierarchy. The antero-posterior and vertical components provide the modulation of the CoM velocity for generating a desired ballistic trajectory. The medial-lateral component is regulated to zero to avoid undesired deviations of the CoM trajectory during the flight phase.

- In order to control the angular momentum at the CoM, a third task is stacked. This task imposes zero momentum around the vertical and antero-posterior (A-P) axes, and a desired angular momentum around the medial-lateral (M-L) axis. It allows the body model to reach a desired posture before landing and to avoid somersaults, and might alleviate torques at the lower limbs as suggested in the literature (see the application case of the previous chapter).

Flight Phase

When the velocity and take-off angle of the CoM trajectory allow to reach a desired horizontal distance, the top level task of the foot placement is removed from the stack of tasks and the flight phase begins. The desired horizontal distance equals to the square of the jump height (as specified in the recording protocol with humans). The horizontal distance d_{flight} that the CoM will travel is calculated during the take-off phase according to ballistic equations as:

$$d_{flight} = \frac{v\cos\theta}{g}\left(v\sin\theta + \sqrt{(v\sin\theta)^2 + 2gh_0}\right), \tag{4.15}$$

where v is the initial speed of the CoM (before the flight phase begins), θ is the take-off angle, g is the gravity acceleration and h_0 is the initial height of the CoM. During the flight phase, the momentum is conserved. A second level task is added to impose a desired posture before contacting the ground. The desired posture was extracted from recorded human motions.

Landing Phase

The landing phase starts at the end of the flight phase and is set as follows:

- At the highest level of the hierarchy, vertical feet position is regulated to keep the current contact position with the ground. A desired flexion of the toes and ankle joints is also imposed.
- At the second level, a 3D linear momentum task is added to decrease the velocity of the CoM to zero.
- At the third level, a task is added to regulate angular momentum to zero in order to avoid tipping motions of the model.
- At the forth level, a task is added to keep the CoM inside the vertical projection of the support polygon (medial-lateral and antero-posterior axis) in order to provide a static equilibrium state until the end of the motion.

4.2.2 Temporal sequence of the whole motion and tasks hierarchies

The temporal sequence of tasks stacked during each motion phase with their hierarchical order is depicted in the following table:

Hierarchy	Preparation	Take-off	Flight	Landing
1	Feet		Momenta	Feet
2	CoM	Linear Mom.	Posture	Linear Mom.
3	Posture	Angular Mom.		Angular Mom.
4				CoM

Table 4.1: Hierarchy of tasks used for generating motion in each phase.

4.2.3 Tasks behaviors

The behavior during each task that is defined by the decay rate of the task function were specified through exponential decay control laws. Weighting matrices multiplying the control input ($\ddot{\boldsymbol{q}}^*$) were tuned for the take-off and landing phases by giving higher gains to lower joints when controlling the linear momentum, and higher gains to upper joints when controlling the angular momentum in accordance to our biomechanical study. As the trunk segment has a significant mass compared to the upper limbs, the gain for the lumbar flexion was lowered to avoid undesirable behaviors of momenta.

4.2.4 Results

The reconstructed human motions and the motions generated based on the task function approach present interesting similarities, specially when comparing the motion of the lower body. Fig. 4.1 shows snapshots of the human motion reconstructed by means of the inverse kinematics method of biomechanics, and snapshots of the motion generated using the robotic framework of hierarchical task control.

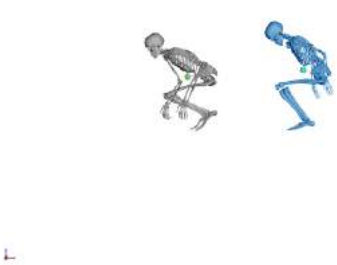

(a) Take-off 1%

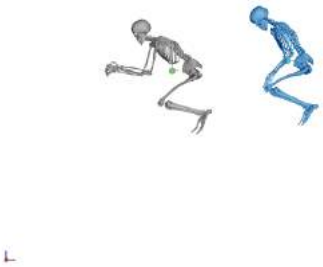

(b) Take-off 50%

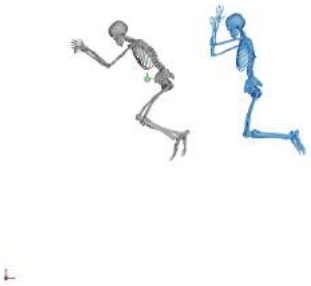

(c) Take-off 100%

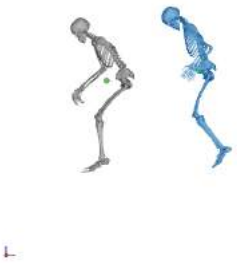

(d) Flight 50%

(e) Landing 1%

(f) Landing 25%

(g) Landing 50%

(h) Landing 100%

Figure 4.1: Snapshots of the take-off phase (**a, b, c**), flight phase (**d**), and landing phase (**e, f, g, h**) at different percentages of the motion phases. The skeleton on the left of each figure, represents the result of the inverse kinematics from motion analysis of a parkour practitioner. The skeleton on the right of each figure, represents the motion generated through hierarchical control.

The profiles of the linear and angular momenta of the experimental and generated motions are shown in Fig. 4.2 and in Fig. 4.3. The momenta profiles of humans represent the mean behavior of parkour experts with the corresponding standard deviation. Table 4.2 shows the difference between the ranges of motion (RoM) of the human group and the simulation model for the principal segments during each motion phase.

	Take-off RoM [deg]		Flight RoM [deg]		Landing RoM [deg]	
	L	R	L	R	L	R
Neck-head flexion-extension	19		22		15	
Trunk flexion-extension	-20		-10		-5	
Upper arm flexion-extension	-1	-1	65	66	-44	-30
Upper arm abduction-adduction	17	33	-2	5	10	9
Upper arm rotation	17	24	44	68	47	54
Forearm flexion-extension	-17	-24	-9	-4	-15	3
Thigh flexion-extension	-2	-2	16	22	2	0
Thigh adduction-abduction	-5	-9	1	-4	2	2
Thigh rotation	-6	0	1	9	8	6
Shank flexion	12	12	30	44	20	23

Table 4.2: Difference in the ranges of motion (RoM) of the analyzed human motions and the generated motion. The table shows the most relevant coordinates during the take-off, flight and landing phases of the parkour precision technique. Negative values mean that the RoM of the generated motion is higher than the RoM of the human experts. Main differences (RoM ≥ 45) are colored in pink while small differences (RoM ≤ 15) are colored in blue.

4.2.4.1 Take-off

- At the beginning of the motion, linear momentum values were different between humans and the model. Throughout the motion, the linear momentum was similar in the medial-lateral component while the antero-posterior and vertical component of the linear momentum behaved differently. More antero-posterior linear momentum was generated by humans at the end of the take-off phase, and more vertical linear momentum was generated by the model at the end of the motion phase.

- Although at the beginning of the motion angular momentum values were different, angular momentum behaved similarly in humans and in the model with time evolution. The angular momentum components around the antero-posterior and vertical axes were almost zero at the end of the motion phase, while the angular momentum component around the medial-lateral axis was not zero at the end of the motion phase.

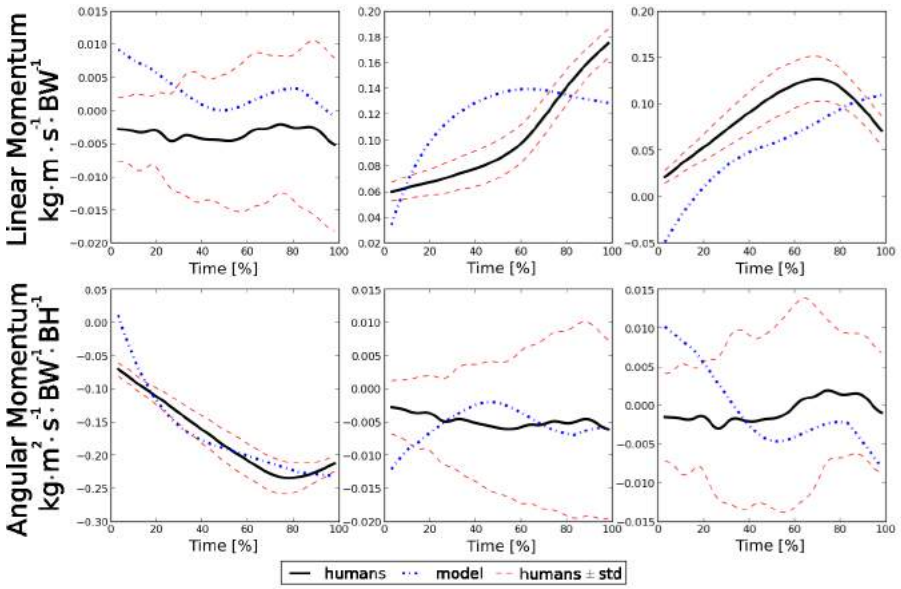

Figure 4.2: Momenta profiles of the human group (± SD), and of the simulation model during the take-off phase. The first row shows the medial-lateral, antero-posterior and vertical components of the linear momentum normalized by the body weight. The second row shows the angular momentum normalized by the body weight and height, about the the medial-lateral, antero-posterior and vertical axis.

- Fig. 4.1 shows that upper-limbs were coordinated differently with the time evolution and that the trunk and hips were more flexed in humans.
- RoM of all coordinates were similar (Table 4.2). RoM of thigh abduction-adduction and forearm flexion-extension were slightly higher in the generated motion, while upper arm abduction-adduction and rotation appear to be higher in humans.

4.2.4.2 Flight

Momenta were not compared because their components are constant during the flight phase according to the momenta conservation principle. Fig. 4.1c and 4.1d show that the motion looks different at the beginning and at 50 % of the flight. RoM were also different, specially in the case of the upper limb movement and the shank flexion-extension (Table 4.2).

4.2.4.3 Landing

- Linear momentum profiles of analyzed human movements and generated motions were globally similar.
- At the beginning of the landing phase, the model generated less angular momentum around the medial-lateral axis, while higher angular momentum was

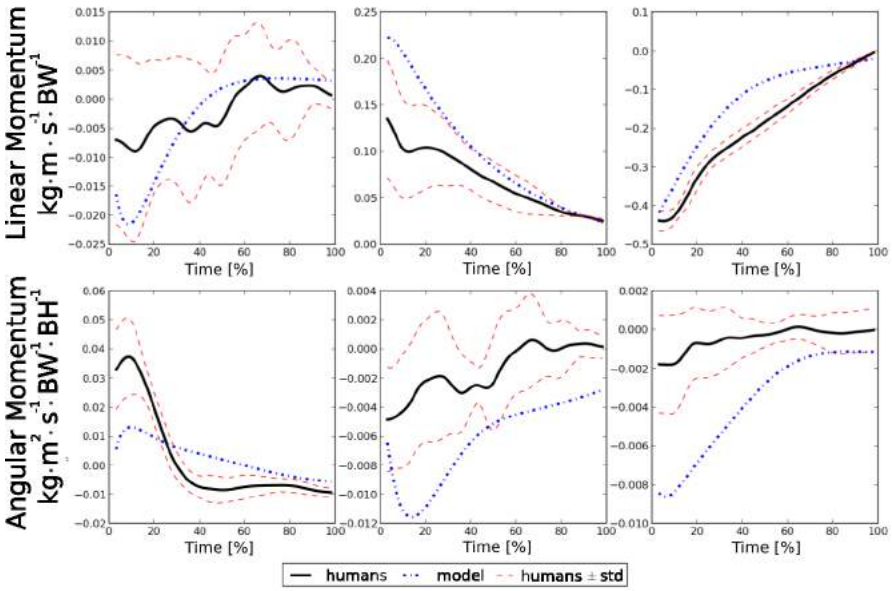

Figure 4.3: Momenta profiles of the human group (± SD), and of the simulation model during the landing phase. In the first row: medial-lateral, antero-posterior and vertical components of the linear momentum normalized by the body weight are displayed. In the second row: angular momentum normalized by the body weight and height around the the medial-lateral, antero-posterior and vertical axis are displayed.

observed around the antero-posterior and vertical axis.

- From Fig. 4.1, we can observe that the humans and the model landed with a similar posture. At 25 % and 50 % of the landing phase, the trunk of the model is more flexed than the the trunk of humans.

- RoM of the upper arm coordinates appear to differ slightly while the RoM of the other coordinates look similar.

4.2.5 Discussion

The analyzed and the generated motion were compared in terms of kinematics and momenta. The results showed that the kinematics of the human group was similar to the kinematics of the simulated model, specially of the lower limbs. Time evolution of momenta was sometimes slightly different during the take-off phase, while it was comparable in the landing phase. Whole-body coordination was congruent between humans and the model, although the upper limbs strategy did not evolve similarly with the time. In the next subsections we analyze the results per phase.

4.2.5.1 Take-off

During the take-off phase, we observed more antero-posterior linear momentum in the motions generated with the model. For generating the desired ballistic profile, the simulation model compensated the lack of antero-posterior linear momentum by increasing the vertical linear momentum. This strategy allowed the model to reach the initial CoM speed for landing at the requested distance. This increase of angular momentum with respect to humans might explain why the model jumped with the trunk more extended than humans (Fig. 4.1c), and why the RoM of the trunk was higher. The time behavior of the vertical and antero-posterior linear momentum was different in the model. This might be due to the task reference behavior which imposes an exponential decay of the error between the actual and desired value (as explained in Section 4.1).

The profiles of angular momentum were similar in humans and with the model. The arms, which contribute to angular momentum, behaved differently with time as shown in Fig. 4.1. The reason might be that upper limbs contributed also to increase the vertical linear momentum (which behaved differently in the model). Note also that the RoM of the forearm flexion-extension motion was higher in the simulation model. In spite of this, the model jumped with an angular momentum that allowed it to prepare properly the body posture for landing (Fig. 4.1e). Controlling the posture before landing allows for a better control of stability and impact damping (See Chapter 3).

On angular momentum control during the take-off phase

(a) Decrease of angular momentum **(b)** Increase of angular momentum

Figure 4.4: Effects on posture at landing when modifying the desired angular momentum during the take-off phase. The motion was generated by using the same hierarchical controller. Only the desired values of the angular momentum were modified during the take-off phase.

We carried on extra simulations by decreasing and increasing the desired angular momentum during the take-off phase. The results showed that when the angular

momentum is decreased, the model lands with a posture that made the model to fall down forwards (Fig. 4.4a). Conversely, if the angular momentum is increased, the model lands with a posture that make it to fall down backwards (Fig. 4.4b). These results highlight the importance of controlling the angular momentum when jumping.

4.2.5.2 Flight

The kinematics of the human body and the model were different during the flight phase. This might be due to the fact that the flight motion of the model was generated without constraining the trunk which has the highest mass. Thus, segments with small masses might have contributed less importantly to keep momenta constant during flight. In fact, the RoM of the trunk was higher in the model whereas the RoM of the upper arm coordinates was higher in humans. Note that the final posture (before landing) does not reflect the higher excursion of the upper arm coordinates in humans. Instants before landing, arms are swung backwards. Later on, when contacting the ground, arms have already been swung forwards in preparation for the landing phase. In the generated model, this swing strategy of the arms was not considered.

4.2.5.3 Landing

Linear and angular momentum were similar in humans and for the model. Nevertheless, upper-body coordination during the landing phase looks different (Fig. 4.1). The model landed with the trunk more flexed than humans. Thus, upper-limbs might compensate this strategy by generating a counterbalancing angular momentum. In fact, the RoM of the upper arm flexion-extension was higher in the model. It turns out that the considered decay rate and hierarchy of tasks allowed the model to replicate the evolution of the momenta in humans.

4.3 Conclusion and Perspectives

In this chapter, we presented an interdisciplinary methodology to generate human inspired motions with anthropomorphic systems such as robots. The approach involves robust biomechanical methods to analyze the human movements and the robotics framework of task hierarchy to generate the motion. We showed that our approach is able to reproduce highly dynamic and complex motions comparable to humans. In this final section we summarize our methodology, we provide a discussion about the interest of using the proposed methodology, we show the limitations of the proposed approach, we give some perspectives for the future work, and we conclude with remarks about the interpretation of our results.

Summary of the method

Important aspects of the proposed motion analysis and generation approach can be summarized as follows:

- A physical model suitable for analyzing and/or generating the motion of interest is selected/created. The model used for the analysis could be different from the model used for generating the motion.

- An experimental protocol for motion analysis is designed and the human movements are recorded by using motion-capture techniques.

- The recorded motion is analyzed using robust biomechanical techniques and key performance variables of the movement are identified (tasks). Then, tasks are assessed through the UCM theory and its extension for verifying if they are being controlled steadily by the brain.

- By understanding how the identified performance variables favor the motion generation in humans, the set of tasks is organized in a hierarchical manner according to their importance in the execution of the motion. A stack of tasks is created.

- The robot controller is further parameterized using information from the control strategies observed in humans by weighting the controller input. Human control strategy is inferred from biomechanical studies in terms of elemental variables (e.g. joint configuration, joint velocities, joint accelerations or joint torques) that affect the performance variables.

- The motion is generated through the robotics framework of hierarchical task control using the synthesized stack of tasks created and the physical model for motion generation.

- The human motion and the motion artificially generated are compared together using the same physical model created for analyzing the motion.

There are interesting aspects of this approach that deserve further discussion. First, our methodology differs from conventional task-space approaches, because it allows for parameterizing the whole-body robot controllers based on the biomechanics of human motion. Quantifying and understanding the mechanics of human motion offers the possibility of parameterizing robotic algorithms based on human expertise to execute movements. This provides a way to generate more robust and efficient motions. Furthermore, generating anthropomorphic motions that look more human-like is of great interest for human-robot interaction. Second, by simulating human movement using the advanced motion generation framework of robotics, comparison of the analyzed human motion and the generated motion is possible. Thus, our methodology also provides an interesting tool for validating or inferring hypotheses about the organization of the human movement based on task hierarchies. Future studies might incorporate the strict task hierarchy observed in the previous chapter.

The feasibility of the motion generated can be assessed in terms of joint torque and joint power by adding inequality constraints (Eq. (4.13)). To this end, the hierarchical controller can be designed using quadratic programming QP as suggested in Subsection 4.1.5. Furthermore, the behavior of the tasks (decay rate of the task function) can also be modified to generate smoother trajectories (see for example [Hoff 1992]). A vision task [Chaumette 2006] could also be added to reflect the importance of vision in humans when performing this type of motions. Other approaches can be used to generate highly dynamic and complex motions by considering the whole trajectory along a finite time horizon, e.g. optimal control. In that case hybrid cost functions, usually described as weighted-sums of elementary criteria, are considered. The difficulty is then to identify the set of weights that lead to the best replication of the observed human movement.

Chapter 5

Conclusion and Perspectives

Contents

This thesis presented an interdisciplinary approach to better understand dynamic human movements and to generate whole-body human motions of anthropomorphic systems. The proposed approach is based on robust biomechanics methods of motion analysis to understand the physics of the motion, on the Uncontrolled Manifold approach of motor control to hierarchically identify hypothesized steadily controlled tasks in human motion, and on the operational space formalism of robotics (task space) to generate motion with anthropomorphic systems. The application of this approach considered highly dynamic and complex movements of parkour. This manuscript also presented epidemiological, biomechanical and motor control studies of targeted parkour movements.

5.1 Summary of Contributions per Chapter

In **Chapter 2**, an epidemiological study of parkour practice in France was presented. This study is important to understand the injury mechanisms in parkour. The parkour precision landing technique was identified as a critical motion based on injury occurrence. This consideration motivated our interest in studying advanced techniques developed by traceurs in order to improve safety and sportive performance. To this end, the parkour precision landing technique and the landing phase of the parkour roll technique were presented through a biomechanical study considering the lower-limbs motion. Several performance variables (tasks) were identified and recommendations for injury prevention, training and performance optimization were provided. Afterwards, a whole-body musculoskeletal human model and a complex recording protocol were built to analyze and generate parkour-like motions. This model can also be used in other whole-body studies of dynamic motions. Then, this model was used to investigate whole-body strategies used in parkour landings

to dissipate and stabilize the body. Results revealed strategies used by traceurs that aim to regulate angular momentum contributions from the whole-body segments expressed at the center of mass during parkour precision landings. At the end of this chapter, performance variables were chosen in order to assess if they are being controlled by the CNS according to the motor control study presented in the sequel.

In **Chapter 3**, a mathematical framework derived from robotics was introduced to formulate motor tasks in human motion. An extension to the Uncontrolled Manifold theory to study redundancy in human motion was presented. This extension permits to analyze the organization of human motion in terms of kinematics and dynamics. Thus, our contribution contemplate the formal study of motor control of dynamic human motions considering. From this study, it is possible to verify if dynamic hypothesized tasks deduced from biomechanical studies are steadily being controlled by the CNS. It also permits to deduce a hierarchical organization of tasks in the execution of the motion in accordance to the motor abundance principle. In particular, we demonstrated that, during take-off and landing, tasks expressed in terms of linear and angular momenta seem to be steadily controlled by the CNS. This study also highlights the importance of studying linear and angular momentum, and their correspondent time derivatives, in the execution of highly dynamic and complex motions.

In **Chapter 4**, the biomechanical and motor control studies were utilized within the robotics task function approach to generate whole-body highly dynamic motions with an anthropomorphic avatar (the whole-body skeletal model introduced in Chapter 2) using a hierarchical task controller. This controller was parametrized according to the previous biomechanical and motor control studies of the parkour precision jump and landing techniques. In this sense, the motion was divided in different phases where tasks were stacked with a given hierarchy and then controlled with a given task behaviour. Mean behaviours of kinematic and dynamic variables from human motion and the results from the simulated motion were then compared. Interesting similarities were observed in human analyzed and simulated motions. In conclusion, the application of the interdisciplinary approach presented in this manuscript provides a strong synergy that permits to better understand and generate human motion using a unified framework.

5.2 Perspectives

5.2.1 On Parkour

In short term, a direct continuation of this research might be to report the unpublished work presented at the end of Chapter 2. In this direction it will be necessary to analyze the biomechanics of parkour vaulting and climbing techniques which were recorded and processed (including the recorded muscular activity). These techniques are key in parkour practice. According to the epidemiological study of parkour in France presented in Chapter 2, these are classified second and third rank

that generate most injuries in parkour. Another short term work will be to study how muscular synergies control steadily the linear and angular momenta tasks of the studied motions. This can be performed using a multiple linear regression approach as described in [de Freitas 2010].

In long term, the biomechanics of the parkour arm jump technique (see our epidemiological study) and techniques which are not stopped but which require a continuation of the movement could be analyzed. For this, a different experimental protocol including a set-up that allows for recording reaction forces on a wall might be needed. These studies might permit to get new insights about how momentum is transferred from one technique to another without breaking fluidity nor stability. Furthermore, biomechanics and motor control analyses have to be correlated with other types of analyses in the context of pain and injury prevention to better understand injury mechanisms in parkour. For example, it might be desirable to integrate biological factors (genetic, biochemical, ...), psychological factors (mood, personality, behavior, ...) and social factors (cultural, familial, socio-economic, medical, ...) in the loop. This could be done by using a biopsychosocial model [Penney 2010].

5.2.2 On modeling the human body

Although in this thesis we built a musculoskeletal model with more degrees of freedom than common humanoid robots, we are still very far from approaching the kinematic redundancy of human movement. Moreover our model included only simple joints such as ball-and-socket and hinge joints. A short term work could be oriented to increase the number of kinematic degrees of freedom of the system and to model complex non-linear joints (e.g. [Seth 2010]). In this direction, it might also be desirable to include more muscles to the model and to consider internal muscles which participate in the generation and dissipation of highly dynamic movements.

5.2.3 On motion generation

The unified approach proposed in this thesis could be applied to generate other dynamic motions. A future study could involve a more controlled set-up which exploits the kinematic redundancy and which puts in evidence a hierarchical organization of the motion. In this direction, the selection of new movements could be oriented to be tested with a humanoid robot such as HRP-2 or Pyrène.

In order to generate more realistic human-like motion, it would be interesting to learn patterns of "good variability" of human motion. Recalling the notions of motor control, good variability does not affect the performance of the task and is used to provide robustness and flexibility to the body. Good variability makes also the movement less stereotyped. In robotics, the remain null space of a stack of tasks is sometimes used to inject posture tasks in order to create more realistic movements. However, a posture task cannot be fully used to represent the variability of human motion. Thus, by using the null space of a hierarchical task controller with models of "good variability" in human motion, it might be possible to create movements

that look more natural and less repetitive.

The unified approach proposed in this thesis favors to identify a hierarchical structure of tasks. Based on this organization, a hierarchical task controller can be implemented to generate a given motion. To control these tasks, an exponential decay behavior is commonly used. In this thesis, exponential control laws were applied to the linear and angular momenta tasks which was useful for simulating some invariants of human motion. In this direction, another future goal could be to learn other behaviours of human tasks to generate a given motion.

Lastly, by using hierarchical control inverse kinematics/dynamics the motion is generated instantaneously. However, it might be desirable to generate motion in a finite time horizon. To this end, other unified approaches based on optimal control could be envisaged. Based on this method, inverse optimal control could be used to identify optimality criteria of biological motions based on motion analyses and in order to build a cost function. Then, the formalism of optimal control in motion generation could be used to control the motion of an anthropomorphic system. Note that a similar approach is used in [Mombaur 2010]. However, only the overall position and orientation of the robot was used in their work. An extension of that approach will be to generate whole-body motion at the joint level.

5.2.4 On rehabilitation robotics

By using the proposed unified approach, several applications in the context of rehabilitation robotics (service robotics, assitive devices, ...) are possible. By generating human-like motion, it is possible to improve human-robot interaction which is highly important in service robotics. Note that the perspectives on human-like motion generation were previously addressed. Thus, in this subsection, we will only focus on assistive devices. In this context, it will be interesting to analyze the variability structure of kinematic and dynamic tasks on human motion based on the proposed extension of the Uncontrolled Manifold (UCM) theory. Studies support that by exploiting variability, the CNS is able to improve motor learning [Singh 2016]. This analysis could lead to developments in active exploration using exoskeletons, in order to improve the learning process of a new motion. In this direction, our approach could be also oriented toward exoskeleton control. There are various methods for controlling exoskeletons, for example, using impedance control [Burdet 2013, Carignan 2008], optimal trajectory generation [Mihelj 2007] and synergies [Crocher 2012]. In [Crocher 2012], kinematic synergies in terms of joint velocities extracted through principal component analysis (PCA) were used to control an exoskeleton on hemiparetic patients during pointing movements. This type of controller imposes patterns of joint coordination without constraining the end-effector during active-assisted exercises. In [Hoellinger 2017], the ability to impose a specific synergy in post-stroke patients was tested. However results did not performed as expected. One of the drawbacks of PCA techniques might be that motion is reduced to a few set of synergies scaled in parallel along time without a explicit direct link to the task stability. In the context of the UCM, synergies are directly

linked to the performance of motor tasks as it has been shown in this thesis. Thus, rehabilitation could be more task-specific ensuring the stable control of a given task by using our proposed framework.

Moreover, a task controller might be designed to induce less variability in the degrees of freedom affecting the task performance and more variability added to degrees of freedom in the null space of the task. Evidence has shown that the application of the UCM theory allows to investigate motion in persons with hemiparesis. For example, it has been shown that these patients benefit from redundancy to stabilize performance variables that were important to successfully complete a reaching task [Reisman 2003]. Thus, within the framework developed in this thesis, it could be interesting to develop a task controller for exoskeletons based on the UCM theory and its extension including complex and dynamic tasks. This controller should be designed to exploit the variability structure of the human motion and might allow for rehabilitating patients to control steadily targeted tasks.

Appendix A

Computation of the UCM Extension

A.1 Partial Derivatives Calculation of Eq. (3.7)

$$B(\boldsymbol{q}, \bar{\dot{\boldsymbol{q}}}) = \frac{\partial J(\boldsymbol{q})\bar{\dot{\boldsymbol{q}}}}{\partial \boldsymbol{q}} \tag{A.1}$$

Let us write $J(\boldsymbol{q})\bar{\dot{\boldsymbol{q}}}$ component-wise:

$$(J(\boldsymbol{q})\bar{\dot{\boldsymbol{q}}})_i = \sum_{k=0}^{n} (J(\boldsymbol{q}))_{ik}\bar{\dot{q}}_k. \tag{A.2}$$

This leads to the component-wise expression of B:

$$B_{ij} = \frac{\partial (J(\boldsymbol{q})\bar{\dot{\boldsymbol{q}}})_i}{\partial q_j} = \sum_{k=0}^{n} \frac{\partial (J(\boldsymbol{q}))_{ik}}{\partial q_j}\bar{\dot{q}}_k. \tag{A.3}$$

Note that $\boldsymbol{q}$ contains rotations which are elements of $SO\mathbf{3}$ (special orthogonal group) which should be operated properly.

A.2 Partial Derivatives Calculation of Eq. (3.8)

A.2.1 Calculation of D

$$D(\bar{\boldsymbol{q}}, \dot{\boldsymbol{q}}, \bar{\ddot{\boldsymbol{q}}}) = \frac{\partial (\dot{J}(\bar{\boldsymbol{q}}, \dot{\boldsymbol{q}})\dot{\boldsymbol{q}})}{\partial \dot{\boldsymbol{q}}}. \tag{A.4}$$

Let us write $\dot{J}(\bar{\boldsymbol{q}}, \dot{\boldsymbol{q}})\dot{\boldsymbol{q}}$ component-wise:

$$(\dot{J}(\bar{\boldsymbol{q}}, \dot{\boldsymbol{q}})\dot{\boldsymbol{q}})_i = \sum_{k=0}^{n} (\dot{J}(\bar{\boldsymbol{q}}, \dot{\boldsymbol{q}}))_{ik}\dot{q}_k. \tag{A.5}$$

This leads to the component-wise expression of D:

$$D_{ij} = \frac{\partial (\dot{J}(\bar{\boldsymbol{q}}, \dot{\boldsymbol{q}})\dot{\boldsymbol{q}})_i}{\partial \dot{q}_j} = \sum_{k=0}^{n} \frac{\partial ((\dot{J}(\bar{\boldsymbol{q}}, \dot{\boldsymbol{q}}))_{ik}\dot{q}_k)}{\partial \dot{q}_j} = \sum_{k=0}^{n} \frac{\partial (\dot{J}(\bar{\boldsymbol{q}}, \dot{\boldsymbol{q}}))_{ik}}{\partial \dot{q}_j}\dot{q}_k + \delta_{jk}(\dot{J}(\bar{\boldsymbol{q}}, \dot{\boldsymbol{q}}))_{ik}, \tag{A.6}$$

with δ the Kronecker delta.

A.2.2 Calculation of E

$$E(\boldsymbol{q}, \bar{\dot{\boldsymbol{q}}}, \bar{\ddot{\boldsymbol{q}}}) = \frac{\partial(\dot{J}(\boldsymbol{q}, \bar{\dot{\boldsymbol{q}}})\bar{\dot{\boldsymbol{q}}})}{\partial \boldsymbol{q}} + \frac{\partial(J(\boldsymbol{q})\bar{\ddot{\boldsymbol{q}}})}{\partial \boldsymbol{q}} \tag{A.7}$$

Let us write $\dot{J}(\boldsymbol{q}, \bar{\dot{\boldsymbol{q}}})\bar{\dot{\boldsymbol{q}}}$ component-wise:

$$(\dot{J}(\boldsymbol{q}, \bar{\dot{\boldsymbol{q}}})\bar{\dot{\boldsymbol{q}}})_i = \sum_{k=0}^{n} (\dot{J}(\boldsymbol{q}, \bar{\dot{\boldsymbol{q}}}))_{ik} \bar{\dot{q}}_k. \tag{A.8}$$

Let us write $J(\boldsymbol{q})\bar{\ddot{\boldsymbol{q}}}$ component-wise:

$$(J(\boldsymbol{q})\bar{\ddot{\boldsymbol{q}}})_i = \sum_{k=0}^{n} (J(\boldsymbol{q}))_{ik} \bar{\ddot{q}}_k. \tag{A.9}$$

This leads to the component-wise expression of E:

$$E_{ij} = \frac{\partial(\dot{J}(\boldsymbol{q}, \bar{\dot{\boldsymbol{q}}})\bar{\dot{\boldsymbol{q}}})_i}{\partial q_j} + \frac{\partial(J(\boldsymbol{q})\bar{\ddot{\boldsymbol{q}}})_i}{\partial q_j}, \tag{A.10a}$$

$$E_{ij} = \sum_{k=0}^{n} \frac{\partial(\dot{J}(\boldsymbol{q}, \bar{\dot{\boldsymbol{q}}}))_{ik}}{\partial q_j} \bar{\dot{q}}_k + \sum_{k=0}^{n} \frac{\partial(J(\boldsymbol{q}))_{ik}}{\partial q_j} \bar{\ddot{q}}_k. \tag{A.10b}$$

A.2.3 Applying the UCM theory to momenta tasks

The similarity between Eq. (3.8) and Eq. (4.14) provides a direct case of application of our extension of the UCM theory. To this end, we compute the partial derivatives of $\dot{\boldsymbol{h}}_c(\boldsymbol{q}, \dot{\boldsymbol{q}}, \ddot{\boldsymbol{q}})$ around the mean performance of one participant ($\bar{\boldsymbol{q}}$, $\bar{\dot{\boldsymbol{q}}}$, $\bar{\ddot{\boldsymbol{q}}}$):

$$\left.\frac{\partial \dot{\boldsymbol{h}}_c}{\partial \ddot{\boldsymbol{q}}}\right|_{\substack{\boldsymbol{q}=\bar{\boldsymbol{q}} \\ \dot{\boldsymbol{q}}=\bar{\dot{\boldsymbol{q}}}}} = A_c(\dot{\boldsymbol{q}}), \tag{A.11a}$$

$$\left.\frac{\partial \dot{\boldsymbol{h}}_c}{\partial \dot{\boldsymbol{q}}}\right|_{\substack{\boldsymbol{q}=\bar{\boldsymbol{q}} \\ \ddot{\boldsymbol{q}}=\bar{\ddot{\boldsymbol{q}}}}} = \frac{\partial(\dot{A}_c(\bar{\boldsymbol{q}}, \dot{\boldsymbol{q}})\dot{\boldsymbol{q}})}{\partial \dot{\boldsymbol{q}}}, \tag{A.11b}$$

$$\left.\frac{\partial \dot{\boldsymbol{h}}_c}{\partial \boldsymbol{q}}\right|_{\substack{\dot{\boldsymbol{q}}=\bar{\dot{\boldsymbol{q}}} \\ \ddot{\boldsymbol{q}}=\bar{\ddot{\boldsymbol{q}}}}} = \frac{\partial(\dot{A}_c(\boldsymbol{q}, \bar{\dot{\boldsymbol{q}}})\bar{\dot{\boldsymbol{q}}})}{\partial \boldsymbol{q}} + \frac{\partial(A_c(\boldsymbol{q})\bar{\ddot{\boldsymbol{q}}})}{\partial \boldsymbol{q}}. \tag{A.11c}$$

Then we apply the presented framework to the first order Taylor expansion of $\dot{\boldsymbol{h}}_c$.

Appendix B

Hierarchical Control

B.1 Basis Multiplication [Escande 2010]

Linear equality constraints of the form $A\boldsymbol{x} = \boldsymbol{b}$ such as task functions, can be solved using hierarchical control. Let us consider the case of L linear constraints (e.g. tasks) $(A_1, \boldsymbol{b}_1) \cdots (A_l, \boldsymbol{l}_1) \cdots (A_L, \boldsymbol{b}_L)$ that have to be satisfied at best and let us consider that constraints are conflicting between them. A strict hierarchy of constraints can be used to solve this problem [Siciliano 1991]. The constrain with the highest priority $(A_1, \boldsymbol{b}_1)$ can be solved at best in a least-square sense by the pseudo-inverse. Then the second constraint $(A_2, \boldsymbol{b}_2)$ is solved in the null space of the first constraint. The generic solution to solve the p levels of the hierarchy can be written as:

$$\boldsymbol{x}_l^* = \sum_{l=1}^{L} (A_l P_{l-1})^+ (\boldsymbol{b}_l - A_l \boldsymbol{x}_{l-1}^*) + \tilde{P}_L \tilde{\boldsymbol{x}}_{L+1}, \tag{B.1}$$

with $P_0 = \mathbb{1}$, $x_0 = 0$ and $\tilde{P}_L = P_{L-1} P_L$ is the projector in the null space of $(A_l P_{l-1})$, x^* denotes the solution for the hierarchy of constraints composed of L linear constraints, P is a projector on the null space of A ($AP = 0$ and $PP = \mathbb{1}$) and $\tilde{x}_{L+1}$ is any vector of the configuration space that can be used to accomplish another objective. In order to fasten the numerical resolution of Eq. B.1 a basis multiplication approach has been proposed [Escande 2010, Escande 2014]. Given a basis Z_1 of the null space of $A1$ ($A_1 Z_1 = 0$), the projector in the null space of A_1 can be written as $P_1 = Z_1 Z_1^T$. Eq. B.1 can be rewritten as:

$$\boldsymbol{x}_l^* = \sum_{l=1}^{L} Z_{l-1} (A_l Z_{l-1})^+ (\boldsymbol{b}_l - A_l \boldsymbol{x}_{l-1}^*) + \tilde{Z}_L \tilde{\boldsymbol{x}}_{L+1}, \tag{B.2}$$

which is more efficient to compute than B.1 due to the size of the matrices.

Bibliography

[Aleshinsky 1986a] S Y Aleshinsky. *An energy 'sources' and 'fractions' approach to the mechanical energy expenditure problem–I. Basic concepts, description of the model, analysis of a one-link system movement.* Journal of biomechanics, vol. 19, no. 4, pages 287–93, jan 1986. (Cited in page 24.)

[Aleshinsky 1986b] S Y Aleshinsky. *An energy 'sources' and 'fractions' approach to the mechanical energy expenditure problem–II. Movement of the multi-link chain model.* Journal of biomechanics, vol. 19, no. 4, pages 295–300, jan 1986. (Cited in page 24.)

[Anderson 1999] Frank C Anderson and Marcus G Pandy. *A Dynamic Optimization Solution for Vertical Jumping in Three Dimensions.* Computer Methods in Biomechanics and Biomedical Engineering, vol. 2, no. 3, pages 201–231, 1999. (Cited in page 34.)

[Asada 2009] M. Asada, K. Hosoda, Y. Kuniyoshi, H. Ishiguro, T. Inui, Y. Yoshikawa, M. Ogino and C. Yoshida. *Cognitive Developmental Robotics: A Survey.* IEEE Trans. on Auton. Ment. Dev., vol. 1, no. 1, pages 12–34, May 2009. (Cited in page 8.)

[Ashby 2002] Blake M. Ashby and Jean H. Heegaard. *Role of arm motion in the standing long jump.* Journal of Biomechanics, vol. 35, no. 12, pages 1631–1637, 2002. (Cited in pages 82 and 88.)

[Ashby 2006] Blake M. Ashby and Scott L. Delp. *Optimal control simulations reveal mechanisms by which arm movement improves standing long jump performance.* Journal of Biomechanics, vol. 39, no. 9, pages 1726–1734, 2006. (Cited in pages 82 and 88.)

[Baker 1974] S P Baker, B O'Neill, W Haddon and W B Long. *The injury severity score: a method for describing patients with multiple injuries and evaluating emergency care.* The Journal of trauma, vol. 14, no. 3, pages 187–96, mar 1974. (Cited in page 32.)

[Bernstein 1967] N Bernstein. The co-ordination and regulation of movements. Pergamon Press, Oxford [etc.], 1967. (Cited in pages vii, 1, 4, 69, 70 and 72.)

[Bisseling 2007] Rob W Bisseling, At L Hof, Steef W Bredeweg, Johannes Zwerver and Theo Mulder. *Relationship between landing strategy and patellar tendinopathy in volleyball.* British Journal of Sports Medicine, vol. 41, no. 7, pages e1–e6, jul 2007. (Cited in page 38.)

[Bisseling 2008] R W Bisseling, a L Hof, S W Bredeweg, J Zwerver and T Mulder. *Are the take-off and landing phase dynamics of the volleyball spike jump*

related to patellar tendinopathy? British journal of sports medicine, vol. 42, no. 6, pages 483–489, 2008. (Cited in pages 38 and 57.)

[Bonci 2014] Tecla Bonci, Valentina Camomilla, Raphael Dumas, Laurence Chèze and Aurelio Cappozzo. *A soft tissue artefact model driven by proximal and distal joint kinematics.* Journal of Biomechanics, vol. 47, no. 10, pages 2354 – 2361, 2014. (Cited in page 18.)

[Breazeal 2003] Cynthia Breazeal. *Toward sociable robots.* Robotics and Autonomous Systems, vol. 42, pages 167–175, 2003. (Cited in page 8.)

[Brown 2004] Cathleen Brown, Scott Ross, Rick Mynark and Kevin Guskiewicz. *Assessing Functional Ankle Instability with Joint Position Sense, Time to Stabilization, and Electromyography.* Journal of Sport Rehabilitation, vol. 13, no. 2, pages 122–134, 2004. (Cited in page 40.)

[Burdet 2013] Etienne Burdet, David W Franklin and Theodore E Milner. *Human robotics: neuromechanics and motor control*, 2013. (Cited in pages 10 and 110.)

[Caine 2005] Dennis Caine and Larry Nassar. *Gymnastics injuries.* Medicine and Sport Science, vol. 48, pages 18–58, 2005. (Cited in page 30.)

[Camomilla 2015] V. Camomilla, T. Bonci, R. Dumas, L. Chèze and A. Cappozzo. *A model of the soft tissue artefact rigid component.* Journal of Biomechanics, vol. 48, no. 10, pages 1752 – 1759, 2015. (Cited in page 18.)

[Carignan 2008] C. R. Carignan, M. P. Naylor and S. N. Roderick. *Controlling shoulder impedance in a rehabilitation arm exoskeleton.* In 2008 IEEE International Conference on Robotics and Automation, pages 2453–2458, May 2008. (Cited in page 110.)

[Carpentier 2015] Justin Carpentier, Florian Valenza, Nicolas Mansard and Others. *Pinocchio: fast forward and inverse dynamics for poly-articulated systems.* https://stack-of-tasks.github.io/pinocchio, 2015. (Cited in pages 61, 84 and 96.)

[Cazenave 2008] N. Cazenave and G. Michel. *Conduites à risques et variation de l'estime de soi chez les adolescents : l'exemple du parkour.* Annales Medico-Psychologiques, vol. 166, no. 10, pages 875–881, 2008. (Cited in pages 12, 28 and 38.)

[Chaumette 2006] François Chaumette and S. Hutchinson. *Visual servo control, Part I: Basic approaches.* IEEE Robotics ib and Automati on Magazine, vol. 13, no. 4, pages 82–90, 2006. (Cited in pages 80 and 106.)

[Cheng 2008] Kuangyou B. Cheng, Chih Hung Wang, Hui Chuan Chen, Chin Dai Wu and Hung Ta Chiu. *The mechanisms that enable arm motion to enhance*

vertical jump performance-A simulation study. Journal of Biomechanics, vol. 41, no. 9, pages 1847–1854, 2008. (Cited in page 82.)

[Chèze 1995] L. Chèze, B.J. Fregly and J. Dimnet. *A solidification procedure to facilitate kinematic analyses based on video system data.* Journal of Biomechanics, vol. 28, no. 7, pages 879 – 884, 1995. (Cited in page 21.)

[Colby 1999] S M Colby, R a Hintermeister, M R Torry and J R Steadman. *Lower limb stability with ACL impairment.* The Journal of orthopaedic and sports physical therapy, vol. 29, no. 8, pages 444–451; discussion 452–454, 1999. (Cited in pages 40 and 44.)

[Cortes 2007] Nelson Cortes, James Onate, João Abrantes, Linda Gagen, Elizabeth Dowling and Bonnie Van Lunen. *Effects of Gender and Foot-Landing Techniques on Lower Extremity Kinematics during Drop-Jump Landings.* Journal of Applied Biomechanics, vol. 23, no. 4, pages 289–299, 2007. (Cited in page 53.)

[Crocher 2012] V. Crocher, A. Sahbani, J. Robertson, A. Roby-Brami and G. Morel. *Constraining Upper Limb Synergies of Hemiparetic Patients Using a Robotic Exoskeleton in the Perspective of Neuro-Rehabilitation.* IEEE Transactions on Neural Systems and Rehabilitation Engineering, vol. 20, no. 3, pages 247–257, May 2012. (Cited in page 110.)

[Da Rocha 2014] Jaime Aparecido Da Rocha, Juan Carlos Pérez Morales, George Schayer Sabino, Bento João Abreu, Diogo Carvalho Felício, Bruno Pena Couto, Marcos Daniel M Drummond and Leszek A Szmuchrowski. *Prevalence and risk factors of musculoskeletal injuries in parkour.* Arch Budo Sci Martial Art Extreme Sport, vol. 10, no. 1, pages 39–42, 2014. (Cited in pages 28 and 31.)

[Danna-dos Santos 2007] Alessander Danna-dos Santos, Kajetan Slomka, Vladimir M. Zatsiorsky and Mark L. Latash. *Muscle modes and synergies during voluntary body sway.* Experimental Brain Research, vol. 179, no. 4, pages 533–550, jun 2007. (Cited in page 72.)

[Dasgupta 1999] A. Dasgupta and Y. Nakamura. *Making feasible walking motion of humanoid robots from human motion capture data.* In Proceedings 1999 IEEE International Conference on Robotics and Automation (Cat. No.99CH36288C), volume 2, pages 1044–1049 vol.2, 1999. (Cited in page 17.)

[de Freitas 2010] Sandra Maria Sbeghen Ferreira de Freitas and John Peter Scholz. *A comparison of methods for identifying the Jacobian for uncontrolled manifold variance analysis.* Journal of Biomechanics, vol. 43, no. 4, pages 775 – 777, 2010. (Cited in page 109.)

[De Ruiter 2001] C. J. De Ruiter and A. De Haan. *Similar effects of cooling and fatigue on eccentric and concentric force-velocity relationships in human muscle.* Journal of Applied Physiology, vol. 90, no. 6, pages 2109–2116, 2001. (Cited in page 57.)

[Decker 2003] Michael J Decker, Michael R Torry, Douglas J Wyland, William I Sterett and J Richard Steadman. *Gender differences in lower extremity kinematics, kinetics and energy absorption during landing.* Clinical Biomechanics, vol. 18, no. 7, pages 662–669, 2003. (Cited in page 54.)

[Dellon 2007] B. Dellon and Y. Matsuoka. *Prosthetics, exoskeletons, and rehabilitation [Grand Challenges of Robotics].* IEEE Robotics Automation Magazine, vol. 14, no. 1, pages 30–34, March 2007. (Cited in page 6.)

[Delp 2007] S. L. Delp, F. C. Anderson, A. S. Arnold, P. Loan, A. Habib, C. T. John, E. Guendelman and D. G. Thelen. *OpenSim: Open-Source Software to Create and Analyze Dynamic Simulations of Movement.* IEEE Transactions on Biomedical Engineering, vol. 54, no. 11, pages 1940–1950, 2007. (Cited in pages 17, 19, 35 and 44.)

[Devita 1992] P Devita and W a Skelly. *Effect of landing stiffness on joint kinetics and energetics in the lower extremity.* Medicine and science in sports and exercise, vol. 24, no. 1, pages 108–115, 1992. (Cited in pages 38, 39, 40, 54, 55, 56 and 57.)

[Di Paolo 2012] Ezequiel Di Paolo and Hanne De Jaegher. *The interactive brain hypothesis.* Frontiers in human neuroscience, vol. 6, 2012. (Cited in page 8.)

[Domkin 2005] Dmitry Domkin, Jozsef Laczko, Mats Djupsjöbacka, Slobodan Jaric and Mark L. Latash. *Joint angle variability in 3D bimanual pointing: uncontrolled manifold analysis.* Experimental Brain Research, vol. 163, no. 1, pages 44–57, may 2005. (Cited in page 72.)

[Duffy 2003] Brian R. Duffy. *Anthropomorphism and the social robot.* Robotics and Autonomous Systems, vol. 42, no. 3, pages 177 – 190, 2003. Socially Interactive Robots. (Cited in page 17.)

[Dumas 2007a] R. Dumas. *Influence of the 3D Inverse Dynamic Method on the Joint Forces and Moments During Gait.* Journal of Biomechanical Engineering, vol. 129, no. 5, page 786, 2007. (Cited in page 23.)

[Dumas 2007b] R. Dumas, L. Chèze and J. P. Verriest. *Adjustments to McConville et al. and Young et al. body segment inertial parameters.* Journal of Biomechanics, vol. 40, no. 3, pages 543–553, 2007. (Cited in pages 19, 20, 34, 44 and 61.)

[Dumas 2007c] R. Dumas, L. Chèze and J.-P. Verriest. *Corrigendum to "Adjustments to McConville et al. and Young et al. body segment inertial parameters" [J. Biomech. 40 (2007) 543–553].* Journal of Biomechanics, vol. 40, no. 7, pages 1651–1652, 2007. (Cited in pages 34 and 61.)

[Dumas 2014] R. Dumas, V. Camomilla, T. Bonci, L. Cheze and A. Cappozzo. *Generalized mathematical representation of the soft tissue artefact.* Journal of Biomechanics, vol. 47, no. 2, pages 476 – 481, 2014. (Cited in page 18.)

[Duprey 2010] Sonia Duprey, Laurence Chèze and Raphaël Dumas. *Influence of joint constraints on lower limb kinematics estimation from skin markers using global optimization.* Journal of Biomechanics, vol. 43, no. 14, pages 2858–2862, 2010. (Cited in page 21.)

[Durkin 2002] JL Durkin, JJ Dowlingm and DM Andrews. *The measurement of body segment inertial parameters using dual energy X-ray absorptiometry.* Journal of Biomechanics, vol. 35, no. 12, pages 1575–1580, 2002. (Cited in page 20.)

[Ehrig 2005] Rainald M Ehrig, William R Taylor, Georg N Duda and Markus O Heller. *A survey of formal methods for determining the centre of rotation of ball joints.* Journal of Biomechanics, vol. 39, no. 15, pages 2798–809, 2005. (Cited in pages 19 and 61.)

[Ehrig 2007] Rainald M Ehrig, William R Taylor, Georg N Duda and Markus O Heller. *A survey of formal methods for determining functional joint axes.* Journal of Biomechanics, vol. 40, no. 10, pages 2150–7, 2007. (Cited in page 20.)

[Escande 2010] A. Escande, N. Mansard and P. B. Wieber. *Fast resolution of hierarchized inverse kinematics with inequality constraints.* In 2010 IEEE International Conference on Robotics and Automation, pages 3733–3738, May 2010. (Cited in pages v, 95, 96 and 115.)

[Escande 2014] Adrien Escande, Nicolas Mansard and Pierre-Brice Wieber. *Hierarchical quadratic programming: Fast online humanoid-robot motion generation.* The International Journal of Robotics Research, vol. 33, no. 7, pages 1006–1028, 2014. (Cited in pages 95 and 115.)

[Fan 2006] Jing Fan, Jiping He and Stephen I. Helms Tillery. *Control of hand orientation and arm movement during reach and grasp.* Experimental Brain Research, vol. 171, no. 3, pages 283–296, may 2006. (Cited in page 73.)

[Feldman 1966] Anatol G. Feldman. *Functional tuning of the nervous system with control of movement or maintenance of a steady posture. II. Controllable parameters of the muscle.* Biophysics, vol. 11, pages 565–578, 1966. (Cited in pages 71 and 74.)

[Feldman 1981] A. G. Feldman. *The composition of central programs subserving horizontal eye movements in man.* Biological Cybernetics, vol. 42, no. 2, pages 107–116, Nov 1981. (Cited in page 74.)

[Feldman 1990] A. G. Feldman, S. V. Adamovich, D. J. Ostry and J. R. Flanagan. The origin of electromyograms — explanations based on the equilibrium point hypothesis, pages 195–213. Springer New York, New York, NY, 1990. (Cited in page 74.)

[Feldman 1995] Anatol G. Feldman and Mindy F. Levin. *The origin and use of positional frames of reference in motor control.* Behavioral and Brain Sciences, vol. 18, no. 04, page 723, 1995. (Cited in pages 17 and 74.)

[Flanagan 1990] J. Randall Flanagan, David J. Ostry and Anatol G. Feldman. *Chapter 2 Control of Human Jaw and Multi-Joint Arm Movements.* In Geoffrey R. Hammond, editor, Cerebral Control of Speech and Limb Movements, volume 70 of *Advances in Psychology*, pages 29 – 58. North-Holland, 1990. (Cited in page 74.)

[Flash 1985] Tamar Flash. *The Coordination of Arm Movements: Mathematical Model.* The Journal of Neuroscience, vol. 5, no. 7, pages 1688–1703, 1985. (Cited in pages 40 and 93.)

[Flash 2005] Tamar Flash and Binyamin Hochner. *Motor primitives in vertebrates and invertebrates.* Current Opinion in Neurobiology, vol. 15, no. 6, pages 660 – 666, 2005. Motor sytems / Neurobiology of behaviour. (Cited in page 71.)

[Frohlich 1979] Cliff Frohlich. *Do spring board divers violate angular momentum conservation?* American Journal of Physics, vol. 47, no. 7, pages 583–592, 1979. (Cited in page 59.)

[Gelfand 1998] I M Gelfand and M L Latash. *On the problem of adequate language in motor control.* Motor control, vol. 2, no. 4, pages 306–13, 1998. (Cited in page 71.)

[Gera 2010] G Gera, S Freitas, M Latash, K Monahan, G Schoner and J Scholz. *Motor Abundance Contributes to Resolving Multiple Kinematic Task Constraints.* Motor Control, vol. 14, no. 1, pages 83–115, 2010. (Cited in pages 71, 73 and 74.)

[Gilchrist 2011] Paul Gilchrist and Belinda Wheaton. *Lifestyle sport, public policy and youth engagement: examining the emergence of parkour.* International Journal of Sport Policy and Politics, vol. 3, no. 1, pages 109–131, 2011. (Cited in pages 12 and 38.)

[Gittoes 2012] Marianne Jr Gittoes and Gareth Irwin. *Biomechanical approaches to understanding the potentially injurious demands of gymnastic-style impact landings.* Sports Medicine, Arthroscopy, Rehabilitation, Therapy & Technology, vol. 4, no. 1, page 4, 2012. (Cited in pages 84 and 89.)

[Goswami 2004] A. Goswami and V. Kallem. *Rate of change of angular momentum and balance maintenance of biped robots.* In Robotics and Automation, 2004. Proceedings. ICRA '04. 2004 IEEE International Conference on, volume 4, pages 3785–3790, April 2004. (Cited in page 59.)

[Grosprêtre 2016] Sidney Grosprêtre and Romuald Lepers. *Performance characteristics of Parkour practitioners: Who are the traceurs?* European Journal of Sport Science, vol. 16, no. 5, pages 526–535, 2016. (Cited in pages 39 and 55.)

[Hamner 2010] Samuel R. Hamner, Ajay Seth and Scott L. Delp. *Muscle contributions to propulsion and support during running.* Journal of Biomechanics, vol. 43, no. 14, pages 2709–2716, 2010. (Cited in pages viii, 33 and 34.)

[Hara 2006] Mikiko Hara, Akira Shibayama, Daisuke Takeshita and Senshi Fukashiro. *The effect of arm swing on lower extremities in vertical jumping.* Journal of Biomechanics, vol. 39, no. 13, pages 2503–2511, 2006. (Cited in page 82.)

[Hasan 2005] Z. Hasan. *The Human Motor Control System's Response to Mechanical Perturbation: Should It, Can It and Does It Ensure Stability?* Journal of Motor Behavior, vol. 37, no. 6, pages 484–493, nov 2005. (Cited in page 70.)

[Hatze 1975] H Hatze. *A new method for the simultaneous measurement of the moment of inertia, the damping coefficient and the location of the centre of mass of a body segment* in situ. European Journal of Applied Physiology, vol. 34, pages 217–226, 1975. (Cited in page 20.)

[Havana 1964] Ernest P Havana. *A mathematical model of the human body (Report AMRL-TR-64-102).* Technical Report, Aerospace Medical Research Laboratory, Ohio, 1964. (Cited in page 20.)

[Hermens 2000] Hermie J Hermens, Bart Freriks, Catherine Disselhorst-Klug and Günter Rau. *Development of recommendations for SEMG sensors and sensor placement procedures.* Journal of Electromyography and Kinesiology, vol. 10, no. 5, pages 361 – 374, 2000. (Cited in page 17.)

[Herr 2008] Hugh Herr and Marko Popovic. *Angular momentum in human walking.* The Journal of experimental biology, vol. 211, no. Pt 4, pages 467–81, mar 2008. (Cited in page 59.)

[Hirose 2001] R Hirose and T. Takenaka. *Development of the Humanoid Robot ASIMO.* Technical Review, no. 1, pages 1–6, 2001. (Cited in page 5.)

[Hodgins 1998] Jessica K Hodgins and Wayne L Wooten. *Animating human athletes.* In Robotics Research, pages 356–367. Springer, London, 1998. (Cited in page 8.)

[Hoellinger 2017] T. Hoellinger, J McIntyre, L. Jami, S. Hanneton, G. Cheron and A Roby-Brami. *A strategy of faster movements used by elderly humans to lift objects of increasing weight in ecological context.* Neuroscience, 2017. to appear. (Cited in page 110.)

[Hoff 1992] B Hoff and M Arbib. *A model of the effects of speed, accuracy, and perturbation on visually guided reaching.* Experimental Brain Research, vol. 22, pages 285–306, 1992. (Cited in pages 93 and 106.)

[Hofmann 2009] a. Hofmann, M. Popovic and H. Herr. *Exploiting angular momentum to enhance bipedal center-of-mass control.* 2009 IEEE International Conference on Robotics and Automation, pages 4423–4429, may 2009. (Cited in page 59.)

[Hogan 1984] N Hogan. *An organizing principle for a class of voluntary movements.* Journal of Neuroscience, vol. 4, no. 11, pages 2745–2754, 1984. (Cited in page 40.)

[Holzbaur 2005] Katherine R S Holzbaur, Wendy M Murray and Scott L Delp. *A Model of the Upper Extremity for Simulating Musculoskeletal Surgery and Analyzing Neuromuscular Control.* Annals of Biomedical Engineering, vol. 33, no. 6, pages 829–840, 2005. (Cited in page 34.)

[Hopper 2014] Diana M. Hopper, Tiffany L. Grisbrook, Mark Finucane and Kazunori Nosaka. *Effect of ankle taping on angle and force matching and strength of the plantar flexors.* Physical Therapy in Sport, vol. 15, no. 4, pages 254–260, 2014. (Cited in page 57.)

[Hrysomallis 2007] Con Hrysomallis. *Relationship Between Balance Ability, Training and Sports Injury Risk.* Sports Medicine, vol. 37, no. 6, pages 547–556, Jun 2007. (Cited in page 39.)

[Hrysomallis 2011] Con Hrysomallis. *Balance ability and athletic performance.* Sports medicine (Auckland, N.Z.), vol. 41, no. 3, pages 221–32, mar 2011. (Cited in page 39.)

[Hsu 2007] W.-L. Hsu, J. P. Scholz, G. Schoner, J. J. Jeka and T. Kiemel. *Control and Estimation of Posture During Quiet Stance Depends on Multijoint Coordination.* Journal of Neurophysiology, vol. 97, no. 4, pages 3024–3035, jan 2007. (Cited in page 72.)

[Jezernik 2003] Sašo Jezernik, Gery Colombo, Thierry Keller, Hansruedi Frueh and Manfred Morari. *Robotic Orthosis Lokomat: A Rehabilitation and Research Tool.* Neuromodulation: Technology at the Neural Interface, vol. 6, no. 2, pages 108–115, 2003. (Cited in page 7.)

[Kamibayashi 2006] Kiyotaka Kamibayashi and Masuo Muro. *Modulation of pre-programmed muscle activation and stretch reflex to changes of contact surface and visual input during movement to absorb impact.* Journal of Electromyography and Kinesiology, vol. 16, no. 5, pages 432–439, 2006. (Cited in page 84.)

[Kaneko 2004] K. Kaneko, F. Kanehiro, S. Kajita, H. Hirukawa, T. Kawasaki, M. Hirata, K. Akachi and T. Isozumi. *Humanoid robot HRP-2.* In Robotics and Automation, 2004. Proceedings. ICRA '04. 2004 IEEE International Conference on, volume 2, pages 1083–1090 Vol.2, April 2004. (Cited in page 5.)

[Kanoun 2009] O. Kanoun, F. Lamiraux, P. B. Wieber, F. Kanehiro, E. Yoshida and J. P. Laumond. *Prioritizing linear equality and inequality systems: Application to local motion planning for redundant robots.* In 2009 IEEE International Conference on Robotics and Automation, pages 2939–2944, 2009. (Cited in page 95.)

[Kato 1973] I Kato. *Development of WABOT 1.* Biomechanism, vol. 2, pages 173–214, 1973. (Cited in page 5.)

[Kavanaugh 1978] J H Kavanaugh, T D Brower and R V Mann. *The Jones fracture revisited.* The Journal of bone and joint surgery. American volume, vol. 60, no. 6, pages 776–82, sep 1978. (Cited in page 57.)

[Khatib 2009] O. Khatib, E. Demircan, V. De Sapio, L. Sentis, T. Besier and S. Delp. *Robotics-based synthesis of human motion.* Journal of Physiology-Paris, vol. 103, no. 3, pages 211 – 219, 2009. Neurorobotics. (Cited in page 10.)

[Kidder 2012] Jeffrey L. Kidder. *Parkour, The Affective Appropriation of Urban Space, and the Real/Virtual Dialectic.* City and Community, vol. 11, no. 3, pages 229–253, 2012. (Cited in pages 12 and 38.)

[Kim 2013] Sangbae Kim, Cecilia Laschi and Barry Trimmer. *Soft robotics: a bioinspired evolution in robotics.* Trends in Biotechnology, vol. 31, no. 5, pages 287 – 294, 2013. (Cited in page 10.)

[Kristianslund 2012] Eirik Kristianslund, Tron Krosshaug and Antonie J. Van den Bogert. *Effect of low pass filtering on joint moments from inverse dynamics: Implications for injury prevention.* Journal of Biomechanics, vol. 45, no. 4, pages 666–671, 2012. (Cited in pages 18, 43 and 61.)

[Kuo 1998] A D Kuo. *A least-squares estimation approach to improving the precision of inverse dynamics computations.* Journal of biomechanical engineering, vol. 120, no. 1, pages 148–59, feb 1998. (Cited in page 23.)

[Latash 2000] M Latash. *There is no motor redundancy in human movements. There is motor abundance.* Motor control, vol. 4, no. 3, pages 259–60, jul 2000. (Cited in pages 72 and 87.)

[Latash 2001] Mark Latash, John Scholz, Frederic Danion and Gregor Schöner. *Structure of motor variability in marginally redundant multifinger force production tasks.* Experimental Brain Research, vol. 141, no. 2, pages 153–165, nov 2001. (Cited in page 73.)

[Latash 2008] Mark L. Latash, Stacey Gorniak and Vladimir M. Zatsiorsky. *Hierarchies of Synergies in Human Movements.* Kinesiology, vol. 40, no. 1, pages 29–38, 2008. (Cited in pages 73 and 81.)

[Latash 2010] Mark L Latash. *Motor synergies and the equilibrium-point hypothesis.* Motor Control, vol. 14, no. 3, pages 294–322, 2010. (Cited in page 73.)

[Latash 2016] Mark L Latash and Vladimir M Zatsiorsky. Biomechanics and Motor Control. Academic Press, 2016. (Cited in page 70.)

[Leva 1996] Paolo De Leva. *Adjustements to Zatsiorsky-Seluyanov's segment inertia paremeters.* Journal of Biomechanics, vol. 29, no. 9, pages 1223–1230, 1996. (Cited in page 34.)

[Levin 1994] Mindy F. Levin and Anatol G. Feldman. *The role of stretch reflex threshold regulation in normal and impaired motor control.* Brain Research, vol. 657, no. 1, pages 23 – 30, 1994. (Cited in page 74.)

[Lu 1999] T.-W. Lu and J.J. O'Connor. *Bone position estimation from skin marker co-ordinates using global optimisation with joint constraints.* Journal of Biomechanics, vol. 32, no. 2, pages 129 – 134, 1999. (Cited in pages 21 and 61.)

[Maldonado 2015] G. Maldonado, H. Bitard, B. Watier and P. Souères. *Evidence of dynamic postural control performance in parkour landing.* Computer Methods in Biomechanics and Biomedical Engineering, vol. 18, no. 1, pages 1994–1995, 2015. (Cited in page 84.)

[Mansard 2009] Nicolas Mansard, Olivier Stasse, Paul Evrard and Abderrahmane Kheddar. *A versatile generalized inverted kinematics implementation for collaborative working humanoid robots: the Stack of Tasks.* In ICAR'09: International Conference on Advanced Robotics, pages 1–6, Munich, Germany, June 2009. (Cited in page 95.)

[Marchetti 2012] Paulo Henrique Marchetti, Danilo Luz Junior, Atanázio, Enrico Gori Soares, Fernando Henrique Silva, Marco Carlos Uchida and Milano Felipe Luis Teixeira. *Differences in Muscular Performance between Practitioners and Non Practitioners of Parkour.* International Journal of Sports Science, vol. 2, no. 4, pages 36–41, 2012. (Cited in page 39.)

[Marshall 2007] Stephen W Marshall, Tracey Covassin, Randall Dick, Lawrence G Nassar and Julie Agel. *Descriptive epidemiology of collegiate women's gymnastics injuries: National Collegiate Athletic Association Injury Surveillance System, 1988-1989 through 2003-2004.* Journal of athletic training, vol. 42, no. 2, pages 234–40, 2007. (Cited in page 31.)

[Mccaw 2013] Steven T Mccaw, Jacob K Gardner, Lindsay N Stafford and Michael R Torry. *Filtering Ground Reaction Force Data Affects the Calculation and Interpretation of Joint Kinetics and Energetics During Drop Landings.* Journal of Applied Biomechanics, vol. 29, no. 6, pages 804–809, 2013. (Cited in pages 18, 43 and 54.)

[McNitt-Gray 1993] Jill L. McNitt-Gray. *Kinetics of the lower extremities during drop landings from three heights.* Journal of Biomechanics, vol. 26, no. 9, pages 1037–1046, 1993. (Cited in page 54.)

[Mihelj 2007] Matjaž Mihelj, Tobias Nef and Robert Riener. *A novel paradigm for patient-cooperative control of upper-limb rehabilitation robots.* Advanced Robotics, vol. 21, no. 8, pages 843–867, 2007. (Cited in page 110.)

[Mombaur 2010] Katja Mombaur, Anh Truong and Jean-Paul Laumond. *From human to humanoid locomotion—an inverse optimal control approach.* Autonomous Robots, vol. 28, no. 3, pages 369–383, Apr 2010. (Cited in page 110.)

[Multon 1999] Franck Multon, Laure France, Marie-Paule Cani-Gascuel and Gilles Debunne. *Computer animation of human walking: a survey.* The journal of visualization and computer animation, vol. 10, no. 1, pages 39–54, 1999. (Cited in page 8.)

[Nakamura 1987] Yoshihiko Nakamura and Hideo Hanafusa. *Optimal Redundancy Control of Robot Manipulators.* The International Journal of Robotics Research, vol. 6, no. 1, pages 32–42, 1987. (Cited in page 95.)

[Nakamura 1991] Yoshihiko. Nakamura and Yoshihiko. Advanced robotics : redundancy and optimization. Addison-Wesley Pub. Co, 1991. (Cited in pages 76 and 92.)

[Nelson 1983] W L Nelson. *Physical principles for economies of skilled movements.* Biological cybernetics, vol. 46, pages 135–147, 1983. (Cited in page 71.)

[Nisky 2014] Ilana Nisky, Michael H. Hsieh and Allison M. Okamura. *Uncontrolled Manifold Analysis of Arm Joint Angle Variability During Robotic Teleoperation and Freehand Movement of Surgeons and Novices.* IEEE Transactions on Biomedical Engineering, vol. 61, no. 12, pages 2869–2881, 2014. (Cited in page 77.)

[Niu 2011] Wenxin Niu, Yang Wang, Yan He, Yubo Fan and Qinping Zhao. *Kinematics, kinetics, and electromyogram of ankle during drop landing: A comparison between dominant and non-dominant limb.* Human Movement Science, vol. 30, no. 3, pages 614 – 623, 2011. (Cited in page 44.)

[Orin 2008] D.E. Orin and a. Goswami. *Centroidal Momentum Matrix of a humanoid robot: Structure and properties.* 2008 IEEE/RSJ International Conference on Intelligent Robots and Systems, pages 653–659, sep 2008. (Cited in page 81.)

[Orin 2013] David E. Orin, Ambarish Goswami and Sung-Hee Lee. *Centroidal dynamics of a humanoid robot.* Autonomous Robots, vol. 35, no. 2-3, pages 161–176, jun 2013. (Cited in pages 80 and 92.)

[Penney 2010] J. Nicholas Penney. *The biopsychosocial model of pain and contemporary osteopathic practice.* International Journal of Osteopathic Medicine, vol. 13, no. 2, pages 42 – 47, 2010. (Cited in page 109.)

[Popović 2013] Marko B. Popović. *Biomechanics and Robotics*, 2013. (Cited in page 10.)

[Puddle 2013] Damien L Puddle and Peter S Maulder. *Ground Reaction Forces and Loading Rates Associated with Parkour and Traditional Drop Landing Techniques.* Journal of Sports Science and Medicine, vol. 12, no. 1, pages 122–129, 2013. (Cited in pages 38, 43 and 54.)

[R Development Core Team 2008] R Development Core Team. *R: A Language and Environment for Statistical Computing.* R Foundation for Statistical Computing, Vienna, Austria, 2008. ISBN 3-900051-07-0. (Cited in page 85.)

[Reisman 2003] Darcy S Reisman and John P Scholz. *Aspects of joint coordination are preserved during pointing in persons with post-stroke hemiparesis.* Brain : a journal of neurology, vol. 126, no. Pt 11, pages 2510–27, 2003. (Cited in page 111.)

[Rosen 2015] A. B. Rosen, J. Ko, K. J. Simpson, S.-H. Kim and C. N. Brown. *Lower Extremity Kinematics During a Drop Jump in Individuals With Patellar Tendinopathy.* Orthopaedic Journal of Sports Medicine, vol. 3, no. 3, mar 2015. (Cited in page 38.)

[Rossheim 2017] Matthew E. Rossheim and Caroline J. Stephenson. *Parkour injuries presenting to United States emergency departments, 2009–2015.* The American Journal of Emergency Medicine, 2017. (Cited in page 31.)

[Saab 2011] L. Saab, N. Mansard, F. Keith, J. Y. Fourquet and P. Soueres. *Generation of dynamic motion for anthropomorphic systems under prioritized equality and inequality constraints.* In 2011 IEEE International Conference

on Robotics and Automation, pages 1091–1096, 2011. (Cited in pages 78 and 95.)

[Saab 2013] L. Saab, O. E. Ramos, F. Keith, N. Mansard, P. Souères and J. Y. Fourquet. *Dynamic Whole-Body Motion Generation Under Rigid Contacts and Other Unilateral Constraints.* IEEE Transactions on Robotics, vol. 29, no. 2, pages 346–362, 2013. (Cited in page 94.)

[Samson 1991] Claude Samson, Bernard Espiau and Michel Le Borgne. Robot control: the task function approach. Oxford University Press, 1991. (Cited in pages 76 and 92.)

[Sardain 2004] P. Sardain and G. Bessonnet. *Forces Acting on a Biped Robot. Center of Pressure—Zero Moment Point.* IEEE Transactions on Systems, Man, and Cybernetics - Part A: Systems and Humans, vol. 34, no. 5, pages 630–637, sep 2004. (Cited in pages 59 and 70.)

[Scholz 1999] John P. Scholz and Gregor Schöner. *The uncontrolled manifold concept: Identifying control variables for a functional task.* Experimental Brain Research, vol. 126, no. 3, pages 289–306, 1999. (Cited in pages 10, 17, 71, 72, 73, 76 and 77.)

[Scholz 2001] John Scholz, Darcy Reisman and Gregor Schöner. *Effects of varying task constraints on solutions to joint coordination in a sit-to-stand task.* Experimental Brain Research, vol. 141, no. 4, pages 485–500, dec 2001. (Cited in page 73.)

[Schubert 2014] Patric Schubert and Marietta Kirchner. *Ellipse area calculations and their applicability in posturography.* Gait & Posture, vol. 39, no. 1, pages 518 – 522, 2014. (Cited in page 45.)

[Schutte 1993] L. M. Schutte, M. M. Rodgers, F. E. Zajac and R. M. Glaser. *Improving the efficacy of electrical stimulation-induced leg cycle ergometry: an analysis based on a dynamic musculoskeletal model.* IEEE Transactions on Rehabilitation Engineering, vol. 1, no. 2, pages 109–125, Jun 1993. (Cited in page 34.)

[Seth 2010] Ajay Seth, Michael Sherman, Peter Eastman and Scott Delp. *Minimal formulation of joint motion for biomechanisms.* Nonlinear Dynamics, vol. 62, no. 1, pages 291–303, Oct 2010. (Cited in page 109.)

[Siciliano 1991] B. Siciliano and J. J. E. Slotine. *A general framework for managing multiple tasks in highly redundant robotic systems.* In Advanced Robotics, 1991. 'Robots in Unstructured Environments', 91 ICAR., Fifth International Conference on, pages 1211–1216 vol.2, June 1991. (Cited in pages 95 and 115.)

[Singh 2016] Puneet Singh, Sumitash Jana, Ashitava Ghosal and Aditya Murthy. *Exploration of joint redundancy but not task space variability facilitates supervised motor learning.* Proceedings of the National Academy of Sciences of the United States of America, vol. 113, no. 50, pages 14414–14419, dec 2016. (Cited in page 110.)

[Sok 2007] Kwang Won Sok, Manmyung Kim and Jehee Lee. *Simulating Biped Behaviors from Human Motion Data.* In ACM SIGGRAPH 2007 Papers, SIGGRAPH '07, New York, NY, USA, 2007. ACM. (Cited in page 17.)

[Standing 2015] Regan J Standing and Peter S Maulder. *A Comparison of the Habitual Landing Strategies from Differing Drop Heights of Parkour Practitioners (Traceurs) and Recreationally Trained Individuals.* Journal of Sports Science and Medicine, vol. 14, no. 4, pages 723–731, 2015. (Cited in pages 38, 39, 54, 84 and 89.)

[Stasse 2017] Olivier Stasse, Thomas Flayols, Rohan Budhiraja, Kevin Giraud-Esclasse, Justin Carpentier, Andrea Del Prete, Philippe Souères, Nicolas Mansard, Florent Lamiraux, Jean-Paul Laumond, Luca Marchionni, Hilario Tome and Francesco Ferro. TALOS: A new humanoid research platform targeted for industrial applications. working paper or preprint, March 2017. (Cited in pages 5 and 11.)

[Steele 1990] J R Steele. *Biomechanical factors affecting performance in netball. Implications for improving performance and injury reduction.* Sports medicine (Auckland, N.Z.), vol. 10, no. 2, pages 88–102, aug 1990. (Cited in pages 38 and 54.)

[Sugano 1987] Shigeki Sugano and Ichiro Kato. Wabot-2: Autonomous robot with dexterous finger-arm - finger-arm coordination control in keyboard performance., pages 90–97. IEEE, 1987. (Cited in page 5.)

[Takagi 1985] A. Takagi, E. Fujimura and S. Suehiro. *A new method of statokinesigram area measurement. Application of a statistically calculated ellipse.*, 1985. (Cited in page 40.)

[Thelen 2003] Darryl G Thelen. *Adjustment of muscle mechanics model parameters to simulate dynamic contractions in older adults.* Journal of biomechanical engineering, 2003. (Cited in page 34.)

[Todorov 2002] Emanuel Todorov and Michael I Jordan. *Optimal feedback control as a theory of motor coordination.* Nature neuroscience, vol. 5, no. 11, pages 1226–35, 2002. (Cited in pages 17 and 71.)

[Todorov 2005] Emanuel Todorov, Weiwei Li and Xiuchuan Pan. *From task parameters to motor synergies: A hierarchical framework for approximately-optimal control of redundant manipulators.* Journal of robotic systems, vol. 22, no. 11, pages 691–710, nov 2005. (Cited in page 73.)

[Tresch 2006] Matthew C Tresch, Vincent C K Cheung and Andrea d'Avella. *Matrix factorization algorithms for the identification of muscle synergies: evaluation on simulated and experimental data sets.* Journal of neurophysiology, vol. 95 4, pages 2199–212, 2006. (Cited in pages 71 and 72.)

[Tsagarakis 2017] N. G. Tsagarakis, D. G. Caldwell, F. Negrello, W. Choi, L. Baccelliere, V.G. Loc, J. Noorden, L. Muratore, A. Margan, A. Cardellino, L. Natale, E. Mingo Hoffman, H. Dallali, N. Kashiri, J. Malzahn, J. Lee, P. Kryczka, D. Kanoulas, M. Garabini, M. Catalano, M. Ferrati, V. Varricchio, L. Pallottino, C. Pavan, A. Bicchi, A. Settimi, A. Rocchi and A. Ajoudani. *WALK-MAN: A High-Performance Humanoid Platform for Realistic Environments.* Journal of Field Robotics, pages n/a–n/a, 2017. (Cited in page 5.)

[Tseng 2006] Ya-weng Tseng, John P Scholz and Martin Valere. *Effects of movement frequency and joint kinetics on the joint coordination underlying bimanual circle drawing.* Journal of motor behavior, vol. 38, no. 5, pages 383–404, sep 2006. (Cited in page 73.)

[Uno 1989] Y Uno, M Kawato and R Suzuki. *Formation and control of optimal trajectory in human multijoint arm movement.* Biological cybernetics, vol. 101, pages 89–101, 1989. (Cited in page 41.)

[Venture 2008] G. Venture, K. Ayusawa and Y. Nakamura. *Motion capture based identification of the human body inertial parameters.* In 2008 30th Annual International Conference of the IEEE Engineering in Medicine and Biology Society, pages 4575–4578, 2008. (Cited in page 20.)

[Wakai 2005] Masaki Wakai and Nicholas P. Linthorne. *Optimum take-off angle in the standing long jump.* Human Movement Science, vol. 24, no. 1, pages 81–96, 2005. (Cited in pages 82 and 87.)

[Wikstrom 2005] Erik a. Wikstrom, Mark D. Tillman, Andrew N. Smith and Paul a. Borsa. *A new force-plate technology measure of dynamic postural stability: The dynamic postural stability index.* Journal of Athletic Training, vol. 40, no. 4, pages 305–309, 2005. (Cited in pages 40 and 45.)

[Winter 2009] David A Winter. Biomechanics and motor control of human movement, Fourth Edition. John Wiley & Sons, Inc, 2009. (Cited in pages 16, 17, 18, 19, 44 and 61.)

[Wu 2002] Ge Wu, Sorin Siegler, Paul Allard, Chris Kirtley, Alberto Leardini, Dieter Rosenbaum, Mike Whittle, Darryl D D'Lima, Luca Cristofolini, Hartmut Witte, Oskar Schmid and Ian Stokes. *ISB recommendation on definitions of joint coordinate system of various joints for the reporting of human joint motion—Part I: ankle, hip, and spine.* Journal of Biomechanics, vol. 35, no. 4, pages 543–548, 2002. (Cited in pages 17, 21, 37, 41 and 61.)

[Wu 2005] Ge Wu, Frans C.T. van der Helm, H.E.J. (DirkJan) Veeger, Mohsen Makhsous, Peter Van Roy, Carolyn Anglin, Jochem Nagels, Andrew R. Karduna, Kevin McQuade, Xuguang Wang, Frederick W. Werner and Bryan Buchholz. *ISB recommendation on definitions of joint coordinate systems of various joints for the reporting of human joint motion—Part II: shoulder, elbow, wrist and hand.* Journal of Biomechanics, vol. 38, no. 5, pages 981–992, 2005. (Cited in pages 17, 21, 37 and 61.)

[Yamane 2003] Katsu Yamane and Yoshihiko Nakamura. *Natural motion animation through constraining and deconstraining at will.* IEEE Transactions on visualization and computer graphics, vol. 9, no. 3, pages 352–360, 2003. (Cited in page 8.)

[Yamane 2010] Katsu Yamane and Kwang Won Sok. *Planning and Synthesizing Superhero Motions.* In Proceedings of the Third International Conference on Motion in Games, MIG'10, pages 254–265, Berlin, Heidelberg, 2010. Springer-Verlag. (Cited in page 17.)

[Yeadon 2010] M.R. Yeadon, M.A. King, S.E. Forrester, G.E. Caldwell and M.T.G. Pain. *The need for muscle co-contraction prior to a landing.* Journal of Biomechanics, vol. 43, no. 2, pages 364–369, 2010. (Cited in pages 56, 84 and 89.)

[Yen 2009] Jasper T. Yen, Arick G. Auyang and Young-Hui Chang. *Joint-level kinetic redundancy is exploited to control limb-level forces during human hopping.* Experimental Brain Research, vol. 196, no. 3, pages 439–451, Jul 2009. (Cited in page 73.)

[Yeow 2009] C. H. Yeow, P. V S Lee and J. C H Goh. *Effect of landing height on frontal plane kinematics, kinetics and energy dissipation at lower extremity joints.* Journal of Biomechanics, vol. 42, no. 12, pages 1967–1973, aug 2009. (Cited in pages 39 and 55.)

[Yun 2011] S. Yun and A. Goswami. *Momentum-based reactive stepping controller on level and non-level ground for humanoid robot push recovery.* In 2011 IEEE/RSJ International Conference on Intelligent Robots and Systems, pages 3943–3950, Sept 2011. (Cited in page 59.)

[Zatsiorsky 1983] Vladimir M. Zatsiorsky and V. N. Seluyanov. *The mass and inertia characteristics of the main segment of human body.* Biomechanics, pages 1152–1159, 1983. (Cited in page 20.)

[Zatsiorsky 2002] Vladimir M Zatsiorsky. Kinetics of Human Motion. Human Kinetics, 2002. (Cited in pages 16, 23, 24 and 44.)

[Zetaruk 2005] M N Zetaruk, M A Violán, D Zurakowski and L J Micheli. *Injuries in martial arts: a comparison of five styles.* British journal of sports medicine, vol. 39, no. 1, pages 29–33, jan 2005. (Cited in page 31.)

[Zhang 2000] S N Zhang, B T Bates and J S Dufek. *Contributions of lower extremity joints to energy dissipation during landings.* Medicine and science in sports and exercise, vol. 32, no. 4, pages 812–819, 2000. (Cited in page 56.)

[Zhang 2008] Wei Zhang, John P Scholz, Vladimir M Zatsiorsky and Mark L Latash. *What do synergies do? Effects of secondary constraints on multidigit synergies in accurate force-production tasks.* Journal of neurophysiology, vol. 99, no. 2, pages 500–13, feb 2008. (Cited in page 74.)

Abstract: This thesis proposes an original and interdisciplinary approach to the treatment of whole-body human movements through the synergistic utilization of biomechanics, motor control and robotics. Robust methods of biomechanics are used to record, process and analyze whole-body human motions. The Uncontrolled Manifold approach (UCM) of motor control is extended to study highly dynamic movements processed in the biomechanical study, in order to determine if hypothesized dynamic tasks are being controlled stably by the central nervous system. This extension permits also to infer a hierarchical organization of the controlled dynamic tasks. The task space formalism of motion generation in robotics is used to generate whole-body motion by taking into account the hierarchy of tasks extracted in the motor control study. This approach permits to better understand the organization of human dynamic motions and provide a new methodology to generate whole-body human motions with anthropomorphic systems. A case study of highly dynamic and complex movements of Parkour, including jumps and landings, is utilized to illustrate the proposed approach.

Keywords: redundancy, whole-body motion, biomechanics, motor control, robotics, human-inspired motion, task space, Uncontrolled Manifold, parkour, highly dynamic motion.

Résumé : Cette thèse propose une approche interdisciplinaire originale du traitement du mouvement humain corps-complet grâce à l'utilisation couplée d'approches issues de la biomécanique, du contrôle moteur et de la robotique. Les méthodes biomécaniques sont utilisées pour l'enregistrement, le traitement et l'analyse du mouvement humain. L'approche « Uncontrolled Manifold » du contrôle moteur est étendue à l'étude des mouvements hautement dynamiques. Ceci permet de déterminer si d'éventuelles tâches dynamiques sont contrôlées et stabilisées par le cerveau, puis d'inférer une organisation hiérarchique des tâches motrices. Le formalisme de l'espace des tâches utilisé en robotique pour la génération de mouvement corps-complet ainsi que la hiérarchie des tâches extraites dans l'étude du contrôle moteur sont utilisés pour simuler des mouvements humains hautement dynamiques. Cette approche permet de mieux comprendre le mouvement humain et de générer des mouvements inspirés de l'humain pour d'autres systèmes anthropomorphes tel que des robots ou avatars. La discipline du Parkour, impliquant des actions hautement dynamiques tels que des sauts et des techniques d'atterisage, est choisie pour illustrer l'approche proposée.

Mots clés : La redondance, mouvement corps-complet, biomécanique, contrôle moteur, robotique, mouvement inspiré de l'homme, l'espace de tâches, Uncontrolled Manifold, le parkour, mouvement hautement dynamique.